LOW- DIMENSIONAL PHOTONIC DEVICES BASED ON HYBRID MATERIALS

Ph.D. Thesis

By

SURESH KUMAR PANDEY

Under the Supervision of

Prof. Mukesh Kumar

DISCIPLINE OF ELECTRICAL ENGINEERING

INDIAN INSTITUTE OF TECHNOLOGY INDORE

AUGUST, 2024

LOW- DIMENSIONAL PHOTONIC DEVICES BASED ON HYBRID MATERIALS

A THESIS

Submitted in partial fulfillment of the requirements for the award of the degree
of
DOCTOR OF PHILOSOPHY

by
SURESH KUMAR PANDEY

Under the Supervision of

Prof. Mukesh Kumar

DISCIPLINE OF ELECTRICAL ENGINEERING
INDIAN INSTITUTE OF TECHNOLOGY INDORE
AUGUST, 2024

INDIAN INSTITUTE OF TECHNOLOGY INDORE

CANDIDATE'S DECLARATION

I hereby certify that the work which is being presented in the thesis entitled **"Low Dimensional Photonic Devices based on Hybrid Materials"** in the partial fulfillment of the requirements for the award of the degree of **Doctor of Philosophy** and submitted in the **Department of Electrical Engineering Indian Institute of Technology Indore**, is an authentic record of my own work carried out during the time period from the July 2019 to July 2024 under the supervision of Prof. Mukesh Kumar, Professor, and Head CAE, Electrical Engineering, Centre for Advanced Electronics, IIT Indore.

The matter presented in this thesis has not been submitted by me for the award of any other degree of this or any other institute.

Suresh Pandey
08/01/2025
signature of the student with date
(SURESH KUMAR PANDEY)

This is to certify that the above statement made by the candidate is correct to the best of my/our knowledge.

08/01/2025
Signature of Thesis Supervisor with date
(Prof. Mukesh Kumar)

SURESH KUMAR PANDEY has successfully given his Ph.D. Oral Examination held on 08/01/2025

08/01/2025
Signature of Thesis Supervisor with date
(Prof. Mukesh Kumar)

ACKNOWLEDGEMENTS

Completing this journey of academic pursuit has been a profound and transformative experience, and it is with sincere gratitude that I express my appreciation to those who have contributed to this endeavor.

First and foremost, I extend my deepest gratitude to my esteemed supervisor, **Prof. Mukesh Kumar**. Your guidance, wisdom, and unwavering support have been invaluable throughout every stage of this research. Your mentorship has not only shaped my academic growth but has also inspired me to strive for excellence in all aspects of my work. Your insightful feedback, patience, and encouragement have been instrumental in shaping this dissertation.

I'm deeply thankful to my doctoral committee members, **Prof. Vimal Bhatia** and **Prof. Shaibal Mukherjee**, for their invaluable guidance and meticulous review of my dissertation. Their advice and support have been crucial to my research journey.

I would like to thank **SIC** at IIT Indore for providing partial technical support, characterization, and fabrication facilities. I gratefully acknowledge the fellowship received towards my PhD from Nano Mission, Department of science and technology **(DST)** and Ministry of Human Resource Development **(MHRD)**.

The financial assistance provided by **DST** and Council of Scientific & Industrial Research (**CSIR**) has enabled me to pursue my academic aspirations and conduct meaningful research in my field. Their investment in my education has been instrumental in advancing knowledge and innovation.

I want to express my deep gratitude to Optoelectronic Nanodevice Research Laboratory (**ONRL**), IIT Indore and colleagues, Lalit Singh, Sourabh Jain, Sulabh, Vishal Kaushik, Swati Rajput, Rahul Dev Mishra, Prem Babu, Santosh Kumar, Ashutosh Kumar, Nikita Mohanta and Shikha Devi who helped me in various ways during my thesis work and for providing invaluable support and motivation.

I am thankful to my beloved wife **Chitralekha Pandey**. Your unwavering support, love, and encouragement have been the cornerstone of my PhD journey. Thank you for standing by me through every challenge and triumph. This achievement is as much yours as it is mine.

To my lovely son **Ved,** your bright smile has been my greatest source of strength throughout this challenging journey. Even in moments of stress, your joyous presence reminds me of what truly matters. Thank you for being my light and for filling my heart with love and happiness.

To my dear parents, **Uma** and **Narendra Prasad Pandey**, I owe a debt of gratitude that words alone cannot express. Your unwavering love, encouragement, and sacrifices have been the cornerstone of my journey.

Finally, I express my gratitude to the divine presence that has guided me throughout this journey. To God, I offer my sincerest thanks for the blessings, strength, and guidance bestowed upon me. Your grace has been my constant companion, providing solace during times of uncertainty and inspiration during moments of clarity.

To all those who have supported and believed in me, whether mentioned here or silently cheering from the sidelines, I extend my heartfelt appreciation. This dissertation stands as a testament to the collective efforts of those who have touched my life in profound ways.

With deepest gratitude,

Suresh Kumar Pandey

© Copyright by SURESH KUMAR PANDEY 2024

All Rights Reserved

"Every accomplishment starts

with the decision to try".

Dedicated to

My Beloved Parents

& My Son Ved.

List of Publication

A. Publications from PhD thesis work

1. **S. K. Pandey**, R. D. Mishra, P. Babu, N. Mohanta, S. Kumar, and M. Kumar, "Optical Field Enhanced Tunable Plasmonic Absorber on Subwavelength Grating waveguide Employing ENZ State of ITO" ***Optics & Laser Technology*,** 2025 **(IF-4.6)**.
2. **S. K. Pandey**, R. D. Mishra, P. Babu, N. Mohanta, S. Kumar, and M. Kumar, "Plasmonic Absorber based on Engineered Cu-ITO Structure on Silicon with Low Voltage Tuning and High Extinction Ratio", ***Journal of Lightwave Technology***, vol 42 no. 10 pp. 3779-3785 May 2024 **(IF-4.7)**.
3. **S. K. Pandey**, S. Rajput, V. Kaushik, P. Babu, R. D. Mishra, and M. Kumar, "Optically triggered AlGaN/GaN semiconductor power transistor with bi-layer anti-reflecting structure", **Optical Engineering**, December 2023, Vol 62 no. 12, pp. 127102 (1-9) **(IF-1.3)**.
4. **S. K. Pandey**, S. Rajput, V. Kaushik, P. Babu, R. D. Mishra, and M. Kumar, "Electrically Tunable Plasmonic Absorber Based on CuITO Subwavelength Grating on SOI at Telecom Wavelength", **Plasmonics**, Vol. 17, pp. 1709–1716, May 2022, **(IF-3)**.

B. Other publications during PhD

B1. in refereed journal

1. R. D. Mishra, **S. K. Pandey**, S. Kumar, A. Kumar, P. Babu N. Mohanta, S. Devi and M. Kumar, "Low Power Nanophotonic Resistive Switch based on Multi-tapered and Engineered Cu-TiO_2 Structure on Silicon with Sensing Capability", **Nanotechnology**, under review, April 2024. **(IF-3.5)**
2. S. Kumar, A. Kumar, R.D. Mishra, P. Babu, **S. K. Pandey**, S. Devi, G. Brunetti, C. Ciminelli and M. Kumar, " Multilevel Nanophotonic Resistive Switching in Ag-ITO-SiO_2 on Silicon with Enhanced Optical Storage Density", **Journal of Lightwave Technology**, under review, May 2024 **(IF-4.7)**.

3. N. Mohanta, S. Devi, P. Babu, V. Kaushik, **S. K. Pandey**, R. D. Mishra**,** and M. Kumar “Electrically Tunable Vertically Coupled Ring Resonator based on Si-ITO Heterojunction”, **Optical and Quantum electronics** Accepted, May 2024**(IF-3)**.
4. R. D. Mishra, **S. K. Pandey**, P. Babu, S. Kumar, A. Kumar, N. Mohanta, and M. Kumar, "Nanophotonic Resistive Switch based on Tapered Copper-silicon Structure with Low Power and High Extinction Ratio", **Optics and Laser Technology**, vol 175, pp. 110833 (1-7), March 2024. **(IF-5)**.
5. V. Kaushik, S. Rajput, P. Babu, **S. K. Pandey**, R.D. Mishra, and M. Kumar, “Electronically Controlled Quantum Confinement for Tunable Plasmonic Metasurfaces” **Journal of Lightwave Technology**, vol 42, no. 10, pp. 3814-3819 May 2024 **(IF-4.7)**.
6. P. Babu, S. Sachan, V. Kaushik, S. Rajput, **S. K. Pandey**, R. D. Mishra, and M. Kumar, "Electrically Tunable Birefringence in Nanophotonic Waveguide with 2D Electron Gas in Semiconductor Heterojunction", **Optik,** vol 299 ,171603 (1-10) January 2024 **(IF-3.1)**.
7. S. Biswas, P. Babu, S. Kumar, S. Devi, **S. K. Pandey**, M. Kumar, "Reconfigurable Optical Add/Drop Multiplexing-Demultiplexing in Arrayed Waveguide Grating with Fold Back Technique", **Optik**, May 2024, **(IF-3.1).**
8. S. Rajput, V. Kaushik, P. Babu, **S. K. Pandey**, and M. Kumar, "All optical modulation in vertically coupled indium tin oxide ring resonator employing epsilon near zero state," Scientific Reports, October 2023, **(IF-3.8).**
9. S. Kumar, R.D. Mishra, A. Kumar, P. Babu, **S. K. Pandey**, and M. Kumar, "Double-Slot Nanophotonic Platform for Optically Accessible Resistive Switching with High Extinction Ratio and High Endurance", **ACS Photonics**, vol 10, no. 11, pp. 4071–4078 October 2023 **(IF-7)**.
10. S. Rajput, V. Kaushik, L. Singh, Sulabh, **S. K. Pandey**, P. Babu, and M. Kumar, "Efficient Optical Modulation in Ring Structure based on Silicon-ITO Heterojunction with Low-voltage and

High Extinction-ratio," **Optics Communication**, May 2023, **(IF-7)**.

11. R. D. Mishra, L. Singh, S. Rajput, V. Kaushik, **S. K. Pandey**, P. Babu, and M. Kumar, "Comb-Like Hybrid Plasmonic Ring Resonator for Large and Voltage Tunable Group Delay", **IEEE Transactions on Nanotechnology**, vol 22 pp. 166-171 March 2023, **(IF-2.4)**.
12. S. Kumar, A. Kumar, P. Babu, R. D. Mishra, **S. K. Pandey**, M. K. Pal, and M. Kumar, "Nanophotonic Ring Resonator based on Slotted Hybrid Plasmonic Waveguide for Biochemical Sensing", **IEEE Sensors Journal**, vol 23 no. 6 pp.5695-5702 January 2023, **(IF-4.3)**.
13. S. Rajput, V. Kaushik, L. Singh, S. Srivastava, **S. K. Pandey**, R.D. Mishra, and M. Kumar, "Efficient Photodetector based on Sub bandgap Transition in Silicon-ITO Distributed-Heterojunctions", Journal of Lightwave Technology, vol 39, no 31, 6886-6892, 2021 **(IF-4.7)**.

B2 in refereed Patents

1. M. Kumar, R.D. Mishra, **S. K. Pandey**, P. Babu, S. Kumar, "Nanophotonic resistive switch with tapered structure and method thereof", Indian Patent, No. 202321045344; published in February 2024.
2. M. Kumar, S. Rajput, V. Kaushik, P. Babu, **S. K. Pandey**, "All optical modulation in engineered indium tin oxide based vertically coupled ring resonator employing epsilon near zero state", Indian patent, No. 202321010734; Published in June 2023.

B3 in refereed conferences

1. V. Kaushik, S. Rajput, P. Babu, **S.K. Pandey**, R. Mishra, H. Ren, S. Maier, V. Sorger, H. Dalir, J. Scheuer, and M.

Kumar, "Electronically Controlled Quantum Confinement for Tunable Plasmonic Metasurfaces (FTu4O.6)", Conference on Laser and Electro-optics (CLEO)-2024-Charlotte, North Carolina, USA, 5-10 May 2024.

2. S. Kumar, A. Kumar, R. D. Mishra, P. Babu, N. Mohanta, **S. K. Pandey** and M. Kumar, "Highly Sensitive Biochemical Sensor Based on Nanophotonic Ring Resonator", Photonics 2023-The International Conference on Fibers and Optical Sensors, IISc Bengaluru, India, 5th to 8th July 2023.

TABLE OF CONTENTS

Error! Bookmark not defined.

LIST OF FIGURES

ACRONYMS

MOS	*Metal Oxide Semiconductor*
MIM	*Metal Insulator Metal*
MIS	*Metal Insulator Semiconductor*
IPE	*Internal Photoemission*
SPP	*Surface Plasmon Polariton*
PIC	*Photonic Integrated Circuit*
SOI	*Silicon on Insulator*
DI	*De-Ionized*
HPW	*Hybrid Plasmonic Waveguide*
NIR	*Near Infra-Red*
I-V	*Current-Voltage*
2DEG	*Two-Dimensional Electron Gas*
GaN	*Gallium Nitride*
AlGaN	*Aluminum Gallium Nitride*
IC	*Integrated Circuit*
CB	*Conduction Bridge*
ER	*Extinction ratio*
UV	*Ultraviolet*
ECM	*Electro-Chemical Metallization*
IL	*Insertion Loss*
OSA	*Optical Spectrum Analyzer*
DUT	*Device Under Test*
QCSE	*Quantum Confined Stark Effect*

eV	*Electron Volt*
CMOS	*Complementary Metal Oxide Semiconductor*
Ag	*Silver*
Au	*Gold*
Cu	*Copper*
ENZ	*Epsilon Near Zero*
FEM	*Finite Element Method*
SEM	*Scanning Electron Microscopy*
SMU	*Source Meter Unit*
Si	*Silicon*
SiO_2	*Silicon Dioxide*
TiO_2	*Titanium Dioxide*
SWG	*Sub-Wavelength Grating*
ITO	*Indium Tin Oxide*
TCO	*Transparent Conducting Oxide*
TE	*Transverse Electric*
TM	*Transverse Magnetic*
UV	*Ultraviolet*
EO	*Electro Optic*
FDE	*Finite Difference Eigenmode (FDE) solver*
FDTD	*Finite Difference Time Domain Solver*

NOMENCLATURE

ε	*Dielectric Constant*
E_a	*Activation Energy*
m_o	*Electron Mass*
λ	*Wavelength*
$h\nu$	*Photon Energy*
Φ_B	*Potential Barrier*
E_{vac}	*Vacuum level Energy*
E_c	*Conduction Band Energy*
E_v	*Valance Band Energy*
E_g	*Energy Band gap*
E_F	*Fermi Level Energy*
n_e	*Electron Density*
K	*Wavenumber*
Q	*Electron Charge*
n	*Refractive Index*
n_{eff}	*Effective Refractive Index*
α	*Attenuation Constant*
β	*Phase Constant*
Λ	*Grating Period*

ABSTRACT

Low Dimensional Photonic Devices Based on Hybrid Materials

by

Suresh Kumar Pandey

Optoelectronic Nanodevice Research Laboratory,
Department of Electrical Engineering,
Indian Institute of Technology Indore

Supervisor: Prof. Mukesh Kumar

Silicon photonics offers a promising platform for creating highly scalable and potentially low-cost on-chip photonic devices. However, due to its poor electro-optic effect, the diffraction limit of silicon waveguides, and weak light-matter interaction, silicon-based tunable absorbers tend to have large device footprints, high power consumption, and low extinction ratios. Consequently, it remains uncertain whether silicon alone can achieve the required performance metrics for tunable absorbers with compact size and extensive tunability. Enhancing silicon photonics with additional materials or identifying a cost-effective active material to combine with silicon is crucial for meeting these performance criteria. Notably, indium tin oxide (ITO) has demonstrated exceptional electro-optic properties for efficient light tuning, while copper (Cu) metal is effective for nanoscale light confinement in plasmonic structures. In this thesis Cu-ITO based tunable plasmonic absorber has been explored to achieve high extinction ratio, low voltage tuning, low power consumption and higher bandwidth devices. This thesis also incorporated optical control power transistor due to various advantages as compared to electrically gate tunable power devices.

An electrically controlled optical absorption is numerically proposed in a plasmonic waveguide on silicon-on-insulator (SOI) consisting of copper-Indium tin oxide (ITO) based subwavelength

grating at 1.55 μm wavelength. The Cu-ITO subwavelength grating in form of a discontinuous Cu layer filled with ITO together with electrically tunable permittivity of ITO provides us with tunable absorption and efficient guidance of plasmonic mode. An n-type ITO is used which exhibits a significant change in the carrier concentration with the applied voltage resulting in a change in optical absorption at a telecom wavelength of 1.55 μm. We numerically observe maximum tuning in absorption at a grating period of 600 nm and a duty cycle of 50%. The proposed device shows a smaller effective mode area of Am= 0.01421 /μm2 and a plasmonic confinement factor of 34.67 %. The device is reported to have an extinction ratio of 10.28 dB for a 100 μm long device at a low voltage of 6V.

An optical controlled AlGaN/GaN semiconductor power transistor with low on-resistance normally-off high electron mobility 2DEG channel is numerically proposed. The device consists of p-GaN region sandwiched between undoped GaN over which n-AlGaN (Al 20 %) is formed. Two-Dimensional Electron Gas (2-DEG) channel is formed at n-AlGaN/GaN heterojunction due to photogenerated electron jumps from valance band to conduction band, when a beam of light having (energy greater than the band gap (3.4 eV) of GaN wavelength 350 nm falls on SiO_2 and TiO_2 Bi-layers antireflecting structure and light penetrates deeper into p-GaN region and generate e-h pairs. Device current can be optically controlled by varying the power intensity of incident beam of light, this device exhibits very low on-resistance which yields very low conduction loss. The switching characteristics of the device are also investigated, and device attain low rise and fall time.

An electrically tunable plasmonic absorber device is experimentally demonstrated at 1550 nm wavelength. The device consists of alternating Cu- ITO grating on the top of a p-type silicon rib waveguide, filled with n-type indium tin oxide (ITO) as a capping layer. The distributed plasmonic mode at the interface of Cu-SiO_2-Si is efficiently coupled with ITO. The electrically tunable permittivity of ITO changes the optical absorption by employing electrically driven carrier depletion and accumulation. We demonstrate large tuning of optical intensity by electrically driven carrier accumulation at ITO interface by applying very low voltage from 0 to -4 V. A 100-μm long device exhibits a high extinction ratio of 22 dB and wide 3 dB bandwidth of 52.2 GHz. Applications for our proposed device include imaging, biosensing, intensity modulators, and other multi-functional nanophotonic devices where change in optical absorption is a key requirement.

In an optical field-enhanced tunable plasmonic absorber integrated on a grating waveguide, utilizing the epsilon-near-zero (ENZ) state of indium tin oxide (ITO). This design enables precise control over light absorption and modulation, resulting in notable performance metrics. The device achieves an extinction ratio of 1.9 dB per micron, indicating its effectiveness in modulating light intensity. It offers a modulation depth of 1.9 dB/μm, ensuring substantial contrast between the on and off states. Furthermore, the device supports a 3 dB bandwidth of 72 GHz, which is suitable for high-speed optical communication applications. The energy required per bit for data transmission is remarkably low, at 56.25 femtojoules per bit, highlighting the device's efficiency in terms of power consumption.

Chapter – 1

Introduction to Integrated Photonics

Integrated photonics is a field that involves the use of photonic circuits to process optical signals on a single chip, like how electronic circuits process electrical signals. This technology leverages the principles of photonics, the science of light, and optics, to achieve various functionalities in a compact and efficient manner. Conventional electronic integrated circuits operate by enabling the flow of electrons through the circuit. Electrons, which are negatively charged subatomic particles, interact with other electrons or particles as they move. These interactions slow down the electrons, thereby limiting the rate of information transfer. Additionally, this process generates heat, leading to energy loss and potential information degradation. To overcome these limitations, photonic integrated circuits, which use photons instead of electrons, are employed [1-2]. Photons move at the speed of light with minimal interference from other photons [3-4]. This greatly improves bandwidth, data transfer rates, and circuit speed, while maintaining low energy loss, thus making photonic integrated circuits (PICs) significantly more efficient.

Integrated photonic technology involves combining multiple photonic functions onto a photonic integrated circuit (PIC) manufactured using wafer-scale integration techniques[5-6]. Figure 1.1 presents the components of photonic integrated circuits (PICs) are interconnected through waveguides that guide and confine light. These chip elements include both passive components (such as couplers, filters, and multiplexers) and active components (such as modulators, switches, amplifiers, and detectors)[7-9]. This integration significantly enhances the performance and reliability of photonic functions while also minimizing size, weight, and power consumption. Integrated photonic technology has a wide range of applications, including telecommunications, data centers, and quantum computing[12].

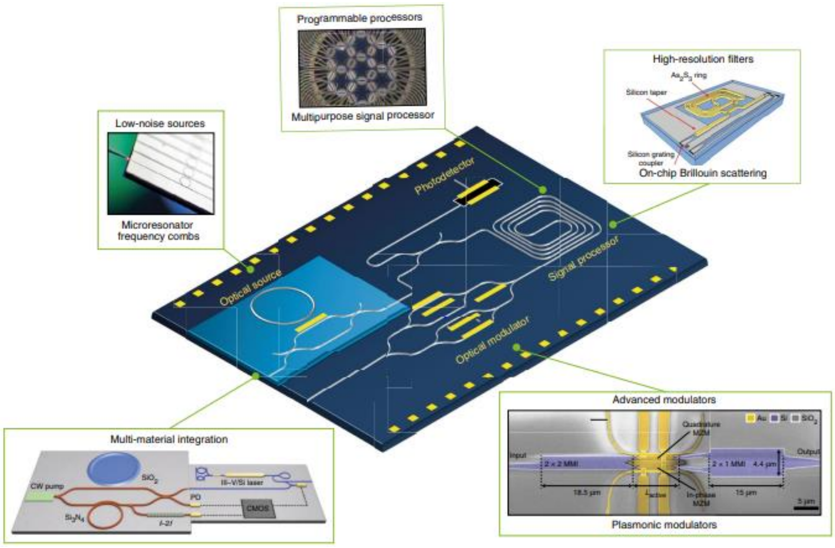

Figure-1.1: Integrated photonic circuit consisting of waveguide, source, modulator, filter, and photodetector [12].

This chapter of the thesis focuses on the role of technological revolution of the next generation silicon photonics. The chapter also highlights the low dimensional photonic devices, hybrid materials significance in integrated phtonics, plasmonic absorbers and applications of plasmonic absorbers.

1.1 Background and Motivation

The global market for silicon photonics was valued at USD 1.29 billion in 2022 and is projected to expand at a compound annual growth rate (CAGR) of 25.8% from 2023 to 2030. Silicon photonics, a rapidly developing technology, is witnessing increasing demand driven by the need for faster data transfer rates and applications requiring high bandwidth [13]. This technology has gained considerable momentum in data centers and telecommunications due to its ability to provide high-speed data transmission, lower power consumption, and seamless integration with existing silicon-based electronic systems. A major benefit of silicon photonics lies in its compatibility with current silicon-based electronic technologies, allowing for the integration of photonic components with electronic circuits on the same silicon chip.

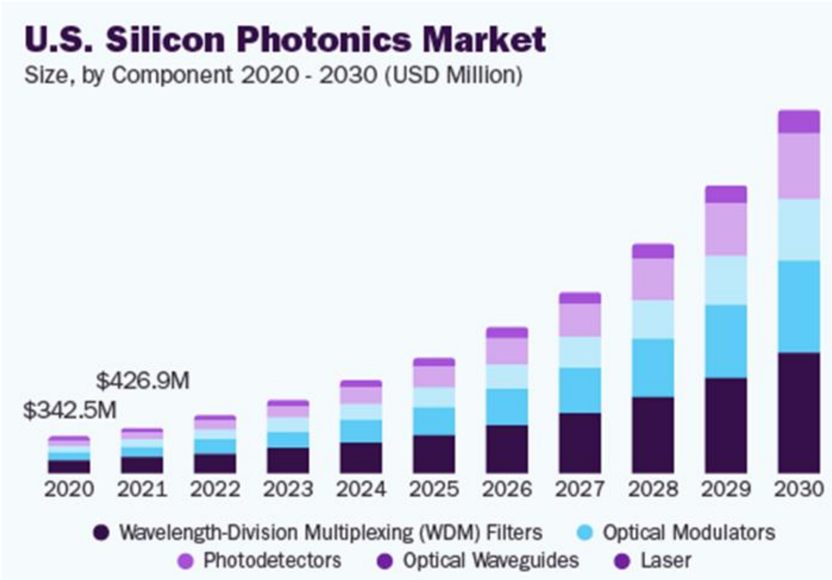

Figure-1.2: Growing market size, by components 2020-2030 (USD Million) of silicon photonics [13].

This compatibility leads to more efficient and cost-effective systems. Significant research and development efforts have been dedicated to enhancing performance, optimizing manufacturing processes, and lowering costs to further advance silicon photonics. Researchers are investigating new materials, fabrication methods, and design approaches to extend the capabilities of this technology.

Low-dimensional photonic devices made from hybrid materials are attracting considerable interest due to their potential to satisfy the increasing market demand for integrated photonics. These devices exploit the unique characteristics of low-dimensional materials, such as improved light-matter interactions and quantum confinement effects, along with the flexibility of hybrid materials, including semiconductors, dielectrics, metals, and organic compounds. This synergy enables the creation of photonic devices with enhanced performance, reduced size, and novel functionalities. As integrated photonics becomes more vital for applications in telecommunications, sensing, and computing, the progress in low-dimensional hybrid material photonics is set to play a key role in meeting these market demands.

1.2 Low Dimensional Photonic Devices

Low-dimensional photonic devices represent a cutting-edge area of research within the broader field of photonics, which deals with the generation, manipulation, and detection of light [14]. These devices utilize materials and structures with reduced dimensions, such as thin films, nanowires, quantum dots, and two-dimensional (2D) materials, to achieve unique optical properties and functionalities that are not possible with bulk materials [15].

1.2.1 Diffraction Limitations:

Diffraction limitation refers to the fundamental limit on the resolution of optical systems due to the wave nature of light. According to the Rayleigh criterion, the minimum resolvable distance d between two points is given by $d = \frac{\lambda}{2\mathrm{NA}}$, where λ is a wavelength of light and NA is the numerical aperture of the system [16]. This limitation constrains the miniaturization and performance of photonic devices, particularly in applications requiring high precision and integration density, such as imaging, sensing, and on-chip data communication [17].

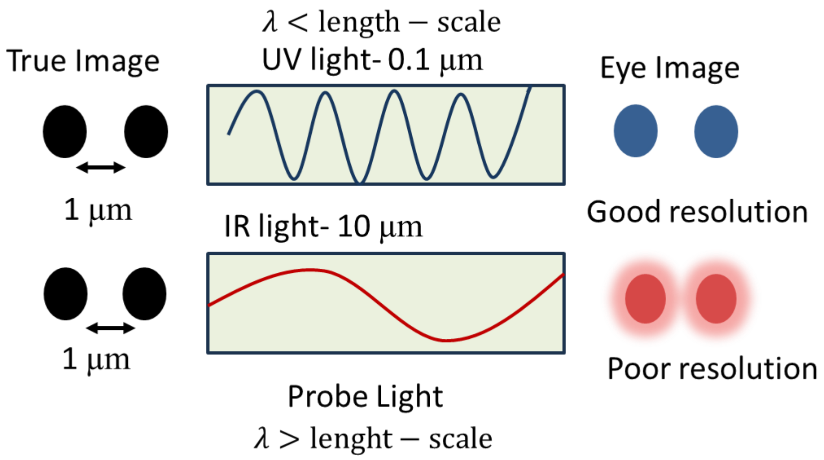

Figure-1.21 Diffraction limitations.

Low-dimensional photonic devices, such as those based on nanophotonic, plasmonic, and metamaterials, offer promising solutions to overcome diffraction limitations [14-15]. These devices exploit the unique properties of materials structured at the nanoscale to manipulate light beyond the diffraction limit. For instance, plasmonic structures utilize surface plasmon resonances to confine light to sub-wavelength dimensions, enabling ultra-compact and highly sensitive sensors. Metamaterials and photonic crystals can engineer the flow of light, achieving super-resolution imaging and efficient light guiding in extremely small volumes. Additionally, two-dimensional materials like graphene and transition metal dichalcogenides exhibit extraordinary optical properties, allowing for the development of highly integrated and tunable photonic devices. Through these advancements, low-dimensional photonic devices pave the way for breakthroughs in various technological fields, pushing the boundaries of optical performance and integration.

1.2.2 Integrated Nanophotonics

Integrated nanophononics is an emerging field that focuses on manipulating and controlling light at the nanoscale, facilitating the integration of photonic components on a single chip. By combining nanotechnology and photonics, this field aims to develop highly compact, efficient, and multifunctional optical devices [18-20].

Essential components of integrated nanophononics include waveguides, resonators, modulators, and detectors, all created using advanced nanofabrication techniques. These components collectively manipulate light in ways unattainable with traditional bulk optics, offering advantages such as reduced size, increased speed, and lower power consumption [21-23].

Integrating these nanophotonic devices onto a single chip is vital for applications in telecommunications, data processing, and sensing. In telecommunications, for instance, integrated nanophotonic devices can significantly enhance data transmission rates and bandwidth while minimizing energy consumption and device footprint. In sensing, nanophotonic sensors provide high sensitivity and specificity due to their enhanced interaction with light.

The use of hybrid materials in integrated nanophononics further boosts device performance. These hybrid materials, which combine properties of various material classes like semiconductors, dielectrics, and metals, enable the creation of devices with tailored optical properties. This flexibility allows for the development of nanophotonic devices with improved efficiency, tunability, and functionality.

As the demand for faster, more efficient, and smaller photonic devices continues to grow, integrated nanophononics is set to play a crucial role in technological advancements [10], driving innovations in fields such as quantum computing, medical diagnostics, and environmental monitoring [24-25].

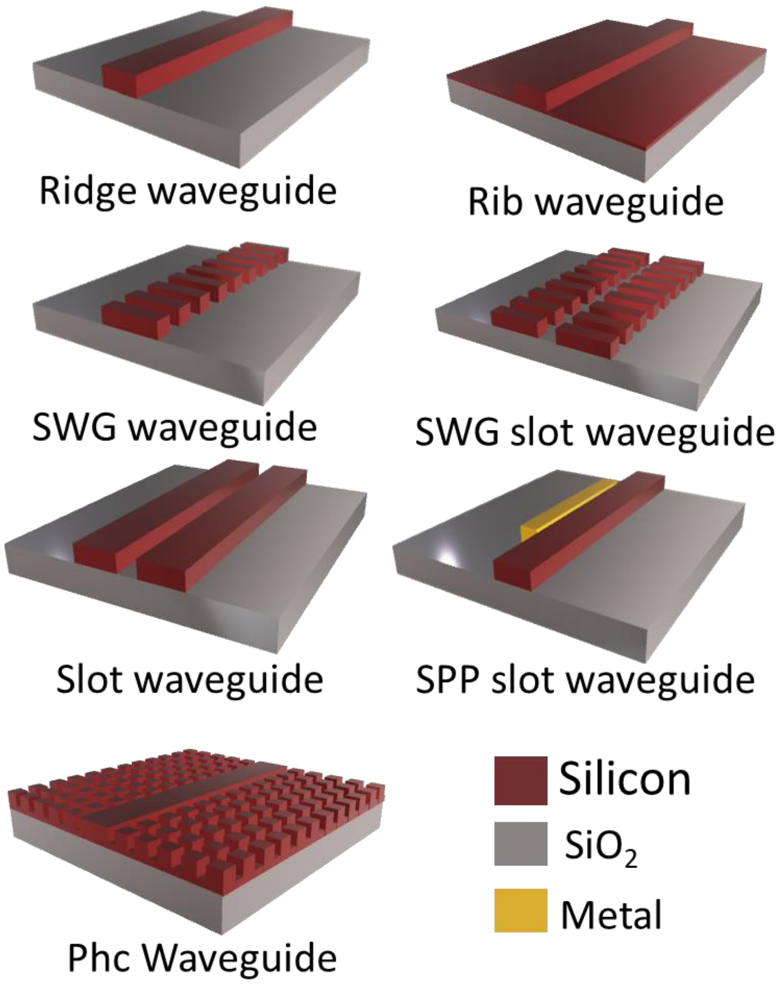

Figure 1.3 Silicon based nanophotonic waveguides find application in optical modulation, detection and sensing.

In today's data-driven world, meeting the requirements of emerging data traffic necessitates devices with high speed and large bandwidth. To achieve this, novel waveguide structures and materials are essential. Traditional waveguides and materials were not compatible with silicon-on-insulator (SOI) technology. However, Almeida et al. in 2004 proposed an SOI-compatible light guidance technique that involves a small gap between two silicon rails, known as a slot waveguide [26], as shown in Figure 1.3. The narrow slot in this configuration has two significant effects. First, the guided light is partially confined within the slot. Second, with the application of a small voltage, an extremely large electric field confinement occurs in the narrow slot. Additionally, this technique is compatible with current silicon technology.

The narrow slot in this configuration has two significant effects. First, the guided light is partially confined within the slot. Second, with the application of a small voltage, an extremely large electric field confinement occurs in the narrow slot. Additionally, this technique is compatible with current silicon technology.

Researchers have found significant benefits in using slot waveguides for optical sensing [27]. These waveguides are particularly effective because they confine over 70% of the guided light near the silicon rails, leading to a much stronger interaction with the analyte than common strip waveguides, which only interact with about 20% of the light. This enhanced light-analyte interaction significantly increases waveguide sensitivity, which has been instrumental in advancing the development of modern integrated optical sensors [28].

Photonic crystals (PhCs)[29-31] are periodic optical structures that can control the flow of light. Multiple reflections from surfaces separated by a distance similar to the wavelength prevent an optical beam from propagating through the crystal. Photonic crystal devices can therefore force light around sharp bands or even trap it entirely. Photonic crystals are advanced optical materials structured with a periodic arrangement of dielectric materials, replacing the role of atoms or molecules in traditional crystals. This periodic structure creates a pattern of varying dielectric constants, forming a periodic dielectric function or index of refraction. When these dielectric materials have significantly different refractive indices and minimal light absorption, they create unique light interactions through multiple refractions and reflections at the interfaces. These interactions mimic the behavior of electrons in atomic crystals, allowing for the manipulation of photons. One of the remarkable features of photonic crystals is their ability to form photonic band gaps, which prevent light from propagating in certain directions and frequencies [32]. This property enables precise control over the flow of light, making photonic crystals invaluable for developing innovative optical devices. Furthermore, photonic crystals can support the propagation of light in novel and advantageous ways, offering new possibilities in fields such as telecommunications, sensing, and quantum computing.

In 1987, Yablonovitch [33] and John proposed the concept of photonic crystals (PhCs). These structures are characterized by periodic variations in the dielectric constant along one, two, or three orthogonal directions as shown in figure 1.3. Depending on these variations, PhCs are classified as one-dimensional (1D), two-dimensional (2D), or three-dimensional (3D). The classification refers to the number of dimensions in which a photonic band gap exists a range of frequencies where light cannot propagate. In 1D PhCs, the dielectric constant varies along one dimension; in 2D PhCs, it varies along two dimensions; and in 3D PhCs, it varies along three dimensions. This modulation of the dielectric constant is on the scale of the wavelength of the light source, which allows PhCs to manipulate light in unique ways. The one-dimensional crystals can be made by depositing an alternate layer of two or more materials. The most widely used fabrication method for 2D photonic crystals is Electron Beam Lithography (EBL) [34]. The fabrication of three-dimensional photonic crystals is complex. Researchers have created 3D crystals using 3D printers, while others have achieved this by stacking multiple layers of 2D photonic crystals. Due to these complexities and the difficulties involved in fabrication, 3D photonic crystals are less popular than other nanophotonic devices. In contrast, one-dimensional (1D) and two-dimensional (2D) nanophotonic crystals are more favored because they are easier to fabricate and provide better control. These photonic structures can confine extremely high-intensity fields within the nanostructured device, making them highly effective for applications in biosensing and optical modulation.

1.2.3 Plasmonics: Light Guidance at Nanoscale

Plasmonics aims to overcome the diffraction limit and achieve subwavelength confinement. One of the initial waveguides that offered strong confinement utilized SOI (Silicon on Insulator) technology [35]. These waveguides can confine light within a small cross-section due to the significant refractive index contrast between the core and the cladding[34-35].

Plasmonics is a specialized area within nanophotonic that examines how electromagnetic fields interact with free electrons in metals. This interaction results in the creation and control of surface plasmon polaritons (SPPs) [11], which are coherent electron oscillations at the boundary between a metal and a dielectric (insulator). Plasmonics merges the concepts of optics and electronics, allowing for the manipulation of light at the nanoscale, beyond the diffraction limit of traditional optics. The Key Concepts in Plasmonics are

Surface Plasmons (SPs): Surface plasmons refer to the collective oscillations of free electrons on the surface of a conductor, usually a metal. These oscillations can be excited by light and travel along the metal-dielectric boundary [166].

Surface Plasmon Polaritons (SPPs): SPPs are the result of surface plasmons coupled with electromagnetic waves. They move along the metal-dielectric interface and can be confined to extremely small dimensions, much smaller than the light's wavelength in free space. SPPs are extremely sensitive to changes in their environment, making them ideal for sensing applications [28].

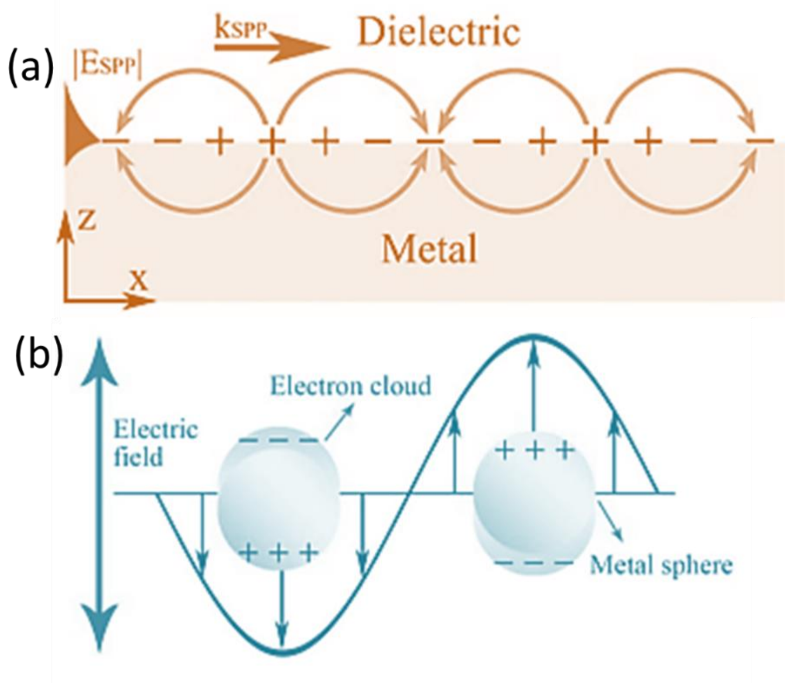

Figure:1.4 Schematic illustration of (a) surface plasmon polaritons (SPPs) and (b) Localized surface plasmon polaritons at the interface between metal nanoparticles and dielectric environment [11].

Localized Surface Plasmons (LSPs): LSPs are non-propagating excitations of conduction electrons in metallic nanoparticles. When light interacts with these nanoparticles, it can induce a collective electron oscillation confined within the nanoparticle. LSPs cause strong light absorption and scattering, leading to effects such as enhanced Raman scattering and local field enhancement [37].

Advantages of Plasmonics

Sub-Wavelength Confinement: Plasmonics enables light to be confined to dimensions significantly smaller than its wavelength, facilitating the creation of extremely compact photonic devices [38].

Enhanced Light-Matter Interaction: The intense confinement of light in plasmonic structures boosts the interaction between light and matter, improving efficiency in applications such as sensing, imaging, and spectroscopy.

High Sensitivity: Plasmonic sensors can detect minute changes in their local environment, making them exceptionally sensitive for use in chemical and biological sensing applications [39].

1.3 Hybrid Materials and their Applications

In recent decades, silicon photonics has gained significant popularity for various applications due to its unique benefits, such as compatibility with CMOS technology and high integration density [40]. High-performance passive silicon photonic devices, which are compact and efficient, have been successfully developed for optical interconnects and sensing applications [41]. Examples include multi-channel optical filters, polarization-handling devices, and multimode photonic devices. However, creating active photonic devices using pure silicon remains challenging because silicon as an active material has a lot of limitations such as weak electro-optic and thermo-optic effects as well as the slow response of plasma dispersion effect. Because of the weak plasma dispersion effect of silicon, there is always a trade-off between the driving voltage and modulation strength [42]. The large driving voltage is considered incompatible with CMOS electronic driving circuits. One of the solutions is to increase the device length, which, however, is not suitable for high-density integration. Moreover, this indicates that travelling electrodes are required which will further increase the device loss and leads to higher power consumption of silicon's inherent material properties, despite considerable efforts in recent years. To address these limitations, silicon-plus photonics has emerged as a promising solution by incorporating additional optoelectronic materials. Various functional materials, including metals, III-V semiconductors, germanium, 2D materials, polymers, magnetic-optical materials, and liquid crystals, have been explored to work alongside silicon. Hybrid materials combine silicon with other materials to overcome these limitations and enhance the performance of low dimensional photonic devices.

1.3.1 Hybrid Materials for Low Dimensional Photonics:

Silicon and III-V Semiconductors: Integrating III-V materials like gallium arsenide or indium phosphide with silicon can lead to improved light emission efficiency and quicker modulation speeds [43].

Silicon and Organic Materials: Organic materials provide better nonlinear optical properties and greater flexibility in adjusting optical features compared to silicon. Therefore, hybrid silicon-organic devices can perform better in specific applications [44].

Silicon and Plasmonic Materials: Merging silicon with plasmonic materials such as gold, copper or silver can boost light-matter interactions, resulting in more effective modulation and absorption at the nanoscale [45].

Silicon and Graphene: Graphene's exceptional electrical and optical properties, when combined with silicon, can enhance device tunability, speed up response times, and reduce losses [46].

Silicon Photonics with Nanophotonic Structures: Adding nanophotonic elements like photonic crystals or metasurfaces to silicon can greatly enhance control over light propagation, allowing for more precise modulation and absorption [47].

In this thesis Indium Tin Oxide (ITO) as active tunable material and copper metal for plasmonic nanoscale light confinement has been explored. Among the various novel plasmonic metals [36-37] like Au, Ag, Al, Cu. Copper found best in class metal due to Plasma frequency fall in NIR wavelength which is operating wavelength of our research.

Table:1 Comparison table of various plasmonic metals [36-37]

Metal Properties	Gold (Au)	Silver (Ag)	Copper (Cu)	Aluminum (Al)
CMOS Compatible	Contaminate	Contaminate	Compatible	-
Damping Coefficient	0.07	0.03	0.07	0.13
Cost	High	High	Low	Low
Low Loss Wavelength	Visible	Visible	NIR	UV
Abundance	Limited	Limited	Abundant	Abundant

Indium Tin Oxide (ITO) for Low Dimensional Devices: Among all these TCOs, indium tin oxide (ITO) is extensively used as an active material for optical modulators. Its popularity stems from its optical transparency and low resistivity, which can be as low as 1.2 x 10^-3 Ω.cm. ITO is utilized in various optoelectronic applications, including displays for mobile devices, laptops, computers, and TVs (i.e., flat displays), as well as in energy conversion devices like photovoltaics and energy-saving window glass [48]. One notable feature of ITO is its ability to exhibit a unity order refractive index change, making it suitable for use as an active material in electro-optic modulators [49]. The optical response of ITO is influenced by free electrons, with their density controlled by adding n-type dopants. The high free carrier concentration in ITO can give it metal-like properties in the near-infrared and mid-infrared ranges, which can be leveraged for subwavelength light manipulation [50]. Unlike the fixed optical properties of noble metals, the permittivity of ITO can be adjusted through doping or the fabrication process [49-51].

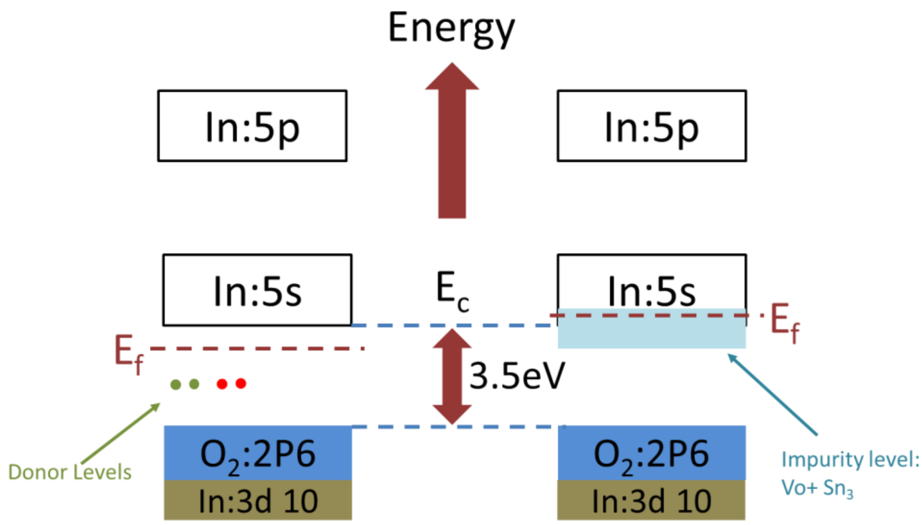

Figure:1.5 Schematic energy-band model for tin doped indium oxide, where Ef, Ey and Ec is the Fermi energy, the violation band energy and the conduction band energy, respectively. Left: low doping level, right: high doping level.

Compared to typical semiconductor materials like silicon and III-V compound semiconductors, ITO exhibits unique optical properties in the telecom wavelength range. Firstly, free carrier concentrations in ITO can reach up to 1×10^{21} cm^{-3} through degenerate doping or gate voltage application. This allows for significant changes in the real part of the refractive index, often exceeding one unit. Secondly, ITO has a much lower high-frequency permittivity compared to Si or III-V semiconductors. With high free carrier concentrations, ITO's real permittivity approaches zero, while its absolute permittivity reaches a minimum due to the small imaginary part. These epsilon-near-zero (ENZ) properties greatly enhance light-matter interactions. When ENZ materials are combined with conventional dielectric or metallic materials, the electric field polarized perpendicular to the interface is strongly confined in the ENZ layer, thanks to the continuity of electric field displacement and ultra-high absorption. Lastly, ITO's electron mobility (50 to 300 $cm^2/V.s$) is much lower than that of single-crystal Si

(~1400 $cm^2/V.s$), resulting in a larger damping factor. As free carriers accumulate, the imaginary part of ITO increases to the same order of magnitude as the real part, leading to an optical absorption 30-140 times greater than that of silicon. Thus, ITO significantly enhances light-matter interactions.

As mentioned earlier, ITO is an excellent representative of TCOs, offering unique advantages such as epsilon-near-zero properties in the near-infrared wavelength and electrically tunable permittivity. The material properties of ITO are highly sensitive to processing conditions. Figure 1.5 shows the schematic band diagram of ITO proposed by Fan in 1977, which qualitatively explains its high optical transparency and high electrical conductivity. In2O3, a component of ITO, has a wide direct bandgap (3.527 eV) that prevents interbond transitions in the visible wavelength range, making it transparent in this range. The Fermi energy Ef is located a few eVs below the conduction band, and its exact level is determined by the n-type doping from tin impurities. The band structure varies with doping density: at low doping density, Ef lies between the donor level and the conduction band minimum; at high doping density, the donor level rises and merges with the conduction band at a critical density n_c. Beyond this critical density, impurities and associated electrons occupy the bottom of the conduction band, forming a degenerate electron gas, which increases ionized impurity scattering and reduces mobility [51].

1.3.2 Semiconductor Heterojunction:

Two different semiconductors, a semiconductor and a metal, or a semiconductor and a carbon-based compound are paired to reduce electron-hole recombination [40]. This combination of materials with different band structures forms a new electronic configuration after hybridization. At the interface of the two semiconductors or components, band bending occurs, creating a potential difference between the two semiconductor regions [41]. This interface generates an electric field within the space charge region, aiding in the spatial separation of photogenerated excitons, a phenomenon known as a 'heterojunction.'

Semiconductor–Semiconductor (S–S) heterojunctions: In general, S–S heterojunction systems can be categorized into two types: p–n semiconductor heterojunctions (Fig.1.6) and non-p–n heterojunction systems. The p–n semiconductor junction is an efficient architecture for effective charge collection and separation. When p- and n-type semiconductors come into contact, they form a p–n junction with a space-charge region at the interfaces due to the diffusion of electrons and holes. This creates a built-in electrical potential that directs electrons and holes to move in opposite directions (Fig. 1.4). When the p–n heterojunction is exposed to photons with energy equal to or greater than the bandgaps of the photocatalysts, the photogenerated electron–hole pairs are quickly separated by the built-in electric field within the space charge region. This electric field drives electrons to the conduction band (CB) of the n-type semiconductors and holes to the valence band (VB) of the p-type semiconductors. This p–n heterostructure offers several advantages: (1) more effective charge separation; (2) rapid charge transfer to the catalyst; (3) longer charge carrier lifetimes; and (4) separation of locally incompatible reduction and oxidation reactions at the nanoscale. These features enhance the photocatalytic performance of p–n heterostructures [42].

Apart from p–n heterostructures, there are other non-p–n heterojunction systems, with the staggered bandgap type being most suitable for photocatalytic applications (Fig. 1.6). In this type, semiconductors A and B with matching band potentials are tightly bonded to **form an efficient** heterostructure. When the CB level of semiconductor B is lower than that of semiconductor A, electrons in the CB of semiconductor A can transfer to that of semiconductor B under visible light irradiation. Similarly, if the VB level of semiconductor B is lower than that of semiconductor A, holes in the VB of semiconductor B can transfer to that of semiconductor A. This internal field promotes the separation and migration of photogenerated carriers, reducing the barrier for electron–hole recombination. Consequently, more electrons on the surface of semiconductor B and holes on the surface of semiconductor A can participate in photo redox reactions, directly or indirectly degrading organic pollutants and greatly enhancing the photocatalytic reaction [41].

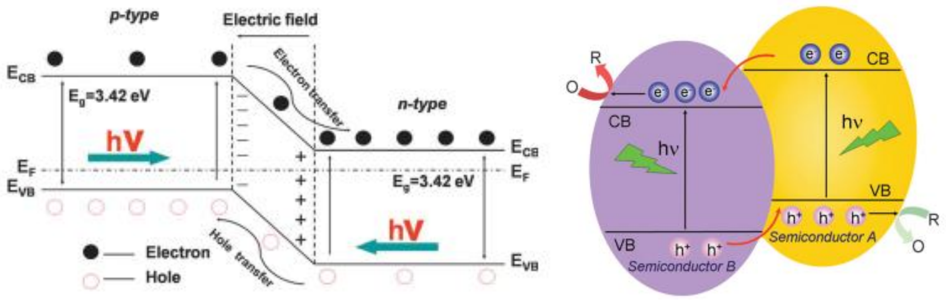

Fig. 1.6 (a) Schematic diagram showing the energy band structure and electron– hole pair separation in the p–n heterojunction. (b)Schematic diagram showing the energy band structure and electron– hole pair separation in the non-p–n heterojunction [41].

Semiconductor–Metal (S–M) heterojunctions: Another effective way to create a space-charge separation region, known as the Schottky barrier, is by forming an S–M junction. At the interface of these two materials, electrons move from one material to the other (from the higher Fermi level to the lower) to align the Fermi energy levels. This commonly occurs in a heterojunction consisting of an n-type semiconductor and a metal. Ideally, the metal's work function is higher than that of the n-type semiconductor (such as TiO2), causing electrons to flow from the semiconductor to the metal to equalize the Fermi energy levels (Fig. 1.7). The Schottky barrier formation results in the metal having excess negative charges and the semiconductor having excess positive charges. Furthermore, the Schottky barrier acts as an efficient electron trap, preventing electron-hole recombination in photocatalysis, often leading to improved photocatalytic performance.

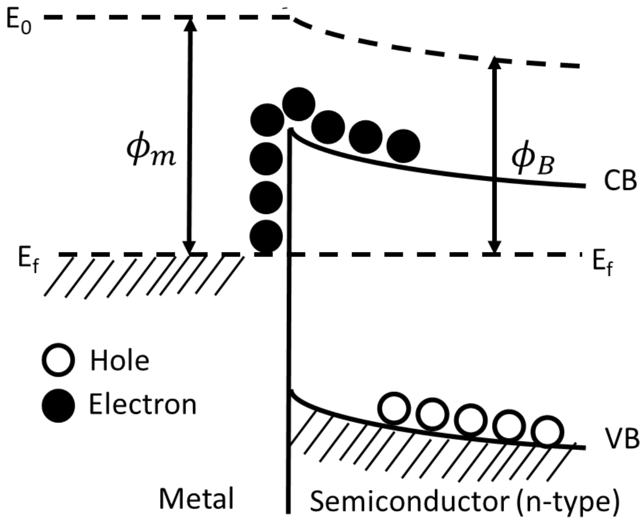

Figure- 1.7 Schematic of the Schottky barrier junction.

1.4 Plasmonic Absorbers and Applications

A plasmonic absorber is a material or structure designed to efficiently absorb electromagnetic radiation, particularly light, through plasmonic effects. These absorbers are made from nanostructured metals like gold, silver or copper, which support surface plasmon resonances. These resonances occur when free electrons in the metal oscillate in response to incident light, resulting in strong absorption at specific wavelengths. The main characteristics of plasmonic absorbers include broadband absorption that can absorb a wide range of wavelengths, making them suitable for applications that require broad spectral coverage.

The resonance effect allows for nearly complete light absorption at designed wavelengths that enhance efficiency. Plasmonic absorbers can achieve high absorption efficiency with very thin layers, often just a few nanometers thick, making them lightweight and flexible. By adjusting the size, shape, and arrangement of the nanostructures, the absorption properties can be finely tuned to specific wavelengths. There are various applications of plasmonic absorber Solar Energy Harvesting, Sensors, Thermal Imaging and Infrared Detection, Stealth Technology.

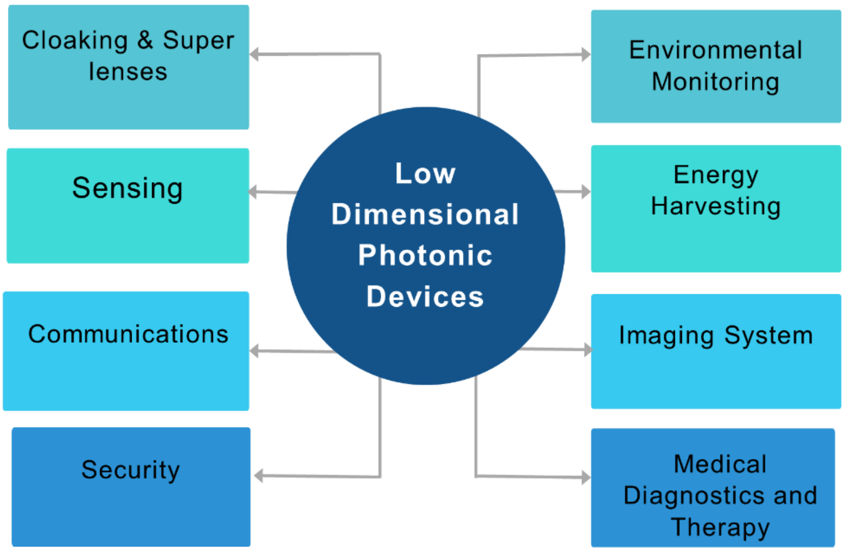

Figure 1.8: Potential applications of Low dimensional photonic devices.

1.4.1 Tunable Absorbers and Tuning Mechanism:

Plasmonic tunable absorbers are sophisticated devices designed to dynamically control the absorption of light at various wavelengths using plasmonic resonances. These devices utilize the unique properties of surface plasmons—coherent oscillations of free electrons at the interface between a metal and a dielectric. The ability to tune the absorption properties makes them valuable for a variety of applications including sensing, imaging, energy harvesting, and photodetection.

Mechanisms of Tunability: Plasmonic tunable absorbers achieve dynamic control over their absorption properties through various external stimuli:

Electrical Tuning: Applying an external voltage can alter the carrier density in materials like graphene or semiconductor layers, shifting the plasmonic resonance and tuning the absorption spectrum. This method provides precise and rapid control over the absorption properties [52].

Thermal Tuning: Changing the temperature can affect the dielectric properties of materials, leading to a shift in plasmonic resonance. Phase-change materials such as vanadium dioxide (VO_2) are commonly used for thermal tuning because they undergo a reversible transition between different phases with distinct optical properties [53].

Mechanical Tuning: Mechanical deformation, such as stretching or compressing the plasmonic nanostructures, can change their geometry and thus alter the resonance conditions. This method allows for reversible and often large tuning ranges [54].

Chemical Tuning: Exposure to different chemical environments can modify the refractive index of the surrounding dielectric or the surface charge density of the plasmonic materials. This approach is useful for applications requiring environmental sensitivity, such as chemical sensing.

In this thesis work our main work is based on electrical tunable device in which we focus more on electrical tuning of the low dimensional photonic devices.

1.4.2 Electro-Optic Effect:

In electro optic effect the optical properties of the light changes with applied electric field. they are further classified as

Pockels and Kerr Effect: On-application of electric-field across any medium, there is a change in the refractive index. When the change is relative to the static electric field, this effect is called Pockels effect and when the change is quadratic at that point it is called Kerr effect or quadratic electro-optic effect. The alteration in the refractive index as a work of the applied static electric field is given by:

$$\Delta n = -r_{33} n_{33} \frac{E_3}{2} \tag{1.1}$$

where n_{33} is the refractive index in the direction of the applied electric field and E_3 is the applied electric field.

The change in the refractive index as a function of the quadratic electric field is given by:

$$\Delta n = s_{33} n_0 \frac{E2}{2} \tag{1.2}$$

where s_{33} is the Kerr coefficient, n_0 is the unperturbed refractive index, and E is the applied electric field. In this case the sign of the refractive index change is not dependent on the direction inside the crystal axis. Pockels effect exists in crystals without inversion symmetry. A few materials that show good Pockels effect are Indium Phosphide, Gallium Arsenide, and Lithium Niobate. The Pockels effect does not exist in Si since it is a centro-symmetric material. Regarding the Kerr effect, it can be measured in Si, but it is a powerless effect [55-57].

Plasma-Dispersion Effect: The change in the charge carrier concentration in a semiconductor alters both the refractive index and the optical losses of the material validating the Kramers-Kronig relations [58]. This is called plasma dispersion effect or free carrier dispersion effect. When the number of charge carriers is increased in a semiconductor like Si, the refractive index decreases while the optical losses of the material are increased. Contrarily, if the charge carriers decrease, we have an opposite effect. The theoretical change in the refractive index and in the optical losses against the concentration of electrons and holes is given by the following Drude-Lorenz equations [57].

$$\Delta n = -\frac{e^2\lambda_0^2}{8\pi^2 C^2 \varepsilon_0 n}\left(\frac{Ne}{m_{Ce}^*} + \frac{Nh}{m_{ch}^*}\right) \tag{1.3}$$

$$\Delta\alpha = \frac{e^3\lambda_0^2}{4\pi^2 c^3 \varepsilon_0 n}\left(\frac{Ne}{-\mu_e (m_{ce}^*)^2} + \frac{Ne}{-\mu_h \left(m_{ch}^*\right)^2}\right) \tag{1.4}$$

where Δn is the change in the refractive index of the medium, Δα is the change in the optical absorption of the medium, e is the electric charge of the electron, λ_0 is the wavelength of the incoming light, c is the velocity of the light in vacuum, ε_0 is the electrical permittivity of vacuum, n is the refractive index of the medium, Ne and Nh are the concentrations of electrons and holes in the medium, μ_e and μ_h are the mobility of electrons and holes and m_{ce} * and m_{ch} * are the reduced effective mass of electrons and holes. Soref and Bennett studied results in the scientific literature to assess the change in the refractive index, Δn, to experimentally create absorption curves for a wide extend of electron and hole densities, over a wide range of wavelengths. They cenetred at 1550 nm, interestingly their comes about were in great assentation with the classical Drude Lorenz model, only for electrons. For holes they noted a $(\Delta N)^{0.8}$ dependence. They produced the following immensely valuable expressions, which are presently utilized all around to assess changes due to injection or depletion of carriers in silicon:

At

λ_0 = 1550 nm:

$$\Delta n = \Delta n_e + \Delta n_h = -[8.8 \times_{10}^{-22} \Delta N_e + 8.5 \times 10^{-18} (\Delta N_h)^{0.8}] \tag{1.5}$$

$$\Delta\alpha = \Delta\alpha_e + \Delta\alpha_h = [8.5 \times_{10}^{-18} \Delta N_e + 6 \times 10^{-18} \Delta N_h] \tag{1.6}$$

where Δn_e = change in refractive index resulting from change in free electron carrier concentration; Δn_h= change in refractive index resulting from change in free hole carrier concentration; $\Delta\alpha_e$=change in absorption resulting from change in free electron carrier concentration; $\Delta\alpha_h$=change in absorption resulting from change in free hole carrier concentrations. From equations 1.5 and 1.6, it has been concluded that holes are more productive than electrons in changing the refractive index of the material. This effect can be accomplished by carrier injection and depletion. Normally this effect is mostly utilized to realize productive phase modulation [46-49].

Franz-Keldysh Effect: The Franz-Keldysh effect leads to the change in the optical absorption of the material for wavelengths near to the direct energy bandgap (e.g., Si and Ge) when an external electric field is applied to the bulk material. Under no applied static electric field into the material, the conduction and valence band are like in Figure 1.9(a). At that point, a photon energy bigger than E_g (energy bandgap of the material) can energize an electron from the valence band to the conduction band. It is represented in Figure 1.9(a). Nevertheless, when an electric field is applied into the material both the valence and the conduction band are tilted as appeared in Figure 1.9(b). In this case the wave-function of the electrons within the valence band can enter the forbidden band by tunnelling. Due to this tunnelling, a photon with less energy than the bandgap of the material E_g can energize an electron from the valence band to the conduction one creating the absorption of light. This increases the optical absorption of the material fair underneath the energy bandgap E_g [58-62].

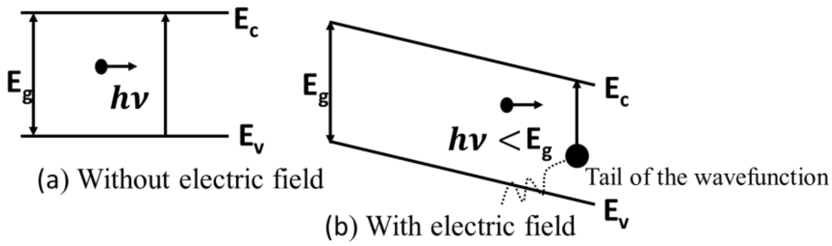

Figure 1.9 Energy diagram of the FKE. In (a) there is not a static electric field while in (b) a static electric field is applied [62].

Quantum-confined Stark Effect: The QCSE is an electro-absorption effect which leads to the changes in the material absorption near the bandgap of the semiconductor upon application of a static electric field. This effect happens in quantum wells. When the quantum well is at equilibrium (in the absence of a static electric field) the wave-function is symmetrical for both electron

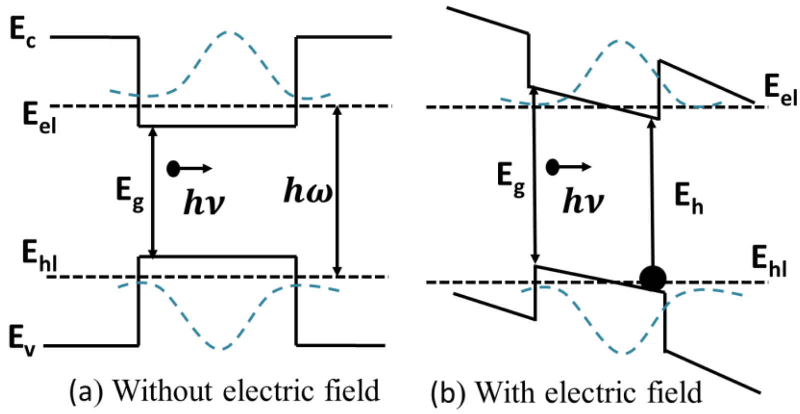

Figure 1.10: Energy diagram of the Quantum confined stark effect. In (a) there is not an electric field while in (b) an electric field is applied [59].

and holes. Furthermore, due to the quantum confinement electrons and hoes are linked by Coulomb forces and form excitons. The absorption of the excitons occurs at photon energy smaller than the bandgap energy of the quantum well material.

This energy is given by

$$h\omega = E_g + E_{el} - E_{hl} - E_{ex}$$

E_g is the energy bandgap of the material, E_{el} and E_{hl} are the electron and holes sub-band energy and E_{ex} is the binding energy of the exciton. When an electric field is applied perpendicular to the quantum well it tilts the energy bands as shown in Figure 1.7(b). Therefore, the energy between E_{el} and E_{hl} is reduced since E_{el} decreases while E_{hl} increases. The binding energy of the excitons E_{ex} is also decreased with an increased static electric field. The electric field pushes the wave functions of the electrons and holes to the sides of the quantum well. This reduces the overlap integral between the wave functions in the valence and conduction band. Thus, the recombination efficiency is also reduced. In this case the energy bandgap is reduced. This increases the absorption of the material in the band-edge of the absorption spectrum [57-58].

1.4.3 Tunable Absorbers:

Tunable absorbers are advanced photonic devices that can dynamically adjust their absorption properties in response to external stimuli, such as voltage, temperature, or light [52-54]. These devices are crucial for a variety of applications, including sensors, modulators, and stealth technology. By incorporating materials with adjustable optical properties, tunable absorbers can selectively control the wavelength and intensity of absorbed light.

Key mechanisms enabling tunability include the use of epsilon-near-zero (ENZ) materials, phase-change materials, and metamaterials. ENZ materials, for instance, can transition between dielectric and metallic states under an applied electric field, resulting in significant changes in absorption characteristics. This tunability allows for precise control over the spectral range and intensity of absorption.

Applications of tunable absorbers span across multiple fields. In telecommunications, they can be used for dynamic filtering and modulation of optical signals. In imaging systems, tunable absorbers enhance contrast and sensitivity. Additionally, they have potential uses in thermal management and energy harvesting by optimizing absorption based on environmental conditions.

The development of tunable absorbers represents a significant advancement in photonic technology, offering flexible, efficient, and responsive solutions for controlling light in innovative ways.

1.5 Thesis Outline

The thesis is organized into seven chapters starting with an introduction to integrated silicon photonics, literature review of past work and problem formulation followed by four major chapters on original research work done and the final chapter on conclusion and the future scope.

Chapter 2. Low dimensional photonic devices based on hybrid materials based on hybrid materials: The second chapter consists of a brief literature review on the significant contributions in tunable absorber specially plasmonic based tunable absorbers and optical switches based on hybrid materials. Followed by this, the chapter highlights the problem formulation.

Chapter 3. This chapter describes the numerical proposal of an electrically controlled optical absorption device in a plasmonic waveguide. the optimization and engineering of Cu-ITO subwavelength waveguide has been done to efficiently guide light at telecom wavelength. The structure features a discontinuous copper layer filled with ITO, whose permittivity can be electrically tuned, allowing for adjustable absorption and efficient plasmonic mode guidance.

Chapter 4. This chapter describes the numerical proposal and analysis of an optically controlled AlGaN/GaN semiconductor power transistor with a low on-resistance, normally-off high electron mobility two-dimensional electron gas (2DEG) channel. The device structure includes a p-GaN region sandwiched between undoped GaN, topped with n-AlGaN. bi-layer antireflecting structure, allowing light to penetrate the p-GaN region and generate electron-hole pairs. The current through the device can be optically controlled by adjusting the power intensity of the incident light beam. The device is resulting in minimal conduction loss. Additionally, the switching characteristics, including low rise and fall times, are examined in this chapter.

Chapter 5. This chapter describes the experimental demonstration of an electrically tunable plasmonic absorber device operating at a wavelength of 1550 nm. The device is composed of a copper (Cu) and indium tin oxide (ITO) grating on top of a p-type silicon rib waveguide, with n-type ITO serving as a capping layer. ITO layer allows for efficient control of optical absorption through electrically driven carrier depletion and accumulation. By applying a low voltage significant tuning of optical intensity is achieved via carrier accumulation at the ITO interface.

Chapter 6. An optical field enhanced tunable plasmonic absorber on a subwavelength silicon (Si) waveguide employing the epsilon-near-zero (ENZ) state of indium tin oxide (ITO) represents a cutting-edge development in nanophononics. This device leverages the unique optical properties of ITO in its ENZ state to achieve significant tunability and absorption enhancements. The core structure of the device consists of a subwavelength Si waveguide integrated with a thin layer of ITO. When ITO is in its ENZ state, it exhibits near-zero permittivity, enabling strong confinement and manipulation of optical fields at the nanoscale. This property is particularly advantageous for creating plasmonic absorbers, as it allows for efficient coupling of light into the ITO layer, leading to enhanced absorption.

Chapter 7. Conclusion and Future Scope: In this chapter, all the contributions are summarized, and the relevant future scope of the work is briefly discussed.

Chapter – 2

2.1 Hybrid Material Photonics: State-of-the-Art

Recent advancements in hybrid material photonics have led to significant improvements. For instance, hybrid photonic devices can achieve high sensitivity and selectivity in sensors, increased bandwidth and speed in communication systems, and superior resolution and efficiency in imaging applications.

One of the key developments is the use of epsilon-near-zero (ENZ) materials, which exhibit unique optical characteristics near zero permittivity, enabling unprecedented control over light-matter interactions. Integrating ENZ materials with traditional photonic structures has resulted in tunable perfect light absorbers and modulators with enhanced performance [63]. The state-of-the-art in hybrid material photonics showcases a promising future where the convergence of different material properties will continue to drive innovations, paving the way for the next generation of photonic technologies that meet the increasing demands of various high-tech industries [64-68].

The primary motivation behind this dissertation is to break the size and speed limits of Si-based tunable absorbers, as compact devices permit higher packaging density, which is essential on chip devices. applications of high-speed optical communications. Silicon plus photonics, i.e., combining Si with other optoelectronic materials and implementing device engineering based on the slow light effect, is an appealing and promising solution to meet the above-mentioned challenges. Many research groups have reported electro-optic tunable absorber devices. In this chapter, the novel waveguiding structures used to incorporate slow light effect along with some of these state-of-art electro-optic tunable devices on hybrid materials are reviewed.

2.2 Tunable Plasmonic Devices

As discussed earlier, in pure silicon linear electrooptic effect does not exist as well as the quadratic electro-optic effect is weak at the telecommunication wavelength, henceforth the silicon-based tunable absorbers have large device footprint or in other words low absorption tuning. Plasma dispersion effect is the most common mechanism employed in pure-Si; however, the speed of these devices is limited because of the slow carrier diffusion time of sub nanoseconds and carrier lifetime of several hundred picoseconds. This raised the necessity for investigating other novel alternative active materials. In this section, some of these state-of-the-art electro-optic devices will be reviewed. The modulators reviewed are based on different structures and several active materials.

Tunable absorbers based on Transparent Conducting Oxide:

Junghyun Park et al. [64] in their work “Electrically Tunable Epsilon Near Zero (ENZ) Metafilm Absorbers” fabricated devices with metal gratings of varying widths and analyzed their reflectance spectra under different states of depletion and accumulation. The ITO layer exhibited an ENZ wavelength of 4.3 μm, influencing the plasmonic cavity resonances at shorter, similar, and longer wavelengths. The experiments demonstrated that applying a positive or negative bias resulted in redshift or blueshift of the reflectance dips, correlating with changes in the mode index. Notably, a significant modulation efficiency of up to 15% was achieved by aligning the optical material resonance with the geometric cavity resonance, despite the limitation of the gate oxide's breakdown field. Furthermore, dynamic control of metafilm absorption was demonstrated with a 3 dB cut-off frequency around 125 kHz, suggesting potential improvements in modulation speed through optimized device geometry. These findings highlight the importance of material and geometric resonance alignment in enhancing modulation efficiency and pave the way for further advancements in photonic device performance.

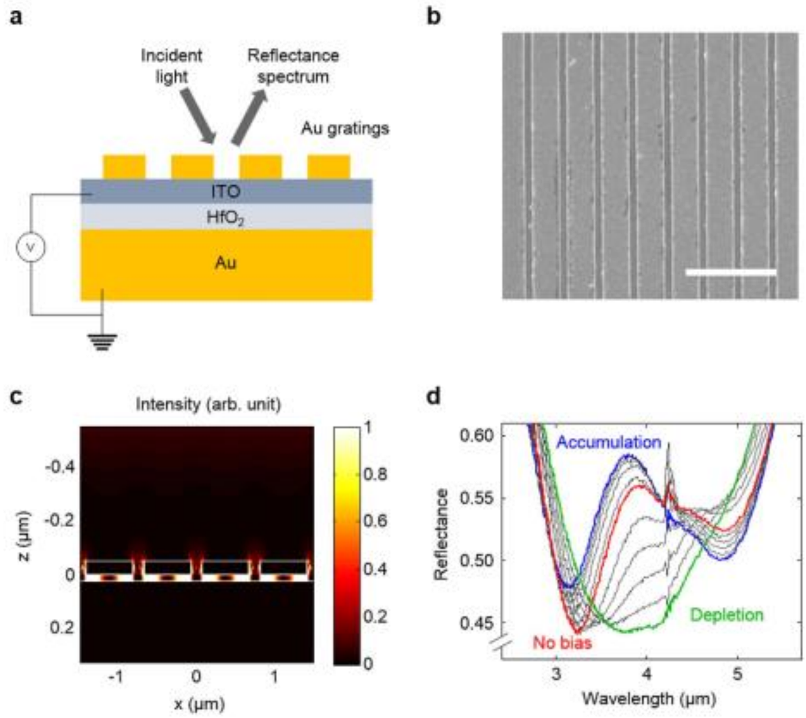

Figure:2.1 Design and performance of an electrically tunable metafilm absorber. (a) Device schematic showing an electrically tunable ITO film clamped between a HfO2-coated Au substrate and an array of Au strips. (b) Scanning electron microscopy (SEM) of the Au strip-array featuring strip widths of 600 nm and periods of 750 nm. Scale bar: 2μm. (c) Intensity distribution in the device driven at a wavelength of 3.8μm, which corresponds to the first-order resonance of the plasmonic cavity formed by the Au strips and the underlying substrate. (d) Reflectance spectra taken from the device

Seyed Sadreddin Mirshafieyan at el. [65] “Electrically tunable perfect light absorbers as color filters and modulators” demonstrates the feasibility of electro-optically tunable perfect light absorbers utilizing epsilon-near-zero (ENZ) materials. The investigated absorber, composed of unpatterned thin-film metal and semiconductor materials, functions as a wavelength-selective light absorber within a Fabry-Perot cavity. By carefully selecting the cavity thickness, the absorption

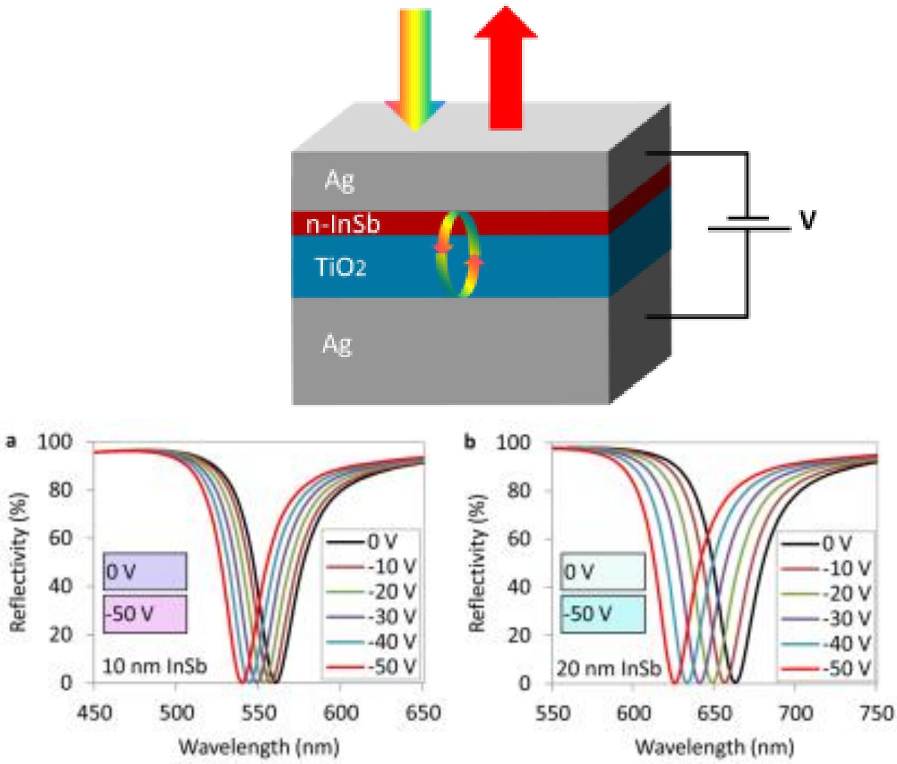

*Figure:2.2 Schematic structure of an electrically tunable perfect light absorber and Calculated reflectance of two tunable perfect light absorbers with n-InSb thicknesses of (**a**) 10 nm, and (**b**) 20 nm. The thicknesses of top Ag, TiO_2, and bottom Ag are 35 nm, 40 nm, and 100 nm, respectively. The reflectivity is calculated at a normal incident angle. The subfigures illustrate the predicted colors of the devices under 0 V and −50 V.*

wavelength can be tuned to fall within the visible range, allowing the reflected color to be modulated with applied voltage. n-InSb was selected as the ENZ material due to its favorable electro-optic properties. Applying a negative voltage increases the carrier density in n-InSb, creating an accumulation region that shifts the material's optical properties from semiconductor-like to metal-like. A spectral shift of 40 nm in the visible range was achieved with a −50 V application, leading to significant color change in the device's reflection. Additionally, the absorption wavelength can be tailored to the 1550 nm telecommunication range, where a high modulation ratio, evidenced by a 95.3% reflectance change with −50 V, is predicted.

Q. Gao et.al-2018 [66] proposed an ultra-compact, broadband gold plasmonic slot waveguide based electro-absorption modulator made up of electrically driven ITO that can achieve epsilon-near-zero state with a modest gate voltage. By coupling two regular silicon waveguides with a 3 μm long, 300 nm wide gold slot waveguide. The active electro-optic modulation area is made up of a metal-hafnium oxide-ITO capacitor that can electrically transform the ITO into ENZ with ultra-high modulation strengths of 1.5 dB/μm. The electro-absorption modulator exhibited uniform electro-optic modulation with a 70 nm optical bandwidth from 1530 to 1600 nm wavelength.

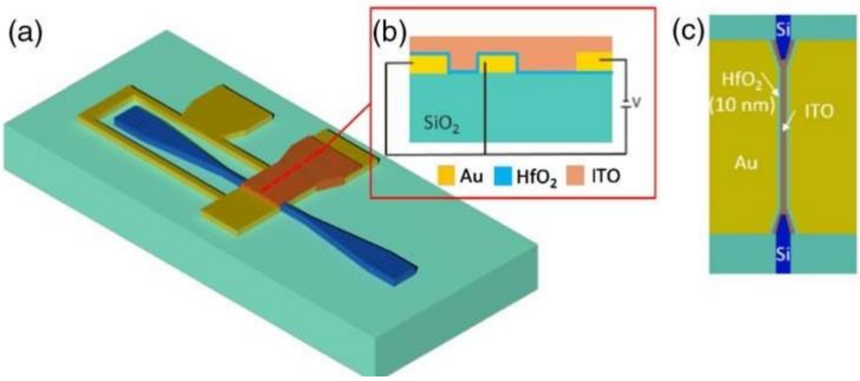

Figure 2.3: (a) 3D Schematic of the plasmonic EA modulator. (b) Enlarged view of the cross-sectional area of the active E-O modulation region and (c) Enlarged view of the Au slot waveguidewith tapers to silicon waveguides [52].

X. Liu et.al-2018 [67] reported a broadband electro-absorption modulator using ITO as the active switching material. To make metal-oxide- semiconductor capacitor-based modulators, silicon strip waveguides are fabricated and covered with 8 nm of Hafnium Oxide and 15 nm of ITO. Figure 2.4 exhibits the design of an ITO based ENZ modulator. The mobile carrier density in the ITO film is controlled by incorporating a post anneal treatment to regulate its permittivity ε to a near-zero value at the working wavelength of 1550 nm. They have shown that achieving an epsilon-near-zero will improve modulation efficiency by increasing the overlap of the directed mode with the active ITO layer using simulations and experiments. The advantages of the optimization of ENZ condition are then demonstrated using silicon waveguides with a central slot filled with ITO. The have obtained a notable 3 dB modulation depth of optical beam in a non-resonant waveguide with a length of 20 μm by using the ENZ effect.

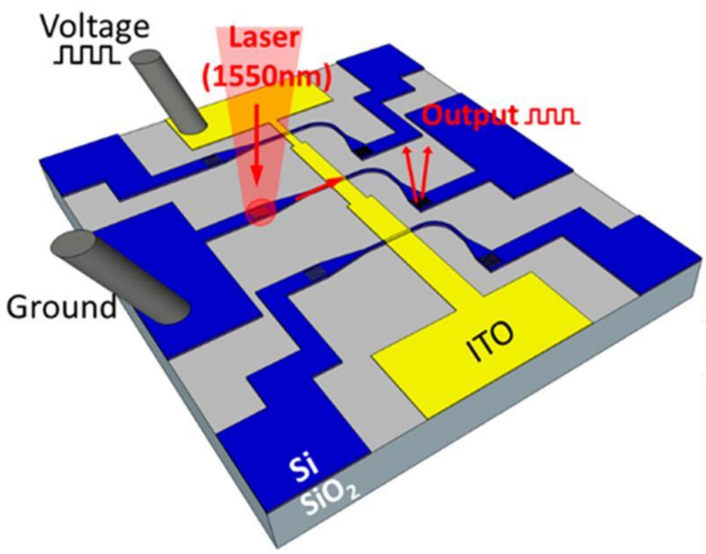

Figure 2.4: Schematic of the ITO based ENZ modulator.[53]

A.P. Vasudev et.al-2013 [68] implemented a concept for a silicon waveguide modulator in which the transmission of a waveguide mode is controlled by electrically inducing an epsilon-near-zero in an adjoining ITO film. This is achieved by inducing loss due to free carrier absorption in the ITO while simultaneously increasing mode overlap with the lossy area where the free carrier absorption occurs. Figure 2.5 demonstrates highly effective electro-absorptive modulation in a silicon waveguide overcoated with ITO. As ITO is brought into an ENZ state locally through electrical gating, this modulator takes advantage of the combination of a local electric field enhancement and improved absorption in the ITO. When gating, this results in significant changes in modal absorption. They discovered that for the fundamental waveguide modes of either linear polarization, a 3 dB modulation depth can be achieved in a non-resonant structure with a length under 30 mm and absorption contrast values as high as 37. They have also shown that 100fJ/bit modulation is possible with an output penalty.

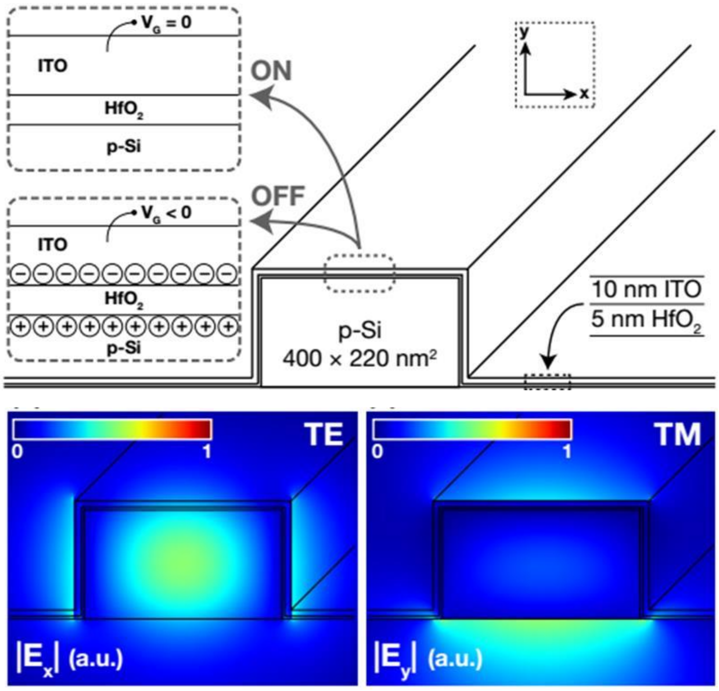

Figure 2.5: Schematic of an electro-absorptive modulator based on silicon waveguide overcoated with ITO. [54]

2.3 Optically Controlled Power Switches:

An optical control power switch is a highly advanced device that uses light to control the flow of electrical power, offering significant advantages over traditional electrically controlled switches. These switches enable jitter-free operation, ensuring precise and stable control with minimal timing variations. They provide complete electrical isolation between the low voltage control circuitry and the high voltage power stage, enhancing safety and protecting sensitive components from electrical surges. Additionally, optical control power switches are immune to electromagnetic interference (EMI), which is crucial for maintaining reliable operation in environments with high levels of electronic noise. With their ability to achieve higher switching speeds and operate at much higher frequencies, optical control power switches are ideal for applications requiring rapid and efficient power modulation, such as in high-speed data communication and advanced power management systems.

Sudip K Mazumdar et al. [69] "Optically Activated Gate Control for Power Electronics". presents and demonstrates a novel optically activated gate control (OAGC) mechanism that dynamically influences power-converter switching loss, dv/dt and di/dt stresses, and electromagnetic emission at the device level. This is achieved by controlling the switching dynamics of the power semiconductor device (PSD) through modulation of its excitation current using a GaAs-based optically triggered power transistor (OTPT). Additionally, the switching initiation delay with the OTPT-based OAGC approach is almost negligible compared to existing fiber-optics-based techniques in power electronics. The key parameter linking the OTPT control to the performance parameters of the power converter is identified and experimentally demonstrated. The work addresses the conflicting dependence of switching loss, and dv/dt and di/dt stresses on the optical intensity of the OTPT, proposing a joint optimization mechanism and demonstrating its effectiveness experimentally

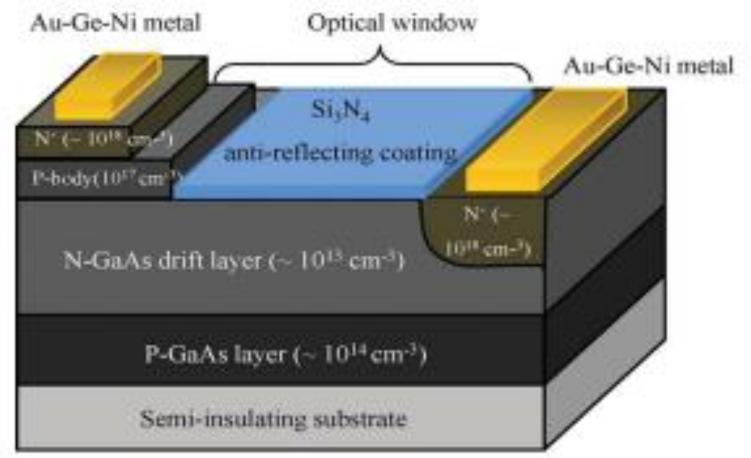

Figure:2.6 Schematic diagram of Optically Activated Gate Control for Power Electronics

Alireza Mojab et al. [70]in their work "Low ON-State Voltage Optically Triggered Power Transistor for SiC Emitter Turn-OFF Thyristor"A new optically triggered power transistor (OTPT) designed for a 100-A load current is introduced. Modifications to the base epitaxial layer have been made to reduce both the ON-state voltage drop and the required optical power for the driving laser. This new structure takes advantage of the fact that an increase in leakage current results in a lower ON-state voltage in power semiconductor devices (PSDs). Despite the proposed structure having a higher leakage current during the OFF-state, this is mitigated by a high-power, low-leakage SiC thyristor connected in series with the OTPT. This configuration allows the use of a leakier OTPT to further reduce the ON-state voltage. The proposed OTPT achieves an ON-state voltage drop of 0.8 V under operating conditions of 100 A and 100 °C with an optical power of 5 W. Compared to conventional low-leakage OTPTs, the proposed design shows a 22% and 92% improvement in the ON-state voltage drop at optical powers of 5 W and 2 W, respectively.

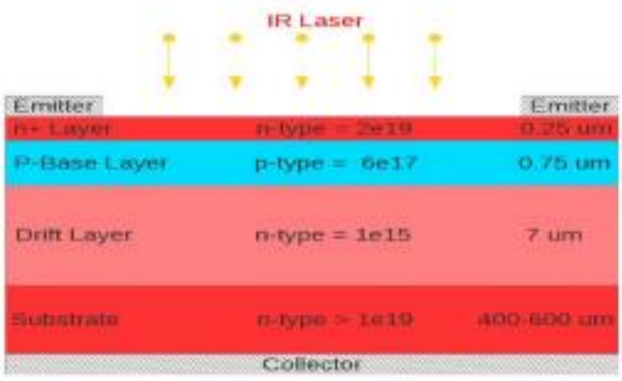

Figure: 2.7 schematic of Low ON-State Voltage Optically Triggered Power Transistor for SiC Emitter Turn-OFF Thyristor [56].

Hossein Riazmontazer et al. [71] "Optically Switched-Drive-Based Unified Independent dv/dt and di/dt Control for Turn-Off Transition of Power MOSFETs" demonstrated to manage the switching dynamics of an optically triggered hybrid device, a photonic-control mechanism. This hybrid device includes a power MOSFET as the primary power semiconductor device (PSD) and a pair of GaAs-based optically triggered power transistors (OTPTs) acting as the drivers for the MOSFET. The switching-transition controller adjusts the turn-off transition of the MOSFET by modulating the optical intensity of the OTPTs. This allows for independent and unified dv/dt and di/dt control of the PSD using a single control circuit, which also anticipates the transition onset between the di/dt and dv/dt control regions. Experimental results demonstrate the effectiveness of the OTPT-based dynamic modulation of the MOSFET's turn-off characteristics. While a SiC MOSFET is used in this study, the proposed photonic-control mechanism can also be applied to Si power MOSFETs.

2.4 Thesis Objectives and Contributions

In the first chapter we have discussed the limitation of pure Si to be used as an active material for Tunable absorbers. We have also discussed the ways which can be implemented to enhance the performance of silicon based low dimensions plasmonic devices by incorporating hybrid material especially high tunable material like Indium Tin Oxide (ITO). Henceforth, after doing the deep literature survey on the past works related to novel waveguiding schemes, state-of-the-art plasmonic tunable absorbers, and optical control power switches, we got motivated and found the following area of improvement and worked through that. Firstly, breaking the size and speed limit of pure Si-based absorbers by material and device engineering. Secondly, to achieve a breakthrough in the wide bandgap semiconductor power switches performance.

Based on the above discussions, following are the objectives of the research work carried out for this thesis:

To achieve these overarching goals, the following specific objectives have been pursued in this thesis work:

- To design an electrically tunable plasmonic absorber using Cu-ITO subwavelength grating on a silicon-on-insulator (SOI) platform, optimized for operation at telecom wavelengths.
- To create an optically triggered AlGaN/GaN semiconductor power transistor incorporating a bi-layer anti-reflecting structure to improve optical triggering efficiency and device performance.
- To develop a plasmonic absorber using a Cu-ITO structure on silicon that achieves low voltage tuning and high extinction ratio for enhanced optical performance.
- To develop an Optical field enhanced tunable plasmonic absorber on subwavelength grating waveguide employing ENZ state of ITO.

Chapter – 3

Numerical Analysis of Cu-ITO based Plasmonic Absorber

3.1 Introduction

The absorption of light energy is a important property of light in which the energy of an electromagnetic wave striking on an object is transferred to several usable types of energies, for example thermal, electrical, chemical, and mechanical. These kinds of devices can be used in a variety of ways like photodetection [72], local heating [73], bio-sensing [74-75], imaging [76], and energy harvesting [77-78]. Noble metals such as copper, gold, and silver are excellent plasmonic materials in the infrared regime (IR). By pattering such types of metals at the nanoscale level, strong absorption can be produced due to the excitation of Surface plasmons polaritons (SPPs) [79-87]. For the integration of nanoscale devices on a single chip, the control and confinement of the light beyond the diffraction limit are major challenges that can be overcome by plasmonic [88-91]. Surface plasmon (SP) excitations in metals allow light to be trapped in the deep-subwavelength zone, which can improve strong light-matter interactions, plasmonic has allowed us to miniaturization of components at a nanoscale level so we can integrate many optical and electronic components on a single chip [92-93]. Controlling and guiding light in on-chip devices via electrical means is a key technology for high-speed computing and embedding data on an optical carrier for efficient data transmission. In that situation, the electrical tuning of a waveguide remains an important function for a variety of devices that can be generated by electrically tuning the charge carrier density of the material to change the optical parameter of the guided wave [94-97]. The carrier concentration of Transparent

Conducting Oxides (TCOs) can be changed to tune the optical properties of light. Among the number of TCOs, Indium Tin Oxide (ITO) is the preferred candidate to tune optical properties. It has received interest as an active electro-optical material because of the significant refractive index change owing to permittivity changes at NIR wavelengths, including the 1.55 µm telecommunication wavelength [98-99]. An integrated platform based on Surface Plasmon Polariton (SPPs) waveguide can be promising for making photonic devices at the nanoscale. Plasmonic waveguide structures offer confinement of optical energy by coupling electromagnetic waves to the oscillation of free charge carriers present at metal-dielectric interface called surface plasmon polariton (SPPs). The oscillation wavelength of resulting plasmon polaritons are considerably smaller as compared to the wavelength of light energy in the vacuum [100].

In this work, an electrically tunable plasmonic absorber on a silicon-on-insulator (SOI) is proposed. The device consists of Copper-Indium Tin Oxide (ITO) based subwavelength grating at 1.55 µm wavelength. The slow light propagates in the device arising from light confinement in the small mode area. The effective mode area of A_m = 0.01421 /µm^2 and plasmonic confinement factor of 34.67% is observed, resulting in enhanced light-matter interaction and significant change in the imaginary part of effective refractive index which shows the absorption of light. The Cu-ITO subwavelength grating in form of a discontinuous Cu layer filled with ITO together with electrically tunable permittivity of ITO provides us with tunable absorption and efficient guidance of plasmonic mode. An n-type ITO is used which exhibits a significant change in carrier concentration with the applied voltage of 4V, resulting in a change in optical absorption at telecom wavelength. In this work the significant change of the imaginary part of the effective refractive index with varying the duty cycle at the grating period of 600nm and we observe maximum tuning in absorption at a grating period of 600 nm and a duty cycle of 50%. The propagation length of the device with varying the duty cycle and with increasing the duty cycle the propagation length decreases. The device has an extinction ratio of 10.28 dB for a 100 µm long device at a very low voltage of 6 V.

3.2 Device Structure and Working Principle

In the proposed device Indium Tin Oxide (ITO) is used as an active absorber material, light absorption can be controlled electrically, the ITO has established itself as one of the highly electrically controllable material and the optical characteristics of the material can be varied significantly by electrical tuning of free charge carrier [91]. ITO exhibits unity order change of effective refractive index due to change in permittivity of the material which can be used for tunable absorber device [106]. Fig.3.1 shows the 3-D geometry of proposed of the electrically tunable plasmonic absorber device. Here x-axis depicts the device's width, the y-axis denotes the device's thickness, and the z-axis represents the propagation direction of the electromagnetic wave. The silicon rib waveguide's thickness(t) and width(w) are 200 nm and 300 nm, respectively, and the device has a buried oxide layer for isolation from the silicon substrate for better confinement of light.

The device consists of a 10 nm thick silicon dioxide layer over which an alternating Cu and ITO grating is formed. Distributed Cu layer is used to reduce metal absorption and to enhance propagation length. ITO material filled between two Cu strips interacts more with SPPs which enhances tuning of carrier concentration ITO layer. The refractive index of Cu and ITO at telecom wavelength (1550 nm) makes a good contrast for the slow light effect which can enhance the light-matter interaction of the device. The grating period of the device is 600nm and the duty cycle is 50%. The optimized thickness of both Cu and ITO grating is 40 nm each over which a 40 nm thick capping layer of ITO is used for better electrical tuning of the device. A 10 nm layer of silicon dioxide dielectric material is used to excite the SPPs at the metal-dielectric interface and to enhance the plasmonic mode. For the simulation of the device Lumerical Eigen Mode, Finite Difference solver is used to study the field confinement of the plasmonic mode and observed that the device supports Transverse Magnetic ™ polarized wave propagation and mode confined at the interface of dielectric and Cu-ITO grating. The working principle of the device is when we shine the light having the wavelength of 1550 nm, The TM polarized plasmonic mode propagates with a high confinement factor and tiny mode area at the Cu-ITO grating and dielectric interface, the inset shows the mode confinement of the device.

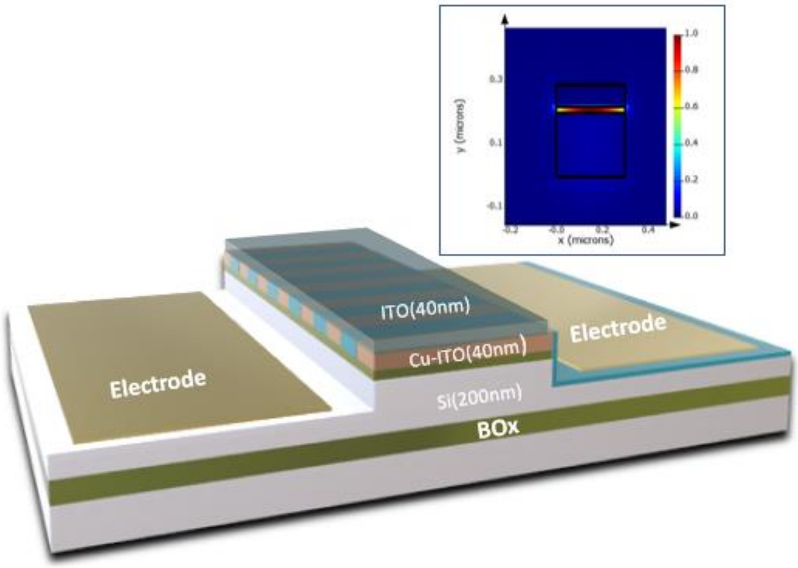

Fig.3.1 3-D diagram of proposed Cu-ITO subwavelength grating assisted electrically tunable plasmonic absorber at 1550 nm wavelength on p-type SOI wafer. Cu-ITO subwavelength grating is utilized to change the imaginary part of the effective refractive index (κ) of the propagating plasmonic mode of the device. Si rib waveguide width is 300 nm, Si thickness is 200 nm, Cu-ITO grating thickness is 40nm, Cu-ITO grating period is 600nm, the Duty cycle is 50% and ITO capping

layer is 40 nm and Plasmonic mode (TM mode) confinement at dielectric and Cu-ITO grating interface of the device. Inset shows confinement of the guided plasmonic TM mode.

The charge carrier accumulates at Cu-ITO grating and dielectric interface, and the accumulated carriers efficiently coupled by propagating electromagnetic waves and form Surface Plasmon Polariton (SPPs) which changes the permittivity of ITO material. The imaginary component of the effective refractive index of the waveguide changes when the permittivity of the ITO changes, indicating a change in light.

3.3 Analysis of Effect of ITO and Propagation Characteristics

The device's optical properties can be electrically modified by varying the carrier (electron) concentration in the ITO layer. It's a good material for tuning intensity at telecom wavelengths with high modulation efficiency because of the substantial fluctuation in carrier concentration caused by the applied voltage. The mobile electron concentration density of the ITO, which acts as a free electron Drude material, is used to monitor its optical characteristics [101].

The optical permittivity of the ITO is denoted by

$$\boldsymbol{\varepsilon_{ITO}} = \boldsymbol{\varepsilon_{\infty}} - \frac{\omega_p^2}{\omega^2 + i\omega\Gamma} \tag{3.1}$$

$$\omega_p^2 = \frac{N_e^2}{\varepsilon_0 m_{ce}^*} \tag{3.2}$$

Here ε_∞ represents dielectric constant of the material, ω depicts the angular frequency of propagating electromagnetic wave and the carrier collision frequency in the ITO layer of the device is denoted by Γ , ω_p is the plasma frequency of the ITO layer, N_e is electron charge magnitude and m_{ce}^* is the effective mass of the electron. The permittivity of the ITO layer can be changed by applying the electrical bias due to the variation of charge carrier density of the ITO layer.

Lumerical charge solver is used to analyze the variation of charge carrier density with applied bias.

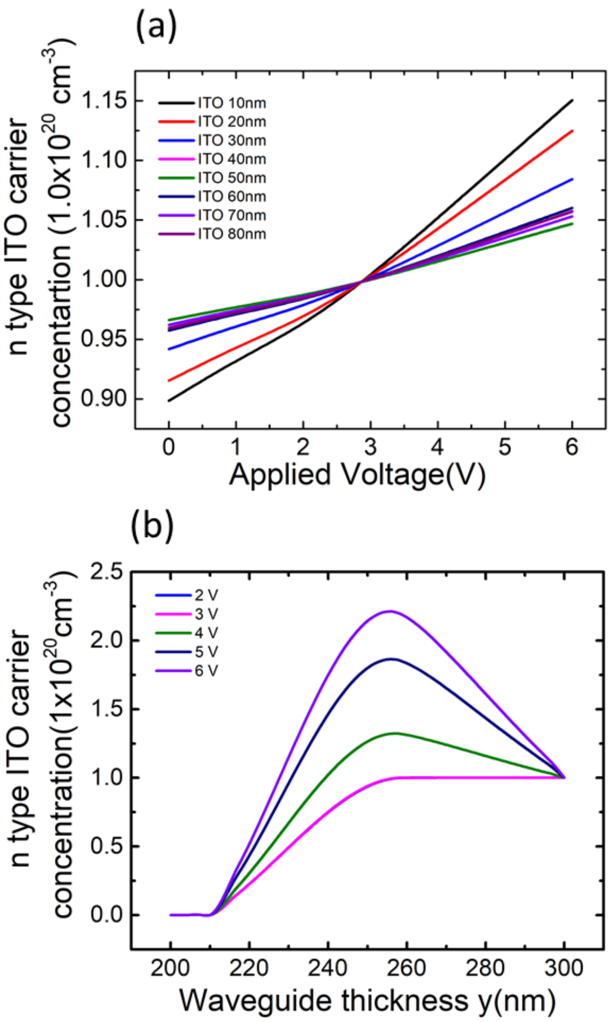

Fig.3.2(a) change of carrier concentration with varying the thickness of ITO layer at different bias voltage, the horizontal axis shows the thickness of waveguide in nm. (b) change of carrier concentration with applied voltage at ITO ($1x10^{20}$ cm^{-3}) thickness of 40 nm. The device exhibits an abrupt change of carrier concentration at 4V.

Fig.3.2(a) shows the change of carrier with applied voltage at different ITO thickness and Fig.2(b) shows the change of carrier concentration versus vertical distance(thickness) of the waveguide and it is observed that the carrier accumulates at the Cu-ITO grating and SiO_2 interface, the accumulated carrier changes the permittivity of the ITO material. A significant change of carrier concentration at the applied voltage of 4 V is observed. The change of carrier concentration results in changes in the effective refractive index of the material due to a change of permittivity of the ITO layer. The perturbed carrier concentration of Lumerical charge solver due to applied bias is imported in Lumerical Finite Difference Time Domain (FDTD) to observe the change of wave propagation. Fig3.3(a) shows the wave propagation, at no bias the plasmonic wave propagate at the interface of dielectric and Cu-ITO grating and we can say that ON state of the device and when we use perturbed carrier concentration at an applied bias of 4V, the intensity of wave propagation reduces and device act as an absorber as Shown in Fig.3.3(b) and we can say OFF state of the device. In the simulation of the device, we have used the Lumerical Finite Difference Eigen Mode (FDE) solver for the analysis of mode confinement.

The effective mode area of the guided mode will be the measure of the nature, whether the localized field is optical or plasmonic mode and it would be the merit of confinement ability, the effective mode area (A_m) of the device can be calculated by taking the ratio of total mode energy flux density, and maximum energy flux density at active region. The effective mode area is denoted by [79]

$$Am(/\mu m\ 2) = \int_{-\infty}^{\infty} P(x,y)\, dx\, dy \ / \ max[P(x,\gamma)] \tag{3.3}$$

Fig.3.4(a) shows the variation of effective mode area with increasing the thickness of the ITO layer and light confined at a very small mode area of 0.01421 /μm^2 at the active region of the device.

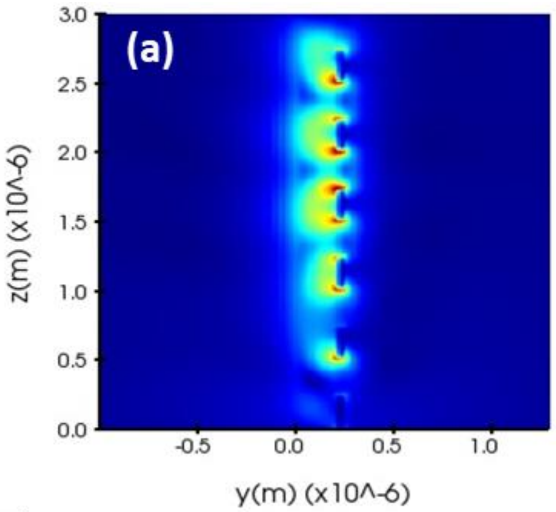

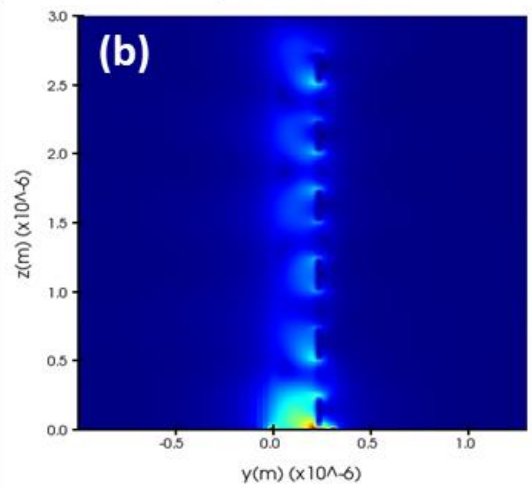

Fig 3.3 (a) plasmonic wave propagation of the device when no bias is applied (ON state), y and z axes represent waveguide thickness and direction of wave propagation respectively and (b) Plasmonic wave propagation at an applied voltage of 4V (OFF state).

The propagation length of the plasmonic wave is depicted as the distance at which the intensity of the propagating wave reduce to a factor of 1/e of the total coupling intensity of the light and the propagation length of the guided plasmonic mode is denoted by [107]

$$\boldsymbol{L_m(\mu m)} = \frac{\boldsymbol{\lambda}}{\boldsymbol{4\pi((n_{eff})img)}} \tag{3.4}$$

Where $\boldsymbol{\lambda}$ is operating wavelength and $(\boldsymbol{n_{eff}})\boldsymbol{img}$ is an imaginary component of the effective refractive index and the model propagation loss is given by

$$\boldsymbol{l_m}(\boldsymbol{dB} \,/\, \boldsymbol{\mu m}) = -\left(2(\boldsymbol{k_0}) \times (\boldsymbol{n_{eff}})\boldsymbol{img}\right) \times \mathbf{4.3} \tag{3.5}$$

where $\boldsymbol{k_0} = \frac{2\pi}{\lambda_0}$ denotes the propagation constant of the plasmonic mode and the negative sign indicates lossy materials.

(a)

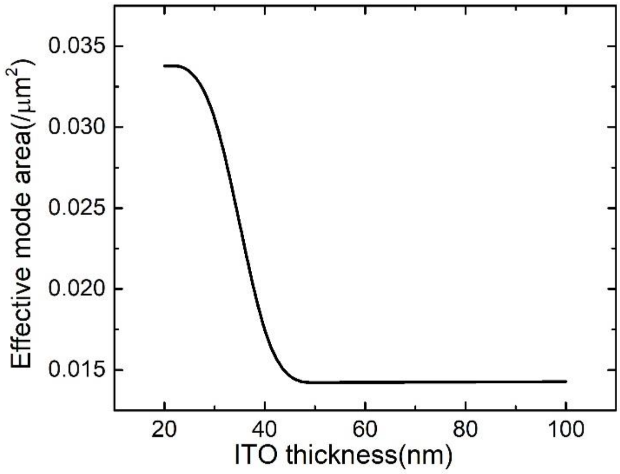

(b)

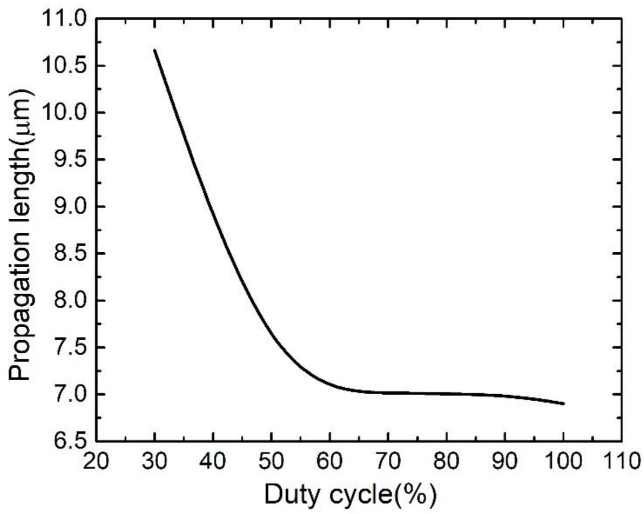

Fig.3.4(a) effective mode area (Am) versus the thickness of ITO layer, mode area decreases with increasing the thickness of ITO layer. (b) Propagation length of the device with varying the duty cycle,

(a)

(b)

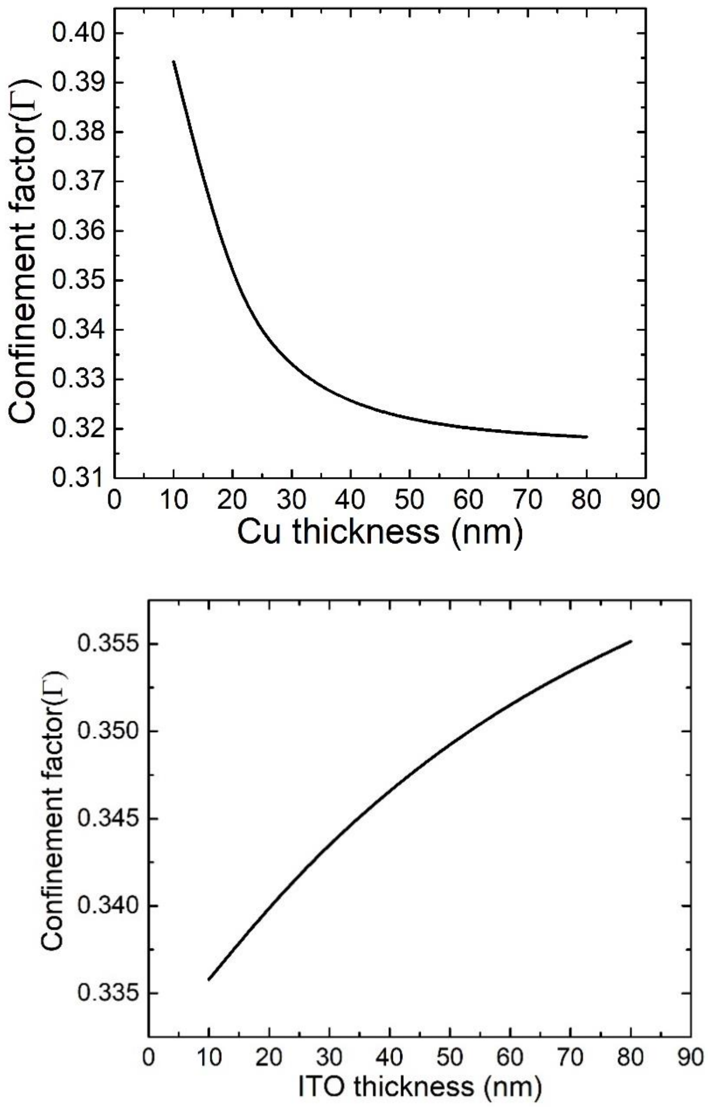

Fig.3.5 (a) Plasmonic mode confinement factor at the different thickness of Cu layer of the device, confinement factor decreases with increasing the thickness of Cu layer. (b) Plasmonic mode confinement at the different thickness of ITO layer of the device, confinement factor increases with increasing the thickness of ITO layer

Fig.3.4(b) shows the propagation length versus duty cycle of Cu-ITO grating and the propagation length decreases by increasing the duty cycle of grating, this is due to the high model propagation loss of the device. So, there is a tradeoff between model propagation loss and propagation length. The optical energy confinement of the device is the propagation of power flowing through the active zone to the total power flowing through the system [89][94][95]. Fig.3.5(a) shows the plasmonic mode confinement of the device with varying the thickness of the active layer (ITO) and the confinement factor increases with increasing the thickness of the ITO layer and Fig.3.5(b) depicts the device's plasmonic mode confinement as a function of Cu layer thickness, demonstrating the mode confinement decreases as Cu layer thickness increases. So, the device exhibits the confinement factor of 34.67% at the optimized layer of 40 nm of the copper layer and 40 nm of the ITO layer.

3.4 Electrically Tunable Absorption

The electrical behavior of the device is numerically investigated by using a Lumerical charge transport solver. The device simulation yields charge transport data of change of charge carrier density of Cu-ITO junction with applied bias. The perturbed charge carrier density of the device is introduced from the Lumerical Device simulation tool through the index perturbation into the Lumerical mode solution for analysis of change of light properties due to applied bias. The Drude model is used to calculate the change in the effective refractive index of the Cu-ITO subwavelength grating. The change of the charge carrier density of the ITO at different voltages has the ability to change the effective refractive index of the device. The complex permittivity of the material is related to its charge carrier density, according to the Drude model hypothesis and depicted as $\boldsymbol{\Delta n} = \frac{\boldsymbol{\Delta\varepsilon}}{\mathbf{2}\sqrt{\boldsymbol{\varepsilon}}}$, the variation of charge carrier density (accumulation or depletion) has ability to change the complex permittivity which yields the change of effective refractive index. The change of complex effective refractive index (real and imaginary components) of the device with variation of carrier density is calculated as

$$\Delta n = \frac{-e^2\lambda_0^2}{8\pi^2 c^2 \varepsilon_0 n}\left(\frac{Ne}{m_c^* e} + \frac{N_h}{m_c^* \cdot h}\right) \tag{3.6}$$

and

$$\Delta \alpha = \frac{e^3\lambda_0^2}{4\pi^2 c^3 \varepsilon_0 n}\left(\frac{Ne}{\mu_e (m_{ce}^*)^2} + \frac{N_h}{\mu_h (m_{ch}^*)^2}\right) \tag{3.7}$$

Here, N_e and N_h represent electron and hole carrier densities, e represents electronic charge, λ_0 represents operation wavelength, μ_e and μ_h represent electron and hole mobility, and m_{ce}^* and m_{ch}^* represent the effective mass of electron and hole, respectively.

The carrier concentration of the ITO layer is $1\text{x}10^{20}$ cm^{-3} and when we applied the voltage carrier concentration of the ITO changes as shown in Fig. 3.2 and electron accumulated at the interface of dielectric and ITO which alters the permittivity of the material yields change in the refractive index of the device when no voltage is applied the refractive index of the material is 2.402+0.0349i and when we applied voltage of 6 V, the refractive index of the material changed to 2.335+0.048i at the operating wavelength of 1550 nm. The change in carrier concentration (accumulation of electron at Cu-ITO grating and dielectric interface) due to applied bias, there is a change of real and imaginary components of the effective index of the device. The change of the real part represents the phase shift, and the change of the imaginary part represents the attenuation of plasmonic wave propagation, The electromagnetic wave's intensity can be changed by changing the imaginary components, which can be done with the applied voltage. Fig.3.6(a) shows the graph between change in the imaginary component of effective refractive index versus applied voltage with varying the thickness of the Cu layer of the device and it shows that the imaginary component of the effective refractive index increases with decreasing the thickness of the Cu layer. We have observed that the maximum tunability of the device is achieved at copper and ITO thickness of 40 nm each. we have optimized the grating period and duty cycle of the device to achieve higher tunability of the plasmonic wave and in Fig.3.6(b) shows the graph between the change of imaginary component of the effective refractive index with varying the grating period of the device.

(a)

(b)

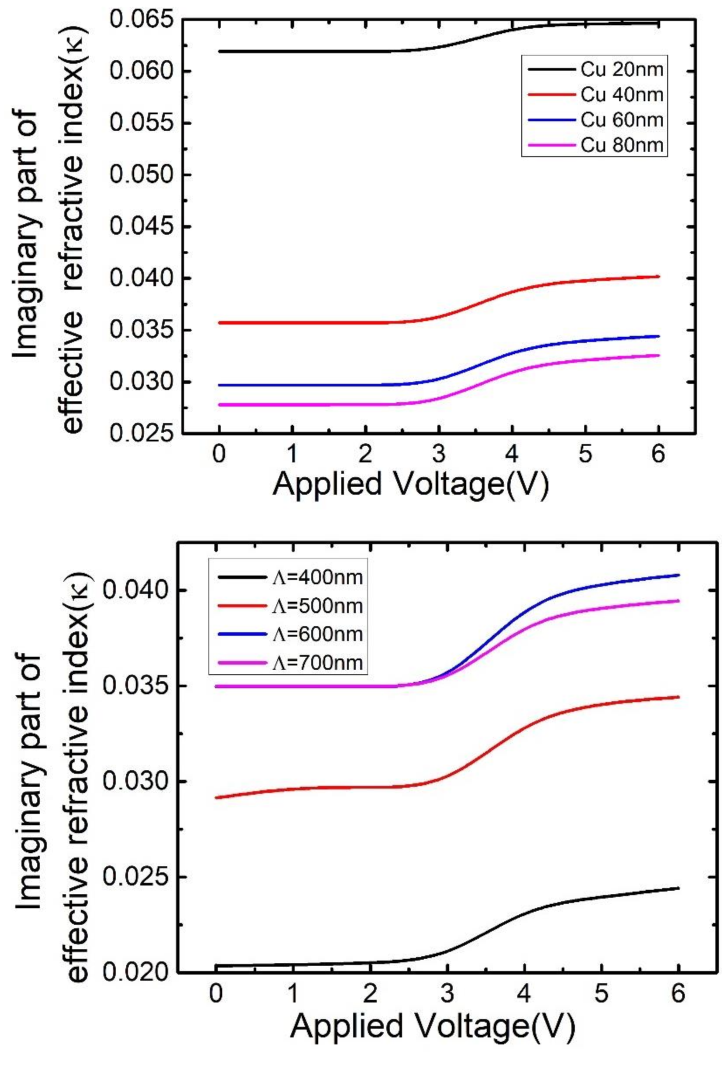

Fig.3.6(a) imaginary component of effective refractive index with applied voltage at different Cu thickness of the device. (b)the variation of imaginary component of the refractive index with applied bias at varying the duty cycle of the grating.

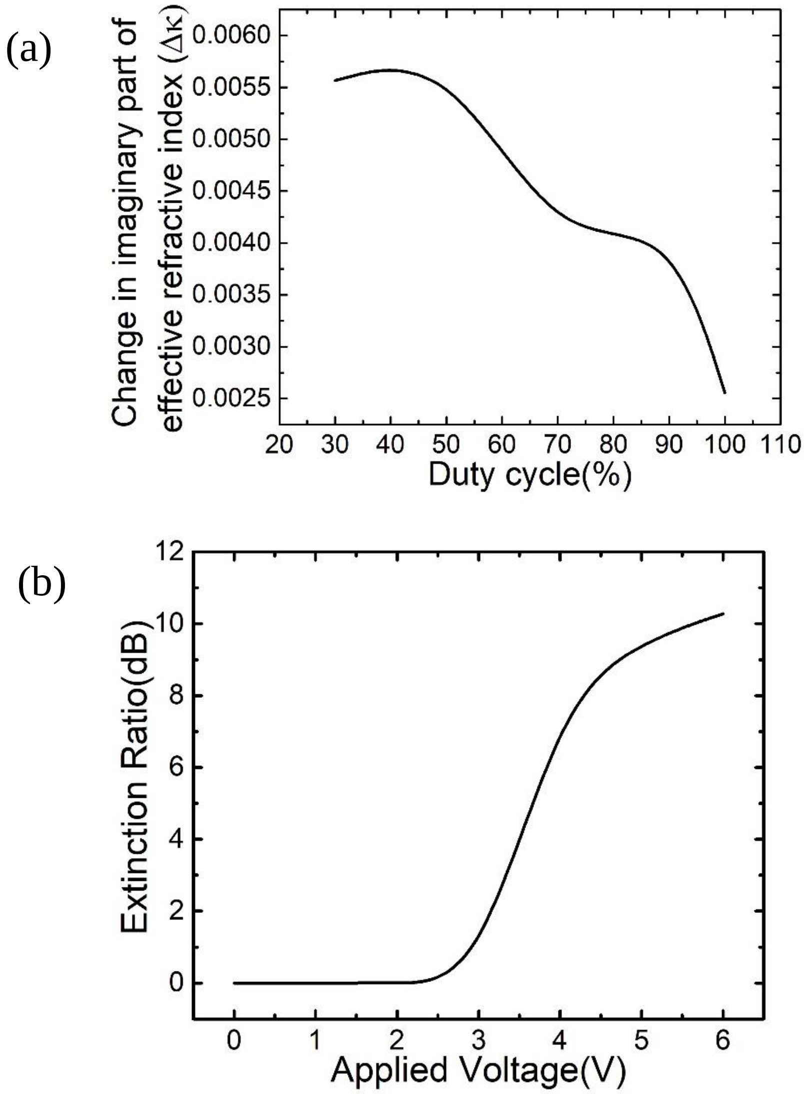

Fig.3.7(a) the imaginary component of the refractive index with applied voltage at varying the grating period of the device, maximum tunability of the absorption (in terms of change in effective refractive index is observed at 600nm grating period. (b)The difference in the states of high and low absorptions i.e., Extinction ratio, versus applied voltage. The device yield extinction ratio of 10.28 dB at the applied voltage of 6 V for 100 µm long device

The change of the imaginary component of the effective refractive index is maximum at the grating period of 600 nm and Fig.3.7(a) depicts the variation of the imaginary component of the effective refractive index versus the duty cycle of Cu-ITO grating and device yield the maximum tunability at the Duty cycle of 50%. We optimized the device for an electrically tunable absorber and observed that at the grating period of 600 nm and duty cycle of 50%, the device yields a maximum change in effective refractive index which represents absorption of electromagnetic wave. The change in the imaginary component of the effective refractive index of the device can be used to tune the attenuation of the intensity (absorption) of the electromagnetic wave. We can calculate the absorption of the light in terms of effective refractive index is given by $\boldsymbol{\alpha = \frac{2\pi k_{eff}}{\lambda}}$. The extinction ratio or modulation depth of the device can be calculated by

$$\boldsymbol{ER = 4.343[\alpha(V) - \alpha(0)]L}. \tag{3.8}$$

Fig. 3.7(b) shows the extinction ratio versus voltage. The ER of the 100 µm long device is calculated to be 10.28 dB. The device length must be increased, or a greater voltage must be provided to improve the extinction ratio. The higher driving voltage is incompatible with CMOS driving circuits, and rising device length is incompatible with high-density integration, therefore there is a tradeoff between high extinction ratio and small device footprint.

3.5 Summary

An electrically tunable plasmonic absorber on SOI is numerically reported. The device consists of copper- Indium tin oxide (ITO) based subwavelength grating which operates at a telecom wavelength of 1.55 µm. The device design with Cu-ITO structure efficiently utilizes electrically tunable permittivity of ITO. We observe that maximum tuning of absorption at a grating period of 600 nm and 50% duty cycle of the Cu-ITO grating. The device shows a very small mode area of A_m= 0.01421 /µm^2 and a higher plasmonic confinement factor of 34.67 %.

our device exhibits the Extinction Ratio (ER) of 10.28 dB at a very low voltage of 6 V for a 100 μm long device. This tunable absorber can be used in many applications where attenuation of intensity is a prime requirement such as intensity modulator, biosensing, imaging, etc.

Chapter – 4

Optically Triggered AlGaN/GaN Power Transistor

4.1 Introduction

The performance of Power Semiconductor Device is extended by the Wide Band Gap Semiconductors (WBG) which offer low conduction and switching losses as compared to equivalent Silicon power devices.[119]-[120]. WBG power devices, with their superior characteristics, offer thinner unipolar devices and have lower on-resistance which means lower conduction losses and higher converter efficiency. WBG devices also exhibit higher breakdown voltages, higher thermal conductivity and operate at higher temperature [126]. The most promising power semiconductor devices for future high power and high frequency applications have been found to be those based on gallium nitride (GaN), which is one of the numbers of WBG materials, because to its greater bandgap, greater breakdown field, greater carrier velocity, greater electron mobility, and greater optical absorption coefficient [120-125], [138-140]. The generation of high mobility two-dimensional electron gas (2DEG) at the AlGaN/GaN heterojunction is a key characteristic of GaN material [130]-[121]. All these properties of GaN make a suitable candidate for optical triggering structure [126].

Electrically powered gate control power devices suffer from being always on, which makes designing and implementing gate drivers for these devices more difficult [127]. Optical triggering of power devices can improve the number of system features, such as reduced electromagnetic interference (EMI), reliable electrical separation, getter-free operation, and separation of the power and control stages [131]. A new generation of power device is needed for power converters in applications where electronic systems based on conventional Si power devices cannot function because Si has some significant limitations in terms of its voltage blocking capability, operation temperature (operates up to 150 ^{0}C of junction temperature) and switching frequency [128].

Thus, in this work we present optical triggering of Semiconductor Power transistor (PSD). The device consists of a p-GaN region which acts as active region for optical triggering sandwiched between undoped GaN, a 30 nm n-$Al_{0.2}GaN_{0.8}$ is formed over GaN region. n-AlGaN/GaN heterojunction formed a 2-DEG channel between source to drain of the device. when beam of light (λ=350 nm) shine on the device, the light absorbed by p-GaN region and photogenerated e-h pairs created, generated electrons jump from valance band to conduction band and form 2-DEG channel, the device current can be controlled by varying the power intensity of light. The device exhibits very low on-resistance, and the device has very low conduction loss. The switching characteristics of the device are investigated by applying the laser pulse of width 200 µm and device exhibits low rise and fall time 0.7 µsec and 0.4 µsec respectively.

4.2 Device Geometry & Working

Optical control of AlGaN/GaN semiconductor power device is shown in fig 4.1(a), the device consists of p-GaN layer sandwiched between two undoped GaN on the top of silicon substrate, a buffer layer between substrate and GaN is incorporated to reduce the lattice mismatch. Here x and y axes depict the width and thickness of the device. The thickness of GaN layer is 1 µm and width of the device is 3 µm. A 30 nm n-AlGaN layer is used on the top of GaN layer and dual layer of SiO_2 and TiO_2 having the thickness of 20 nm each is used as an antireflecting layer to reduce the reflection of the light and

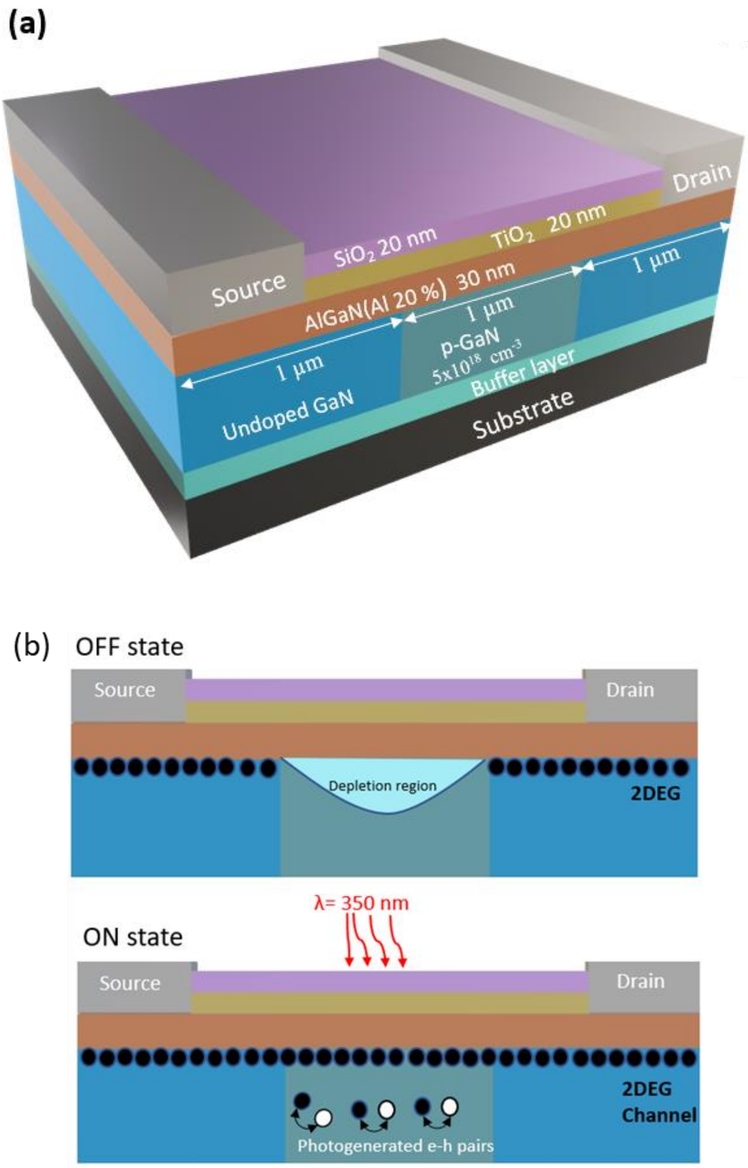

Fig. 4.1 (a) 3-D diagram of proposed optical triggered AlGaN/GaN semiconductor power transistor, thickness of GaN layer is 1 µm, width of p-GaN($5x10^{+18}cm^{-3}$) layer is 1 µm sandwiched between undoped layer having the thickness 1 µm each, the device width is 3 µm, a 30 nm n-AlGaN(Al 20 %) ($2x10^{+18}cm^{-3}$) barrier layer is used on top of GaN layer to form 2DEG channel, Dual layer of SiO_2 and TiO_2 having the thickness of 20 nm each is used as an antireflecting layer to reduce the reflection of the light and surface passivation of the device (b) Normally Off state of the device, 2DEG channel is formed between

undoped GaN and n-AlGaN layer at applied bias and 2DEG channel is depleted between p-GaN and n-AlGaN at optically off state and On state of the device, when light shine, it absorbed by p-GaN region and e-h pairs generated, generated electrons jump to conduction band and form 2DEG channel

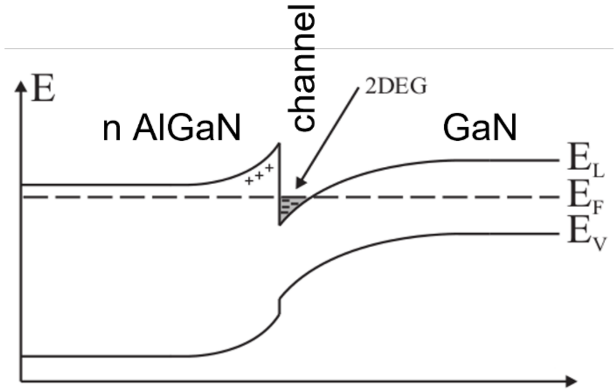

Fig 4.1(c) Two-dimensional electron gas (2-DEG) formed at n-AlGaN/GaN heterojunction

surface passivation of the device. SiO_2 is chemically stable at high temperatures and has good passivation and scratch resistance qualities [133]. Another material is TiO_2 which has suitable refractive index (2.9 at λ=350nm) and low absorption. In addition, TiO2 is well-known for its chemical resistance, mechanical toughness, and low moisture absorption [135]. p-GaN having the hole concentration of 5×10^{18} cm^{-3} is used in order to deplete 2DEG channel to keep the device in normally off state. The operating principle of the proposed device is based on the photogeneration of electron hole pair. Initially the device is off state when there is no light shine in the device and at the applied bias between source and drain, the charge accumulate at heterojunction interface between n-AlGaN and undoped GaN layer, the conduction band of the undoped GaN bend below the fermi level and electron of n-AlGaN tunnel into the GaN layer and formed 2DEG at the interface, when there is no light shine on the device the fermi level of p-GaN region is near the conduction band and there is no 2DEG channel is created and the device is normally in off state. Fig.4.1(b) shows the off state of the device p-GaN region is depleted when the beam of light is off state. When we shine the beam of light having the energy of wavelength greater than the band gap of p- GaN layer the light is absorbed by the p-GaN region and it is transmitted by n-AlGaN region due to higher band gap of the n-AlGaN layer.

Dual layer of SiO_2 and TiO_2 is act as an antireflecting layer to reduce the reflection of the light, the absorbed light generates electron hole pair in p-GaN region and at the applied bias between source and drain the generated electron jumps valance band to conduction band and drift towards the n-AlGaN/p-GaN interface, the accumulated electron form 2DEG channel at heterojunction.

The 2DEG channel creates a conduction path and charge carriers flow from source to drain and device remains in on state till the beam of light is on. Fig.4.1(c) shows the ON state of the device in which the 2DEG channel is formed when a beam of light shines on the device and current flows from drain to source of the device. When the beam of the light turned off the generated electron hole pairs recombine, and the device turned to OFF state. Fig.2 shows the 2-DEG channel formation at n-AlGaN/GaN heterojunction, photogenerated electrons jump from valance band to conduction band, the conduction band bending below the fermi level and form 2-DEG channel, charge flows from source to drain, and device remains in on state, when the light turned Off the generated electron hole pairs recombine and 2-DEG channel disconnected, and device turned Off.

3.3 Optical Characteristics of the Device

The optical characteristic of the device is numerically investigated by Lumerical Finite Difference Time Domain (FDTD)

(a)

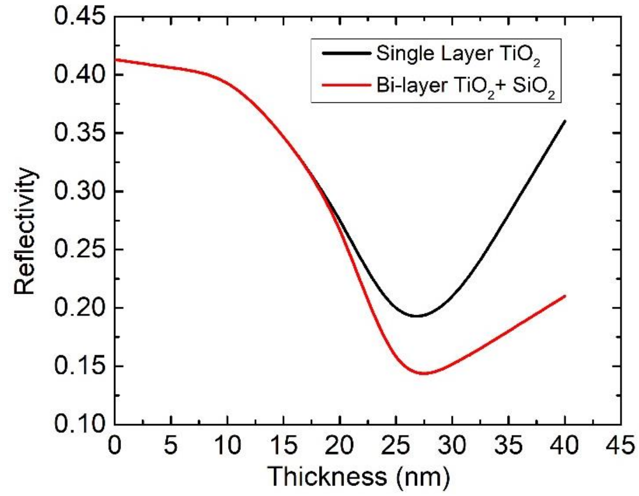

(b)

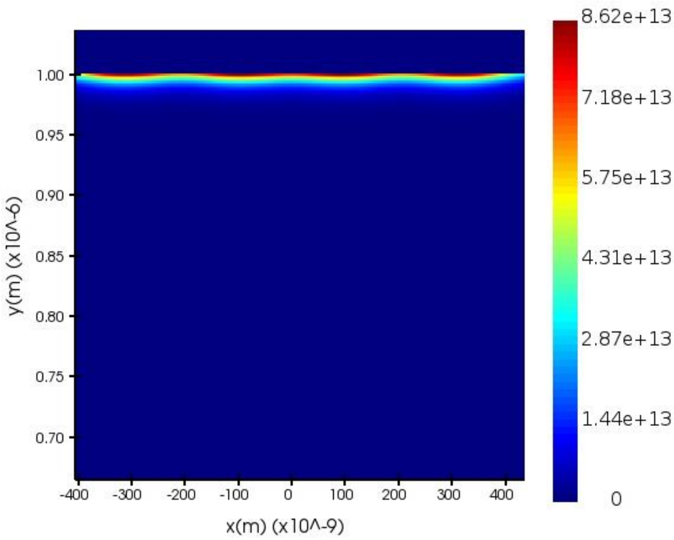

Fig.4.2(a) graph between reflectivity verses anti reflecting layers, reflectivity reduces from 42 % to 20 % at TiO2 thickness of 25 nm, further it reduces to 15 % by using SiO_2+TiO_2 anti reflecting layers to enhance the efficiency of the device (b) Absorbed power (P_{abs}) of incident beam of light λ=350nm, light absorbed at the surface of p-GaN region.

analysis, to enhance the efficiency of the device a bi-layer anti-reflecting structure of SiO_2 and TiO_2 is used to reduce the reflection of light. Fig.4.2(a) shows the graph between reflectivity verses thickness of anti-the band

gap the light

absorbed l

(c)

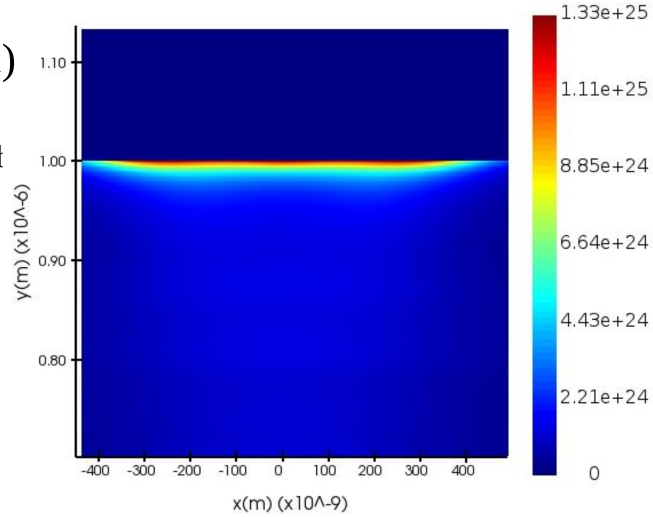

(d)

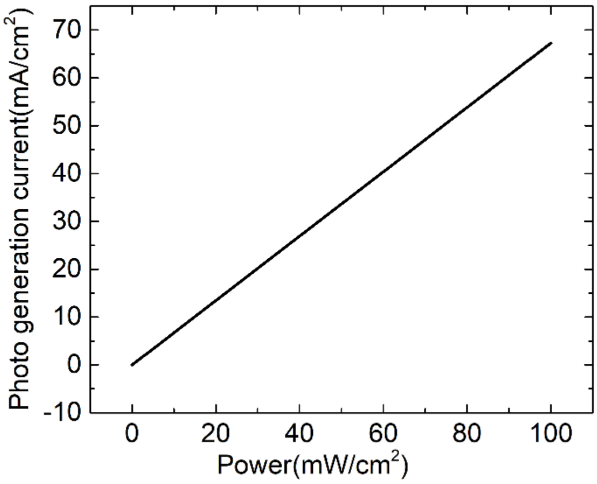

Fig.4.2 (c) Optical generation rate (G): e-h pairs created at the p-GaN region. (d) This graph depicts photogeneration current verses applied optical power, the photogeneration current increases with increasing the optical power of the light source.

device through the excitation of charge and excited electrons at valance band jumps to conduction band and leaves behind vacancy called hole, this process is called electron hole pairs generation. Fig.4.2(b) shows the absorbed power of incident light on to the device, most of the light absorbed (P_{abs}) at the surface of the p-GaN layer and absorptions of light decaying with respect to depth. The absorbed photons excite the electron hole pair generation. Fig.4.2(c) shows the photo generation of electron hole pairs at the surface of p-GaN layer. The most of the photogeneration occurs at the surface of the p-GaN layer and its gradually decrease with depth of the optical generation rate is calculated with varying different laser power by script command and generation rate files imported in Lumerical DEVICE simulation for electrical simulation of the device. Fig.4.2(d) shows the graph between photogeneration current verses different laser power, and it is observed that the photogeneration current increases with increasing laser power.

4.4 Electrical Characteristics of the Device

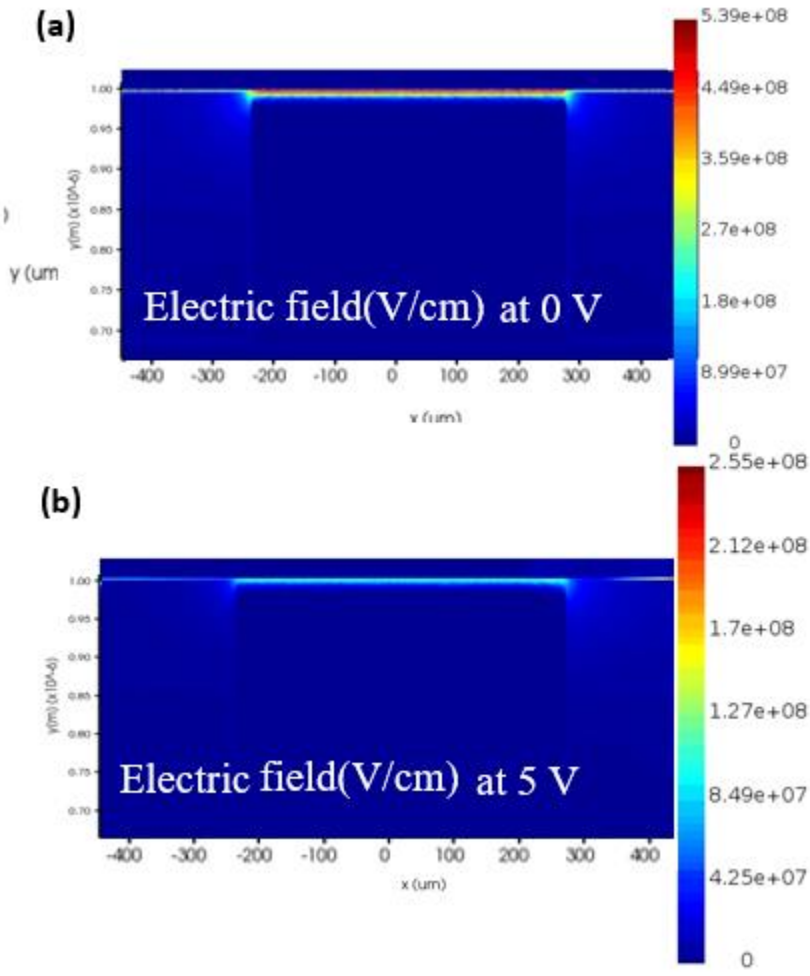

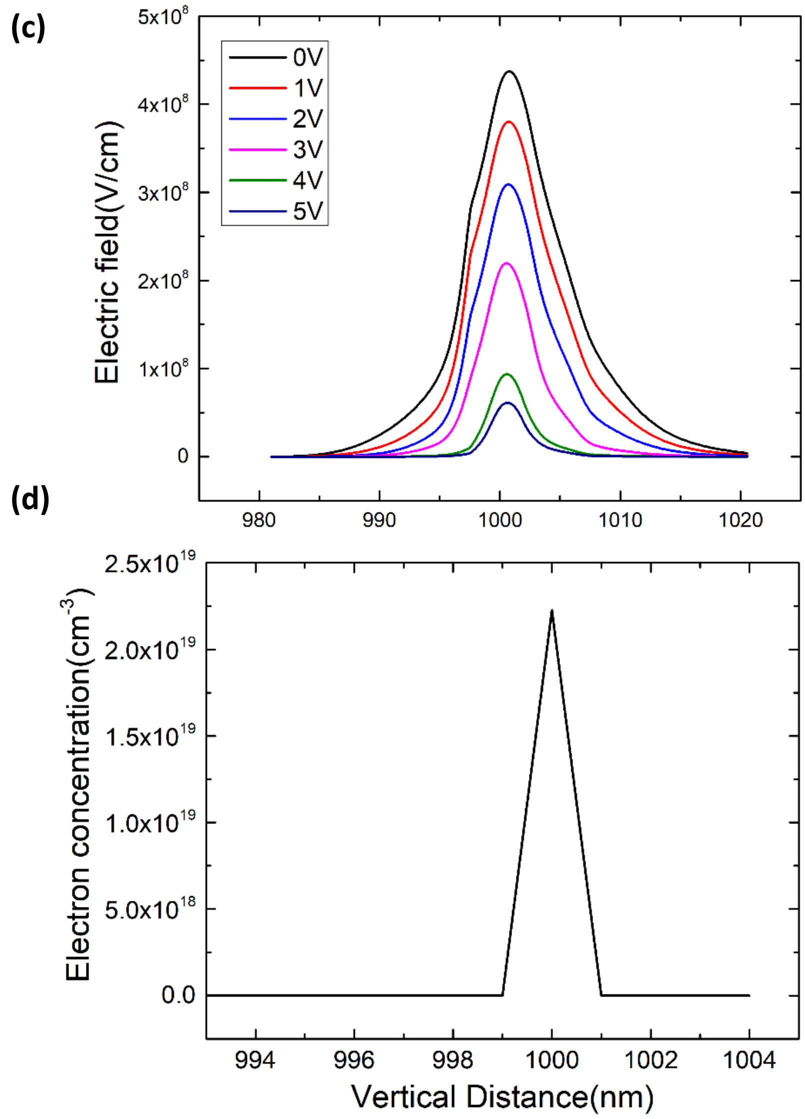

Fig.4.3(a) Electric field strength at n-AlGaN/GaN interface at no bias, due to higher depletion region the electric field strength is high (b) Electric field strength at n-AlGaN/GaN interface at applied voltage of 5V the depletion region vanishes at electric field strength is low (c) fig. shows the variation of electric field strength with varying the applied voltage between source to drain at the heterojunction (d) carriers (electrons) concentration at 2-DEG channel

The electrical characteristic of the device is numerically calculated by Lumerical DEVICE simulation tool [112]-[114]. The CHARGER solver is run in steady state mode and transient state mode to calculate device current and switching characteristics respectively. The optical generation rate files at different laser powers are imported from Lumerical FDTD to calculate the device current at applied laser powers. Fig.4.3 shows the electrical characteristics of the device. Fig.4.3(a) shows the electric filed strength at the interface of n-AlGaN and p-GaN layer and electric field is higher when there is no applied voltage and channel is in depletion region and when the applied voltage is increases the depletion region vanishes. Fig.4.3(b) shows the depletion region at 5V, and Fig.4.3(c) depicts graph between the electric field versus thickness of the device, at the zero bias the electric filed is higher at n-AlGaN/p-GaN interface due to depletion region. When we increase the applied potential then the width of the depletion region starts to decrease, and electric field strength also decreases with increasing the applied potential. Fig. 4.3(d) shows the graph between carrier concentration verses device thickness, the peak depicts the carrier accumulated at AlGaN/GaN heterojunction (high 2DEG density)

4.5 Optical Switching

The numerical investigation of switching characteristics and switching speed of the device has been carried out by transient analysis of Lumerical DEVICE simulation. In transient analysis the optical generation rate imported from FDTD is activated for the duration of 0-200 μsec. During the turn On time of the laser pulse (in form of photogenerated electrons) with different laser powers are introduced and found that the current flows from source to drain and drain current saturates beyond 2 V Fig.4.4(a) shows the drain current vs applied laser pulse for the duration of 0-200 μsec with varying the laser powers and it shows that the drain current is high when the optical generation rate is activated and it down to zero when the optical generation rate deactivated. So, the switching of the device can be controlled optically by applying laser power. Thus, unlike electrical controlled power transiter device optical control power transistor device can improve the number of system features, such as reduced electromagnetic interference (EMI), reliable electrical separation, getter-free operation, and separation of the power and control stages.

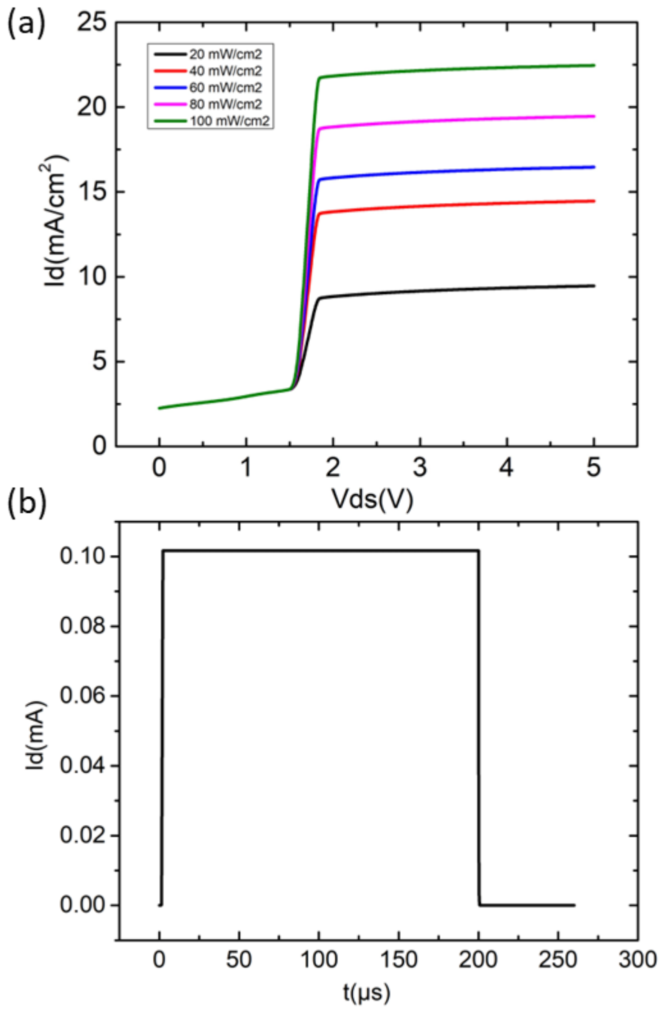

Fig.4.4(a) graph between drain to source voltage verses drain current density at different laser power, drain current increases with increasing the laser power (b) the graph depicts the drain current verses applied laser power at 0-200 us pulse duration and it shows that the drain current rain high till the optical generation rate is activated and it down to zero when optical pulse (optical generation rate) turned off.

The switching speed of the device is evaluated by transient analysis of Lumerical DEVICE simulation, the photogenerated results imported from FDTD at applied laser power of 40 mW/cm^2 and activated at pulse duration of 0-200 μsec and turn On and turn Off time of the device is calculated. The transient simulation of the device shows the good switching characteristics with rise and fall time (10-90%) of 0.7 μsec and 0.4 μsec respectively due to high optical absorption and short carrier lifetime of GaN.

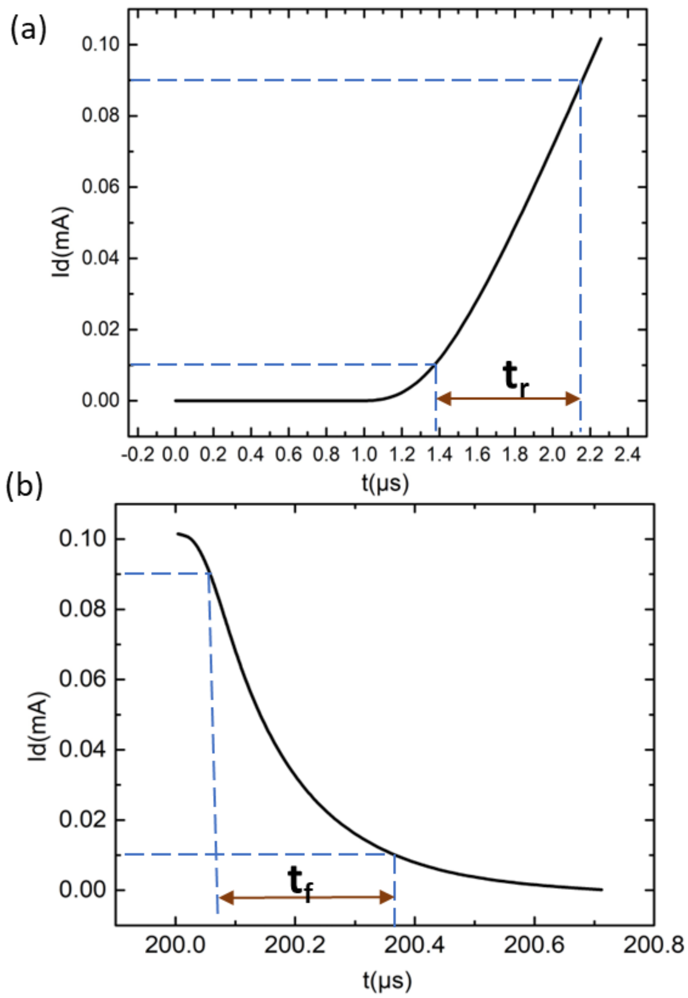

Fig.4.4(c) fig. shows the rise time (10 to 90% of drain current) of drain current when the generation rate is turned on (d) figure shows the fall time (90 to 10 % of drain current) of the drain current when the optical generation rate is turned off.

Fig.4.4(b) shows the graph between the activated photogeneration current duration period versus the drain current of the device at applied laser power of 40 mW/cm^2. Fig. 4.4(c) and (d) show the turn on time and turn off time of the power transistor verses drain current of the device. The optical switching characteristics of the device is fast enough for application of high frequency power devices.

4.6 Summary

In this work we have proposed and numerically evaluated optical triggering of n-AlGaN/GaN power semiconductor device. The device is normally an OFF device in the electrical domain and controlled by optical triggering in optical domain. The device current flows from source to drain when 2-DEG channel is formed due to absorption of photon of incident light and channel current can be controlled by varying the intensity of incident beam of light. The device exhibits low resistance which means it consumes low power and amount of heat generated is less and device yields low conduction loss. The switching characteristics of the device are also investigated, and device attain very low rise and fall time 0.7 μsec and 0.4 μsec respectively which can be used for high-speed application. The optical controlled power devices can be used for high frequency, high speed switching devices, high voltage and high current devices, power converter in applications where electronic system based on traditional Si power devices cannot operate.

Chapter – 5

Tunable Plasmonic Absorber on Cu-ITO Structure

5.1 Introduction

Tunable plasmonic absorbers have drawn increased interest because of their numerous applications such as sensing [131,132], imaging [133], energy conversion [134,135], filters [136], photodetection [138,139], and modulation [133]. There have been several methods reported to achieve either narrow or broadband light absorption in the microwave [137], terahertz [138], infrared [139,140], and visible spectral range [141,142]. To produce tunable plasmonic absorbers, several nanostructures have been developed that couple the plasmonic effects in a system. [131,143,144]. Noble metals, like copper, silver, and gold, are ideal plasmonic materials by patterning such metals at the nanoscale level, a significant absorption of light can be achieved due to the excitation of plasmonic resonance in the infrared (IR) regime [145-148]. The excitation of surface plasmons (SP) in novel metals enables light confinement in the deep-subwavelength regime and can improve strong interactions between light and matter at the nanoscale. Plasmonic has made it possible to miniaturize components at the nanoscale level, allowing the integration of several optical and electronic devices on a single chip [149,150]. Unfortunately, pure metal-based plasmonic absorbers are prone to highly metallic and scattering loss of light which can be overcome by incorporating Transparent Conducting Oxides (TCOs) [153,154]. Light's optical characteristics of the light can be tuned by using a variety of Transparent Conducting Oxides (TCOs) such as Indium zinc oxide (IZO) and aluminum zinc oxide (AZO) are two examples of the many TCOs. The most effective material to tune the optical properties of light is indium tin oxide (ITO)

[153,154]. It has recently been discovered that employing indium tin oxide (ITO) in a metal-oxide-semiconductor arrangement enables substantial voltage-controlled tuning in the refractive index to be generated through the accumulation of carriers through the electric field effect [155-157]. In this work, we experimentally demonstrated a tunable plasmonic absorber based on Copper-Indium Tin Oxide (Cu-ITO) plasmonic gratings that can efficiently control the absorption of light at near-infrared (NIR) wavelength. The peak intensity of Ag, one of the many plasmonic materials (Cu, Au, Ag, and Al), is poor in the infrared region, while absorbers with Cu, Au, and Al have strong infrared absorption abilities. The Al absorber has a lower absorption intensity in the visible and near-infrared area compared to the Cu and Au absorbers. Also, the highly narrow absorption band for Ag absorber. The absorption spectra of Cu and Au absorbers are comparable, despite Au being a precious metal. Cu has thus been taken as the metal component for the suitable absorber material [159]. The structure is numerically proposed in our published work [158], and it is now an experimental demonstration with fabrication and confirmation of this kind of tunable plasmonic absorber.

Here we use distributed copper grating filled with ITO material. Distributed copper grating not only reduces metallic losses but also enhances the confinement of plasmonic mode at the metal-dielectric interface and filled ITO material used to couple plasmonic mode for efficient tuning of propagating plasmonic mode by applied bias [149]. Cu-ITO grating with discontinuous Cu strips filled with ITO and electrically controllable ITO permittivity gives us tunable absorption and effective plasmonic mode guidance. The employed n-type ITO demonstrates a considerable variation in charge carrier density with the applied voltage of -4 V, changing the optical absorption at telecom wavelength. The intensity of light varies from -35.57 dB to -57.77 dB at

0 V and -4 V respectively. The 100 µm long device shows an extinction ratio of 22.2 dB, 3 dB modulation bandwidth is 52.2 GHz, and the switching energy of the tunable absorber (high to low transmission and vice versa) is 60 p-Joule/bit.

5.2 Device Structure & Working

This mechanism of the electrically tunable plasmonic absorber device with distributed copper (Cu) gratings filled with n-type Indium Tin Oxide (ITO) material for efficient coupling of plasmonic modes is described for working at a 1550 nm wavelength. The suggested mechanism's concept is to electrically tune the absorption of the light by changing the permittivity of ITO while efficiently coupling light in a Cu-ITO grating based on a silicon rib waveguide. The schematic view of the proposed device is displayed in Figure 5.1(a). The illustrated structure is designed to fabricate on p-type (100) silicon wafer with resistivity 0.001-0.005 Ω-cm. The device has an integrated input/output coupler made of a homogeneous, periodic, single-layer silicon-air grating. The benefits of in-coupling (or fiber-to-chip) and out-coupling (or chip-to-fiber) are offered by high index contrast and subwavelength silicon grating. We optimized the grating parameters in our previous work [158] to efficiently couple 1550 nm wavelength with low loss. To acquire a proficient plasmonic tunable absorber we optimized device parameters to efficient coupling and propagation of plasmonic mode is calculated by Lumerical FDTD (Finite Difference Time Domain) analysis and MODE analysis, the grating period of input/output coupler is 600 nm, Duty cycle 50 % and grating height is 200 nm. On the top of 200 nm thick silicon rib waveguide, 10 nm SiO2 is thermally grown and we use magnetron sputtering system to deposit 40 nm thick copper layer and patterned distributed copper grating (Period 600 nm and Duty cycle 50 %) by using maskless lithography system, and 40 nm Indium Tin

Oxide (ITO) filled between Cu grating and 40 nm thick ITO is used as a capping layer to efficiently tuning of plasmonic mode of the device.

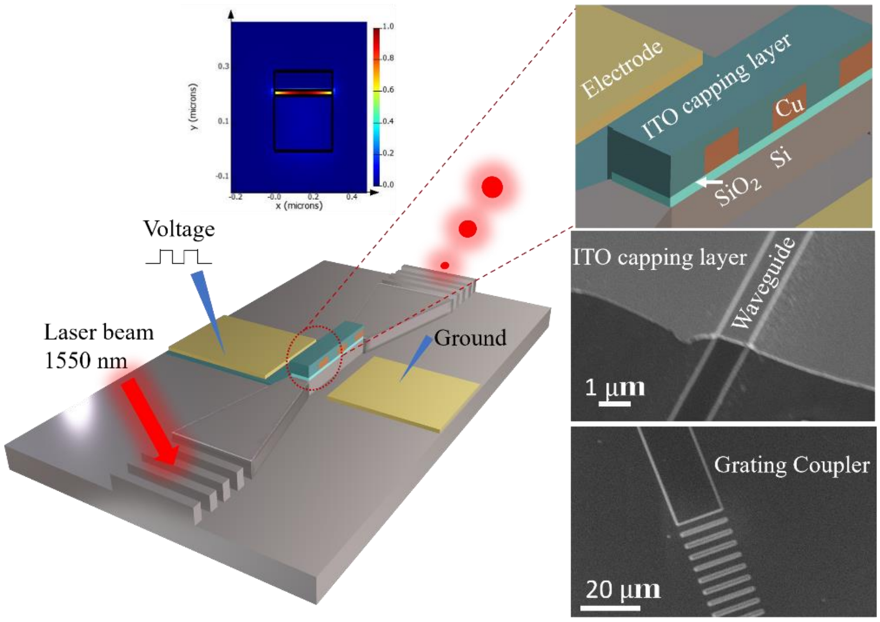

Figure-5.1. Structure of plasmonic absorber with electrical tuning based on Cu-ITO distributed grating at 1550 nm wavelength fabricated on p-type silicon wafer, the height of coupler and silicon waveguide is 200 nm and 10 nm of SiO_2 is thermally grown at active region of the device and the device length is 100 um. The device consists of distributed copper grating with grating period of 600 nm and duty cycle 50 %, Cu-ITO thickness is 40 nm on the top 40 nm capping layer of ITO material on the top of silicon rib waveguide, inset displays the confinement of the 1550 nm optical beam in a guided plasmonic TM mode. At the Cu-ITO grating/SiO_2 interface. Scanning Electron Microscopic view of the top surface of the Silicon-air grating coupler for efficient coupling of fiber to chip light along with taper waveguide and SEM image of active area of the Cu-ITO plasmonic tunable device on the top of capping layer of ITO for efficient tuning of light absorption.

When we shine a beam of light with a wavelength of 1550 nm, a fiber-to-chip input coupler couples the light, and the optical mode propagates through a silicon waveguide. At the active region of the waveguide, the device's Cu-ITO grating and SiO_2 interface propagate the TM polarized plasmonic mode, and the inset shows the device's mode confinement. The tuning of light absorption of the device is governed by the applied bias of the electrode when we apply negative bias at the top of the ITO electrode and the electrode on the silicon layer is kept grounded. The negative bias pushes the electron on the ITO layer towards the junction and charge careers accumulated at the interface, the accumulated electrons at the junction of Cu-ITO and dielectric interface are efficiently coupled through the propagation of electromagnetic waves and create Surface Plasmon Polaritons (SPPs). The absorption of light by collective oscillation of accumulated electrons changes the intensity of light.

5.3 Electrical & Optical Characteristics of the Device

Lumerical simulation is used to evaluate the electrical and optical properties of the proposed device. The device consists of distributed Copper grating which not only enhances light matter interaction due to low and high index of Cu-ITO grating but also reduces plasmonic metallic loss. The absorption of light is influenced by the charge carrier variation of the device due to applied bias. The side view of a single Cu strip filled with ITO material is shown in Fig. 5.2(c), we analyze the charge carrier perturbation by using the Lumerical CHARGE solver module. The change in charge carrier density caused by applied bias in ITO materials exhibits a change in permittivity in ITO material resulting in a change in the Effective Refractive Index of the device according to the formula.

$$\Delta n = \Delta\varepsilon / (2\sqrt{\varepsilon}) \tag{1}$$

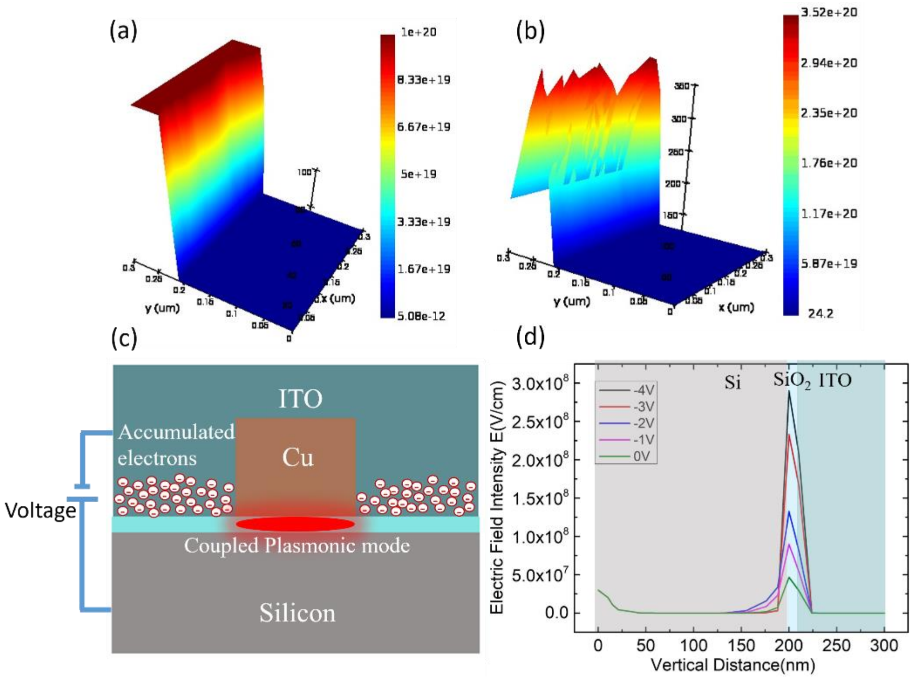

Figure- 5.2 Illustrative view of operational principle of the device and plasmonic mode coupling of distributed Cu-ITO grating i.e., charge coupling analysis of single Cu strip surrounded by ITO material. (a) At ON state of the device light propagates through the device, charge carrier density of the device at 0V (b) At applied bias of -4 V the device acts as OFF state, the light absorbed by accumulated charge carrier at the interface of Cu-ITO grating and SiO_2 (c) figure shows the cross sectional view of single Cu strip filled with ITO material, propagating plasmonic mode coupled with accumulated charge carrier density and changes the intensity of light (d) figure represents the enhanced electric field at the junction of the device at the applied voltage of -4V.

when we apply negative bias at the ITO electrode the charge carrier accumulated at the interface of Cu-ITO grating and dielectric, figure 5.2 (a) shows the charge carrier density when bias is applied, and figure 5.2(c) shows the accumulated charge carrier when we applied – 4 v the charge carrier changes from $1x10^{20}$ to $3.2x10^{20}$ cm^{-3}. The accumulated electron changes the electric field intensity as shown in Fig. 5.2 (d). By changing the concentration of carriers (electrons) in the

ITO layer, the device's optical characteristics can be electrically changed. The high variability of carrier concentration due to the applied voltage makes it a suitable material for fine-tuning at telecom wavelengths at high modulation efficiencies. The optical characteristics of ITO materials are observed by their mobile electron

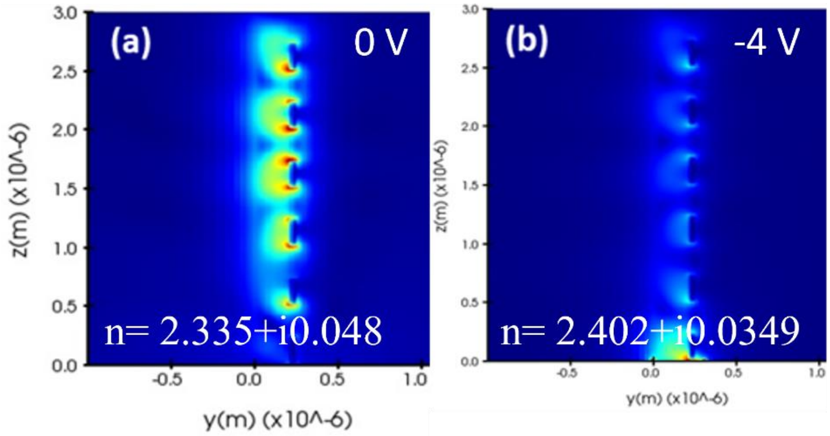

Figure 5.3 (a) Device plasmonic wave propagation in the absence of bias (ON state), Waveguide thickness and wave propagation direction are shown by the y and z axes, respectively and (b) propagation of a plasmonic wave at a -4 Volt applied voltage (OFF state).

concentration, which behaves as per a free electron Drude model [161].

We use a Lumerical EME solver and FDTD to analyze the optical characteristics of the device. The generated np density file from the Lumerical CHARGE solver is imported to the Lumerical EME solver to observe the variation of the effective refractive index of the device and it changes from 2.335+i0.048 to 2.402+i0.0349 at the applied voltage of -4 V. the imaginary part of an effective refractive index represents the change of intensity of light with applied bias. We use FDTD to observe the wave propagation of the device. Figure 5.3 (a) shows the wave propagation at 0 V and the wave propagates through the device called ON state of the device. Figure 5.3(b) depicts the wave propagation at -4 V the intensity of the light attenuates, and the device is called in OFF state.

5.4 Device Fabrication and Measurements

To demonstrate the electrical tuning of plasmonic absorption of the device we deposited the ITO on a glass sample for optimization of ITO carrier concentration with distinct oxygen partial pressure. The ITO layer will have a varied electron density depending on the oxygen partial pressure used during ITO deposition [163]. When oxygen flow increases, oxygen atoms fill the gaps, reducing the number of defect states and the decrease in conductivity. This is why the ITO layer formed at 0 sccm O_2 looks more conducive [164-166]. RF magnetron sputtering is used to deposit an optimized ITO layer at 40 sccm. Ar gas and 1 sccm oxygen gas at partial pressure of $1x10^{-6}$ torr to achieve n-type ITO having carrier concentration of $1x10^{20}$ cm^{-3}. After ITO's electron charge density is optimized to achieve a carrier concentration of $1x10^{20}$ cm^{-3}, the Cu-ITO grating on the top of the silicon rib waveguide with silicon-air grating coupler is fabricated using the standard fabrication procedure shown in Figure 5.4(a). Which shows the process flow of device fabrication. The device was fabricated on a p-type (100) 4 ‘’ silicon wafer having resistivity (0.001-0.009Ω-cm). 10 nm oxide layer is thermally grown by dry oxidation method and patterned by maskless lithograph for selective removal of oxide. The unwanted oxide is removed by buffer hydrofluoric (HF) acid, and we etched the silicon 200 nm deep, which makes the silicon rib waveguide along with the silicon air grating coupler. To create distributed copper grating over a silicon rib waveguide, the maskless lithograph is used to create a positive photoresist pattern and then the 40nm copper layer was deposited by RF magnetron sputtering. A 40 nm thick ITO layer was first deposited, then an additional 40 nm layer of ITO was deposited as a capping layer on top of the Cu-ITO grating structure by RF magnetron sputtering method, and finally aluminum metal was deposited for electrode formation by the lift-off method.

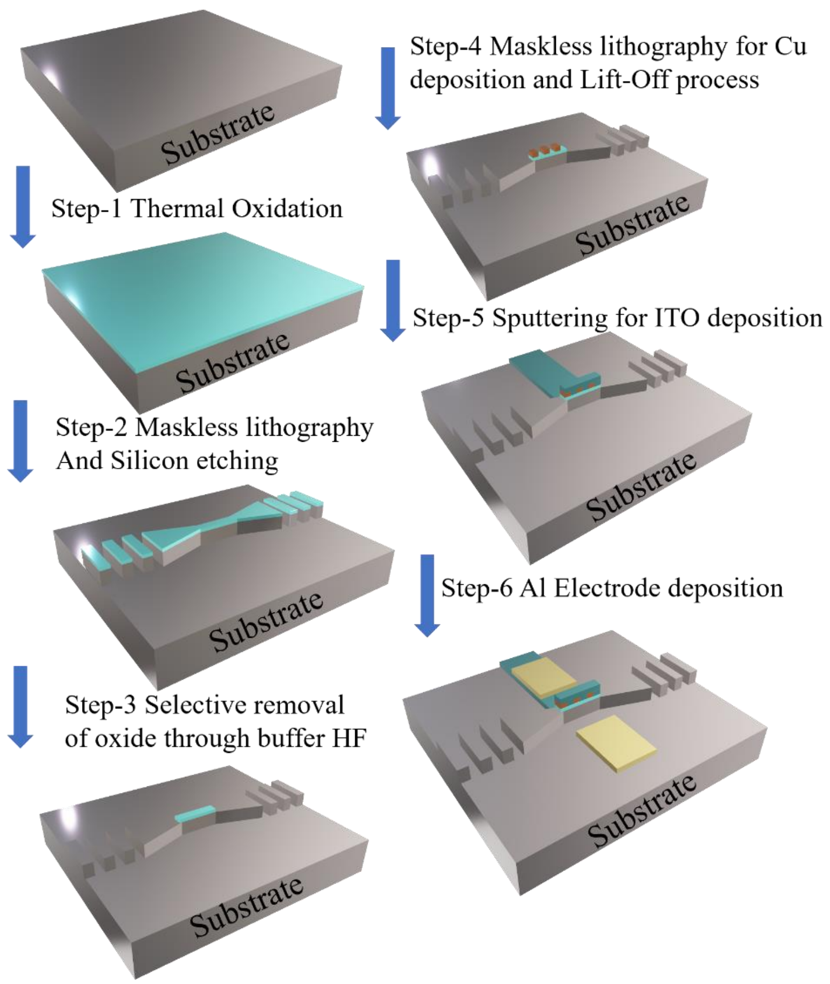

Figure 5.4 (a). Diagram showing the proposed structure's typical fabrication process on a p-type silicon wafer.

The fabricated device is characterized electrically and optically. The electrical measurement was performed to assess the modulation bandwidth and power usage. The capacitance's charging and discharging time (RC time), serves as a major constraint on the device's modulation bandwidth. The 3-dB modulation bandwidth is calculated using the expression [160-162]:

$$f_{3\,dB} = \frac{1}{2\pi R_s C_{Total}} \quad (5.6)$$

Rs represents the series resistance of the device, which is inversely proportional to device length, Rs includes ITO sheet resistance (160 Ω/*sq*) and metal contact resistance (40 Ω/*sq*) and the measured value of device capacitance is 14 pF. The 3 dB bandwidth of the device is calculated to 53 GHz.

The per-bit switching energy of the modulator is computed using the relation

$$E_{bit} = \frac{1}{4} C_{Total} V_{pp}^2 \tag{5.7}$$

Where V_{pp} stands for peak-to-peak driving voltage, which is 4 V and the measured value of E_{bit} is 60 p-Joule/bit.

An illustrative diagram of the optoelectronic measurement setup is shown in Figure 5.5. The setup includes a highly precise optical spectrum analyzer (OSA), a microscope, a polarization controller, a device under test (DUT), and a tunable laser source operating between 1527 and 1566 nm in wavelength. The polarization controller receives the tunable laser source's fiber-optic output and activates the TM-polarized mode before feeding it via the lensed fiber to the input coupler of the device under test (DUT), i.e., Transmitted light is gathered at the opposite end of the DUT by a silicon-air grating coupler and collimator fiber. To calculate the maximum coupled to power and note that we receive the most power at the output coupler, the single-mode lensed fibers for the input and output are oriented at 0°, 5° and 10° about the test device's surface normal. We receive maximum output power when the input fiber is kept at an angle of 10°. An optical microscope is used to place the electrical probe arms on the contacts with high precision.

BNC cables are used to link these probe arms to the source measurement device.

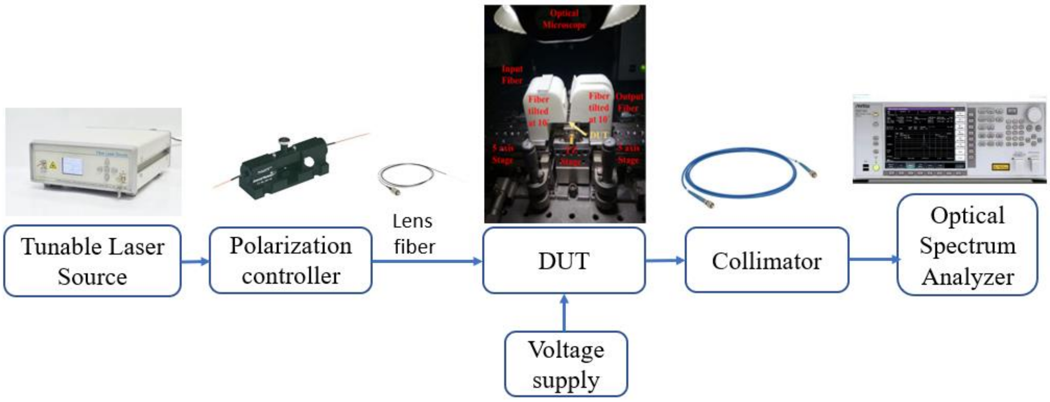

Figure- 5.5 Illustration of an experimental setup for optoelectronic characterization that includes a vacuum stage, source measurement unit, single-mode lensed fiber (SMF), polarization controller, high-resolution optical spectrum analyzer, tunable laser source, and optical microscope.

5.6 Results & Discussion

Figure 5.6 shows the experimental result of the measured transmission spectrum of the fabricated device, when there is no bias the maximum output power received at the Optical Spectrum Analyzer (OSA) keeping Input/Output coupling fibers at an angle of 10^0 from the normal. When we apply the negative bias on the top of the ITO electrode, the accumulated charge carriers at the junction lead to variations of the complex model of the device's refractive index. For the reverse bias, the intensity of the propagating beam is altered by the alteration in the complex effective index due to applied bias. The intensity of light reduces as we increase the reverse bias voltage. Figure 5.6 (a) displays the graph between the power transmission spectrum in dB versus the wavelength of the light at various reverse-bias voltages and it shows that the intensity of light reduces with applied reverse-bias voltages. the output power normalized to input power.

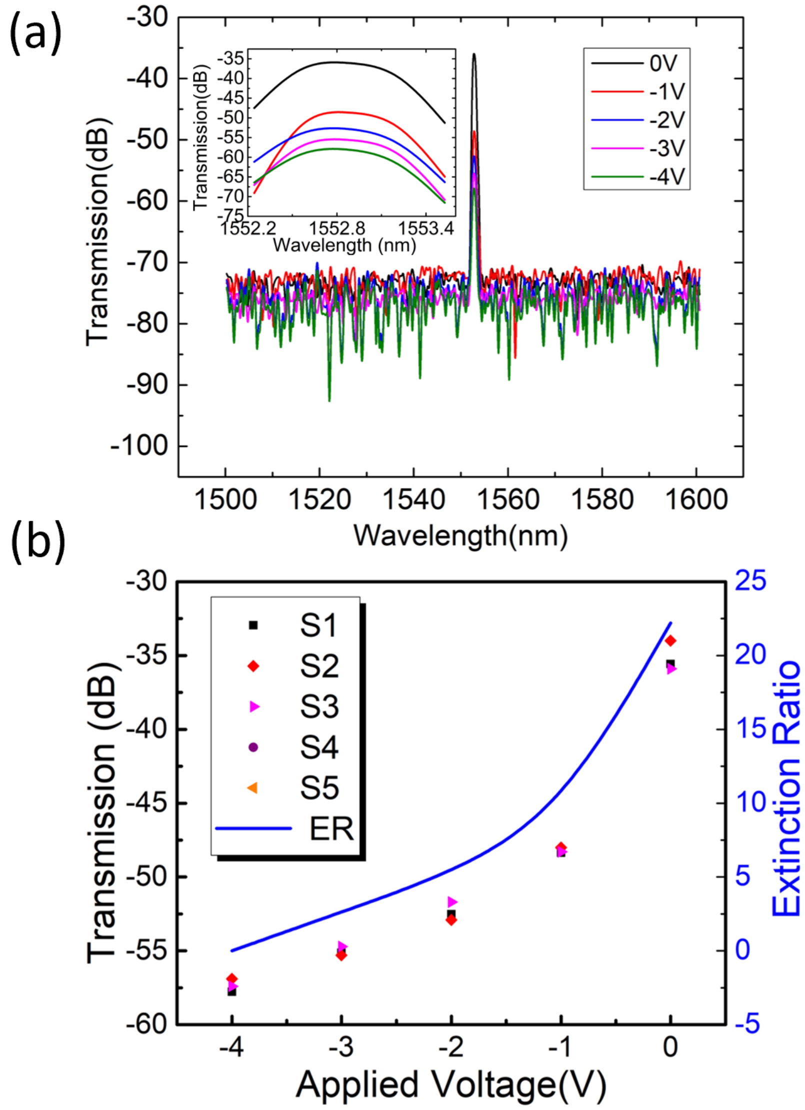

Figure 5.6(a) Experimentally measured transmission spectrum with increasing reverse-bias voltage and inset shows zoom- in image of transmission spectrum at working wavelength (b) graph between extinction ratio verses applied reverse bias at fixed wavelength of 1552 nm and Experimental fitting of transmission versus voltage at a fixed wavelength of 1552 nm for different sets of measurements on five sets of devices.

The output power minimum and maximum are -35.57 dB and -57.77 dB at an applied bias of 0 V and -4 V respectively. inset shows the change of intensity at the working wavelength, and it depicts that the device attains maximum extinction ratio at the wavelength of 1552 nm. Figure 5.6(b) shows the graph between extinction ratio versus applied reverse bias voltages; the extinction ratio of the device is the ratio of maximum power received (at no bias) at the output to the minimum power (at an applied bias of -4 V) received at the output of the device. The device depicts the extinction ratio or modulation depth as 22 dB at the applied voltage of -4 V and the length of the device is 100 µm.

The experiment of tunable absorber is performed for five sets of samples and transmission spectrums are recorded. Figure 5.6(b) shows the experimental fitting of transmission versus voltage for various sets of measurements on five distinct samples at a fixed wavelength of 1552 nm. Fig depicts the variation of the transmission spectrum for applied voltages. The percentage error (variation of transmission spectrum in distinct devices) may be caused by fabrication tolerance and environmental effects during the device fabrication and/or fiber misalignment of chip-to-fiber or fiber-to-chip coupling during measurements.

5.7 Summary

A plasmonic absorber with an electrical tunable based on an engineered Cu-ITO structure with low voltage tuning and high extinction ratio is experimentally demonstrated. Operating at a telecom wavelength of 1.55 µm, the device is composed of a distributed grating based on copper and Indium Tin Oxide (ITO) with a capping ITO layer. The permittivity of the ITO layer changes with applied bias, which results in attenuation of intensity due to variation in the imaginary component of the effective refractive index. We observe that the intensity of light tunes from -35.57 dB to -57.77 by applying the voltage of -4 Volt. the 3 dB modulation bandwidth is 52.2 GHz and the switching energy of the tunable absorber (high to low transmission and vice versa) is 60 p-Joule/bit. our device displays the extinction ratio of. 22 dB at a very low voltage of -4 V for a 100 μm long device. There are several uses of tunable absorbers where the tuning of light absorption is a prime requirement such as intensity modulator, biosensing, imaging, etc.

Chapter – 6

Optical Field Enhanced Plasmonic Absorber

6.1 Introduction

The quest for highly efficient optical devices has driven significant advances in the field of plasmonic tunable absorbers. One promising area of research is the development of optical field-enhanced tunable plasmonic absorbers, particularly those utilizing epsilon-near-zero (ENZ) states in materials such as Indium Tin Oxide (ITO) [162]. These absorbers are designed to leverage unique optical phenomena at subwavelength scales to achieve enhanced performance in applications such as modulation, sensing, imaging and energy harvesting [160].

Plasmonic absorbers utilize the resonance of surface plasmons—collective oscillations of free electrons in metals—interacting with incident light [154-158]. By carefully designing the geometry and materials of these absorbers, it is possible to achieve high absorption efficiencies at specific wavelengths. Subwavelength grating waveguides are a key component in modern optical devices due to their ability to manipulate light at scales smaller than the wavelength of light itself [157]. These structures consist of periodic patterns with features smaller than the wavelength of light, enabling efficient light confinement and propagation [154]. When integrated with plasmonic absorbers, these waveguides can enhance the interaction between light and the material, leading to increased absorption and improved device performance.

Indium Tin Oxide (ITO) is a widely used transparent conductive oxide with notable optical properties. When ITO is engineered to operate near its epsilon-near-zero (ENZ) state, its permittivity approaches zero, resulting in unique optical behaviors such as enhanced field confinement and reduced reflection. The ENZ state allows for substantial enhancement of the optical field within the material, which can be exploited to significantly improve the performance of plasmonic absorbers.

The ability to tune the absorption properties of plasmonic devices is crucial for many applications. By adjusting parameters such as the wavelength of operation or the geometrical configuration of the absorber, it is possible to achieve targeted absorption profiles. The integration of ENZ materials like ITO into these systems provides an additional degree of tunability, allowing for dynamic control over the absorber's performance.

The development of optical field-enhanced tunable plasmonic absorbers on subwavelength grating waveguides using the ENZ state of ITO represents a significant advancement in photonic technology. This approach combines the advantages of subwavelength waveguides, which allow for miniaturized and efficient optical components, with the unique properties of ENZ materials, leading to enhanced performance and new functionalities.

Modern integrated photonics is swiftly advancing towards compact devices that offer a variety of signal processing capabilities [167].

Epsilon-near-zero (ENZ) materials have recently garnered significant interest in the research of plasmonic optics and nanophotonic devices due to their unique optical properties [168-169]. By adjusting the real part of permittivity to approach a near-zero value at certain wavelengths, ENZ materials can easily achieve a near-zero refractive index, n as given by the formula n= $\sqrt{\mu\varepsilon}$ [5-6]. Their near-zero permittivity and refractive index result in exceptional optical properties that surpass those of typical dielectric materials. These include extremely high optical nonlinearity [170-172], significant field intensity enhancement (FIE), improved control over light-matter interactions [140-145], and directional emission.

Among the various optical methods to achieve an ENZ condition, transparent conducting oxides (TCOs) have been extensively studied due to their wide ENZ regions, spanning from ultraviolet to near infrared, their lower costs, and their simpler structural complexity. Indium tin oxide (ITO) is the most widely used type of transparent conductive oxide (TCO), known for its near-infrared epsilon-near-zero (ENZ) region and compatibility with CMOS technology.

In this work device described is an optical field-enhanced tunable plasmonic absorber integrated on a grating waveguide, utilizing the epsilon-near-zero (ENZ) state of indium tin oxide (ITO). This design enables precise control over light absorption and modulation, resulting in notable performance metrics. The device achieves an extinction ratio of 1.9 dB per micron, indicating its effectiveness in modulating light intensity. It offers a modulation depth of 1.9 dB/μm, ensuring substantial contrast between the on and off states. Furthermore, the device supports a 3 dB bandwidth of 72 GHz, which is suitable for high-speed optical communication applications. The energy required per bit for data transmission is remarkably low, at 56.25 femtojoules per bit, highlighting the device's efficiency in terms of power consumption. These attributes make this plasmonic absorber a promising candidate for advanced integrated photonic systems, particularly in applications requiring high-speed, low-energy optical modulation.

6.2 Device Structure & Working

The optical field enhanced tunable plasmonic absorber described here leverages the epsilon-near-zero (ENZ) state of indium tin oxide (ITO) integrated with a subwavelength grating waveguide to achieve remarkable control over light absorption and manipulation at the nanoscale. This device utilizes the unique optical properties of ITO when it approaches its ENZ state, where the dielectric permittivity becomes very small, leading to significant enhancement of the local electromagnetic field. By carefully tuning the ITO's permittivity, we can achieve precise control over the device's absorption characteristics.

The core of this device is the subwavelength grating waveguide, Subwavelength grating waveguides offer significant advantages in photonics by enabling precise control over light propagation at scales smaller than the wavelength of light., allowing for enhanced light confinement and manipulation within a compact footprint. The primary benefits include reduced device size and weight, improved integration with other photonic components, and the ability to achieve strong light-matter interactions. This waveguide facilitates the coupling of light into surface plasmon resonances supported by the ITO layer. The subwavelength grating's periodicity and geometry are meticulously designed to match the wavelength of interest, allowing efficient excitation of plasmonic modes that interact strongly with the incoming light. The grating also helps to enhance the interaction between the optical field and the ITO layer by trapping and guiding light in the vicinity of the material.

The ITO layer, positioned on top of the grating, is engineered to operate near its ENZ state. At this point, the real part of the dielectric permittivity of ITO is close to zero, which significantly amplifies the optical fields localized at the interface. This amplification of the optical field is crucial for achieving high absorption efficiency.

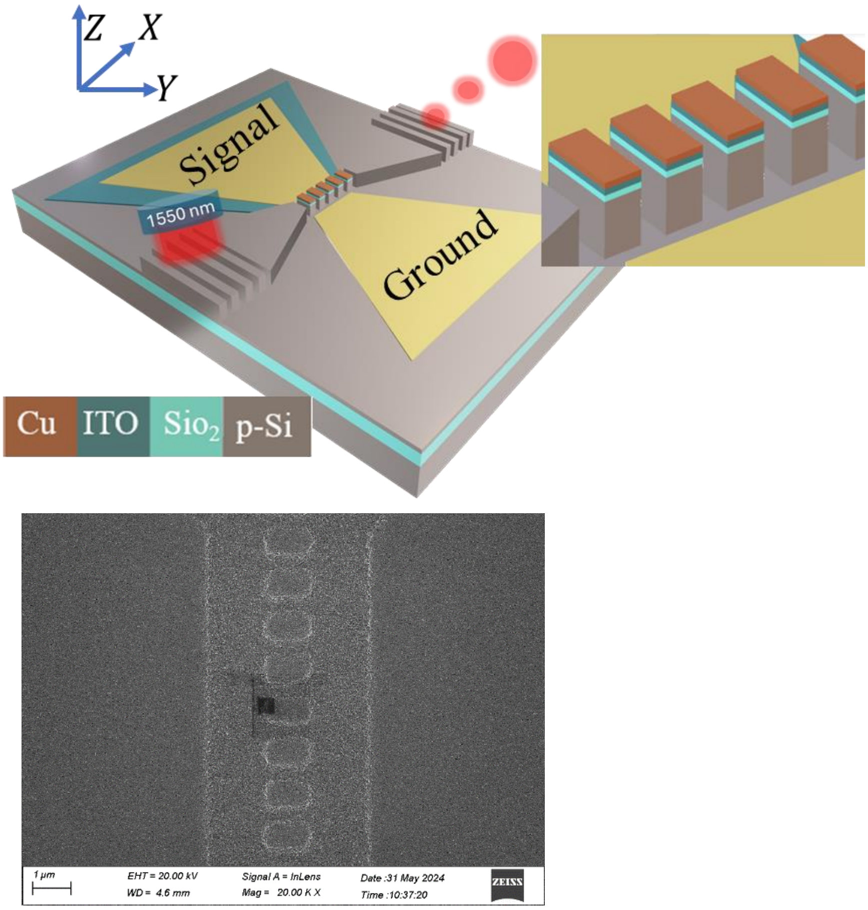

Fig.6.1 3-D diagram of proposed Optical field enhanced tunable plasmonic absorber on subwavelength silicon grating waveguide assisted electrically tunable plasmonic absorber at 1550 nm wavelength on p-type silicon wafer. Si rib waveguide width is 600 nm, Si thickness is 300 nm, oxide thickness is 10 nm, ITO thickness is 40nm, Cu thickness is 40 nm, silicon strip width is 600nm, the Duty cycle is 50% and Plasmonic mode (TM mode) confinement at interface.

The optical field-enhanced tunable plasmonic absorber is designed using a subwavelength grating waveguide structure is shown in figure, The device consists of a periodic array of silicon subwavelength gratings fabricated on a silicon substrate having height 300 nm. These gratings are made from a high-refractive-index silicon material, creating narrow slits that allow for strong confinement and enhancement of the optical field. A thin (10 nm) layer of silicon dioxide is thermally grown, and ITO (40 nm) is deposited over the grating structure using RF- sputtering process, capitalizing on its ENZ properties in the near-infrared region. This configuration enables precise control over the plasmonic resonance, facilitating tunable absorption at 1550 nm wavelength. The optimized parameters of silicon input/output grating coupler to efficiently couple 1550 nm of wavelength is reported in our previous work []. These parameters are taken to fabricate the device to propagate 1550 nm of light. The working principle of the device is based on tuning of permittivity of ITO by applying the electrical bias, when we apply the voltage, the enhanced electric field induced at ITO layer due to boundary condition (permittivity near zero of ITO), in a result the light absorption increase.

6.3 Tuning Mechanism of the Device

In this study, a Lumerical simulation was conducted to analyze the behavior of an epsilon-near-zero (ENZ) device based on indium tin oxide (ITO) under varying carrier concentrations. Initially, the ITO was simulated with a carrier concentration of $4.2\text{x}10^{20}$ cm^{-3}, achieving an ENZ state that exhibited unique optical properties. By applying a voltage of -4 V, the carrier concentration within the ITO layer was modulated, shifting to a new concentration of $6\text{x}10^{20}$ cm^{-3}. This change induced a significant alteration in the optical response of the material, transitioning from its initial ENZ state to a modified state with different refractive index characteristics. The simulation results demonstrated a marked change in light absorption and reflection properties, confirming the effectiveness of electrical tuning in controlling the ENZ behavior of ITO. This electrically tunable ENZ device showcases the potential for dynamic optical modulation in integrated photonic circuits. the tuning mechanism of the device is numerically analyses by using Lumerical simulation tool. Lumerical CHARGE solver is used to analyses electrical characteristic of the device and Lumerical Finite Difference Time Domain (FDTD) is used to analyses optical characteristics of the device. To achieve ENZ state of ITO material at 1550 nm of wavelength. We optimize the doming carrier concentration and tuning voltage at which the plasma frequency of ITO material the propagating light through the device

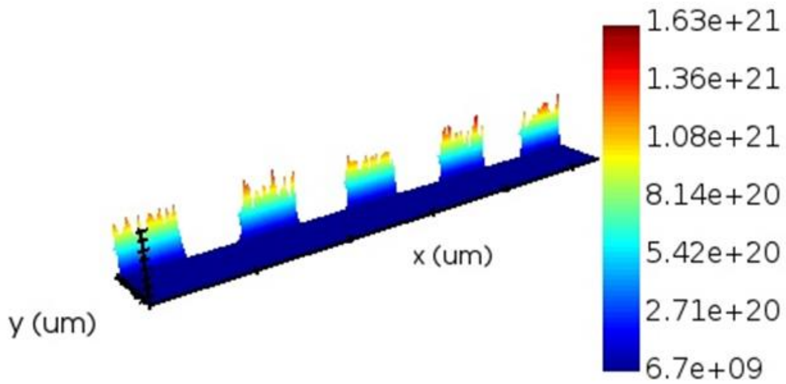

Figure -6.2 this figure shows the variation of charge carrier concentration at applied voltage of -4 V. this depicts the carrier concentration of ITO 6x10^{20} cm^{-3} achieve with applied voltage of -4 V. which matches the plasma frequency at the propagating wavelength of 1550 nm.

we achieved a baseline electric field strength as shown in figure(a) under no bias conditions. This initial simulation provided a detailed understanding of the device's inherent optical properties without any external influence. Upon applying a voltage of -4 V, the electric field strength increased significantly as shown in figure(b) which enhances the absorption of the light. This change demonstrates the device's tunability and responsiveness to electrical modulation. The ability to dynamically control the electric field strength with an applied bias is crucial for applications requiring precise optical manipulation, this simulation confirms the effectiveness of our design in achieving

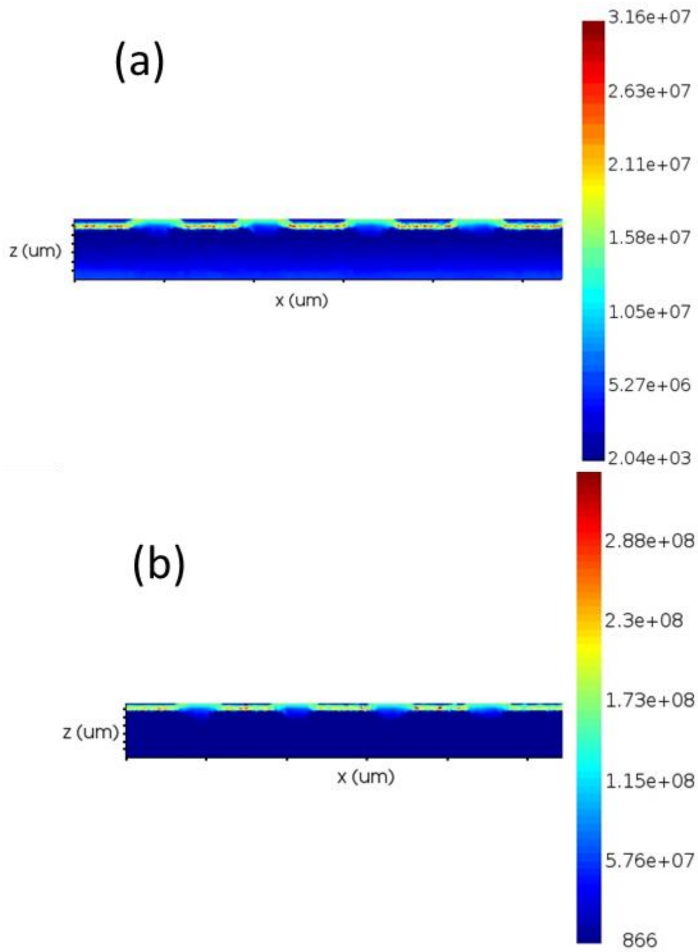

Figure:6.3 this figure shows the electric field strength at applied bias (a) show the electric field at no bias and (b) show the electric field strength at applied bias of -4 V in V/cm

significant electric field modulation, highlighting its potential for advanced photonic applications. After rigorous electrical simulation to achieve carrier concentration of ITO at which it shows the ENZ state of the IITO analyze the optical characteristics of the device using Lumerical FDTD simulation tool. In our study, we utilized Lumerical FDTD simulations to investigate the enhanced electric field strength in a device incorporating indium tin oxide (ITO) with epsilon-near-zero

(ENZ) properties. By applying a voltage of -4 V, we significantly altered the permittivity of the ITO layer, bringing it close to zero. This adjustment in permittivity, coupled with carefully chosen boundary conditions, facilitated the confinement and amplification of the electric field within the device. The ENZ behavior of ITO at -4 V creates an accumulation region where the material exhibits metal-like properties, drastically enhancing the local electric field strength. The simulation results demonstrated that this configuration leads to a substantial increase in field intensity, proving the effectiveness of ENZ materials and optimized boundary conditions in achieving superior performance in photonic devices. This enhancement is particularly beneficial for applications requiring strong light-matter interactions.

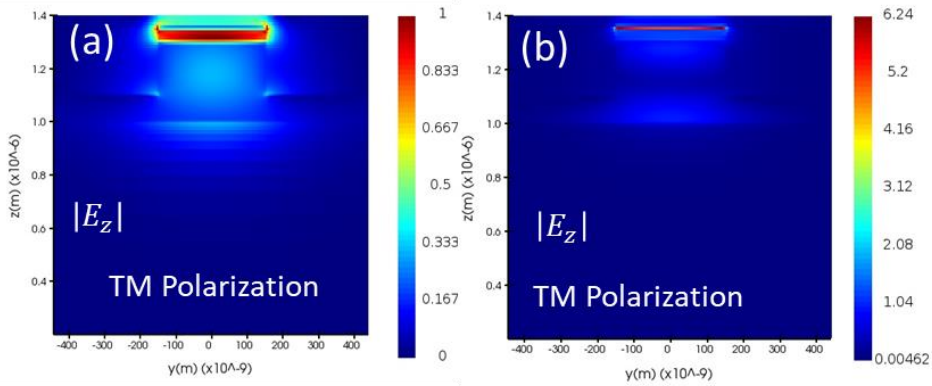

Figure:6.4 this figure(a) shows the electric field strength of the propagating light at applied bias in V/cm (b) show the electric field strength at applied bias of -4 V in V/cm

Figure shows the electric field enhancement of the light at applied voltage of -4 V. in figure (a) show the electric field strength in V/cm at the ITO region and it drastically enhanced as shown in figure (b) which enhance the light absorption in the device. After carefully electrical and optical analysis of the device we concluded that at doping concentration of $4.2x10^{20}cm^{-3}$ of the ITO material we can tune the carrier concentration to $6x10^{20}$ cm^{-3} which depicts plasma frequency at 1550 nm wavelength to achieve maximum tunability of the light.

6.4 Material Processing for ENZ state of ITO

To experimentally verify the strong electro-optic effects in ITO using the ENZ-effect, ITO is deposited on p-type SOI wafer at three distinct oxygen partial-pressure followed by an annealing treatment. Depositing ITO at various oxygen partial-pressure will yield different electron-density in the ITO layer [151]. The optical constants of the ITO layer can be electrically tuned by the variation of its electron charge- density. When the electron charge density of the ITO layer is optimized at a zone where its permittivity is in close proximity to zero i.e., the ENZ-state, a larger change in the attenuation of the ITO can be seen making it a potent-candidate for intensity modulation across 1550 nm with a larger modulation- efficiency [163]. ITO acts as a free-electron Drude material whose optical-attributes are monitored by its motile electron-concentration. The optical permittivity of ITO is given by: The optical permittivity of the ITO is denoted by

$$\boldsymbol{\varepsilon_{ITO}} = \boldsymbol{\varepsilon}_{\infty} - \frac{\omega_p^2}{\omega^2 + i\omega\Gamma} \tag{7.1}$$

$$\omega_p^2 = \frac{N_e^2}{\varepsilon_0 m_{ce}^*} \tag{7.2}$$

Here ε_∞ represents dielectric constant of the material, ω depicts the angular frequency of propagating electromagnetic wave and the carrier collision frequency in the ITO layer of the device is denoted by Γ , ω_p is the plasma frequency of the ITO layer, N_e is electron charge magnitude and m_{ce}^* is the effective mass of the electron [162].

To attain optimal modulation efficiency, the optical properties of the ITO-layer deposited on highly doped p- type SOI wafer at three distinct oxygen partial pressure i.e., i)1 sccm O2 & 40 sccm Ar, ii) 2 sccm O2 & 40 sccm Ar and iii) 0 sccm O2 & 30 sccm Ar are examined. The p-type SOI wafers are ultrasonically cleaned and ion- assisted e-beam deposition unit is utilized to carry out the deposition at an oxygen partial pressure of i) 1 sccm & 40 sccm Ar, ii) 2 sccm & 40 sccm Ar and

iii) 3 sccm & 40 sccm Ar iv) 3 sccm & 40 sccm Ar using a commercially available ITO ceramic target and 99.99% pure. Inside the deposition chamber, the background and working pressure is maintained at 5.7 x 10^{-7} mbar and 7.5 x 10^{-3} mbar, respectively whereas the ion beam voltage and power is kept at 190 V and 80 W, respectively. The deposition is carried out at a rate of 10 nm /min. After the deposition, the wafers are annealed at 200°C for half an hour. The carrier density and conductivity of the deposited ITO films is measured on a room temperature hall-effect measurement set-up having Vander-Pauw geometry at 0.6 Tesla magnetic field and 1 mA current. The deposited ITO thin films as represented in Figure 6.4 exhibits n-type conductivity and the carrier density measured are shown in figure the carrier concentration verses the variation of the partial pressure of the oxygen gas.

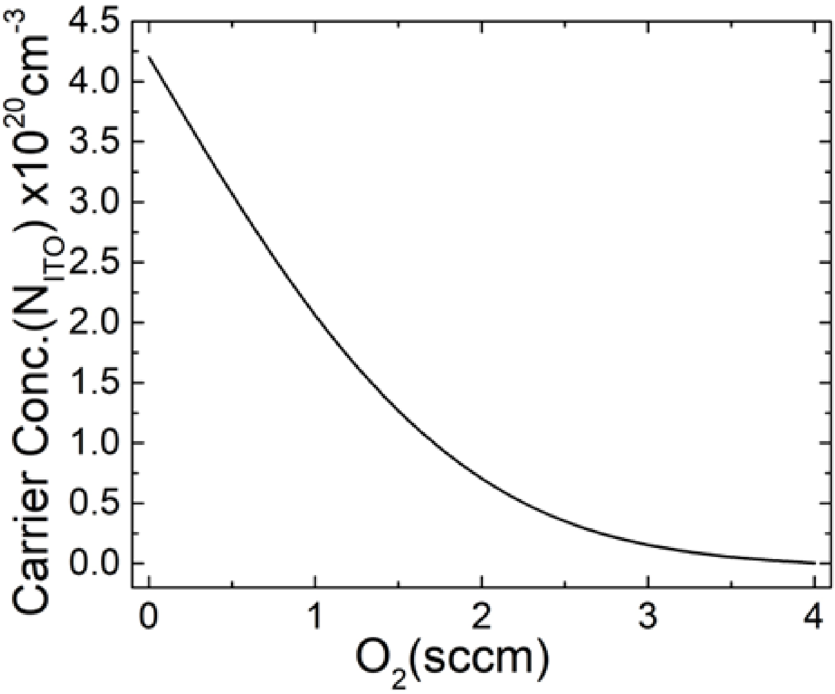

Figure:6.5 this shows the charge carrier density of the ITO material with RF sputtering deposition vs varying the partial pressure of the oxygen gas at 40 sccm of Ar gas at 80 W of RF power.

The permittivity of the ITO comes close to zero as reported in our group [149] there comes a dramatic alteration in the real and imaginary part of the refractive index of ITO. Henceforth, on the ITO coated si wafer with a carrier concentration of 4.2 x $10^{20}/cm^3$, the real and imaginary part of the refractive index with respect to reverse- bias voltage of 4 Volt.

6.5 Fabrication Process of the Device

Fabrication Process of the Tunable Plasmonic absorber is shown in figure. The fabrication process is as fallows

1. Wafer Cleaning: Begin with a silicon wafer and perform a thorough cleaning to remove any contaminants. This typically involves using a series of solvents such as acetone, isopropyl alcohol (IPA), and deionized (DI) water, followed by a drying step using nitrogen gas. Further cleaning can be done using piranha solution (a mixture of sulfuric acid and hydrogen peroxide) to remove organic residues and RCA cleaning to eliminate any remaining particles and metallic impurities.
2. Thermal Oxide Growth: Grow a layer of silicon dioxide (SiO_2) 10nm on the cleaned silicon wafer through thermal oxidation. dry oxidation (using oxygen gas). The thermal oxidation process is performed at high temperature 1050°C) in a furnace to form a uniform oxide layer of desired thickness.
3. ITO Deposition: Deposit a thin film(40nm) of indium tin oxide (ITO) onto the silicon dioxide layer. This can be achieved using techniques RF sputtering at 40 sccm, Ar gas and 80 W RF power.
4. Lithography Patterning: Apply a photoresist layer onto the ITO-coated wafer using spin coating. Soft bake the wafer to evaporate the solvent and harden the photoresist. Develop the exposed photoresist in a developer solution to reveal the pattern on the ITO layer.

5. Selective Removal of Oxide and ITO: wet etching using HCl and DI water (1:4) etching technique to selectively remove the exposed areas of the ITO layer, following the developed photoresist pattern. After the ITO etching, use a buffered oxide etch (BOE) solution or hydrofluoric acid (HF) to selectively etch away the exposed silicon dioxide, leaving behind the patterned ITO and oxide layers.
6. Wet Etching of Silicon: Remove the remaining photoresist using a solvent such as acetone. Perform wet etching of silicon using tetramethylammonium hydroxide (TMAH) solutions.

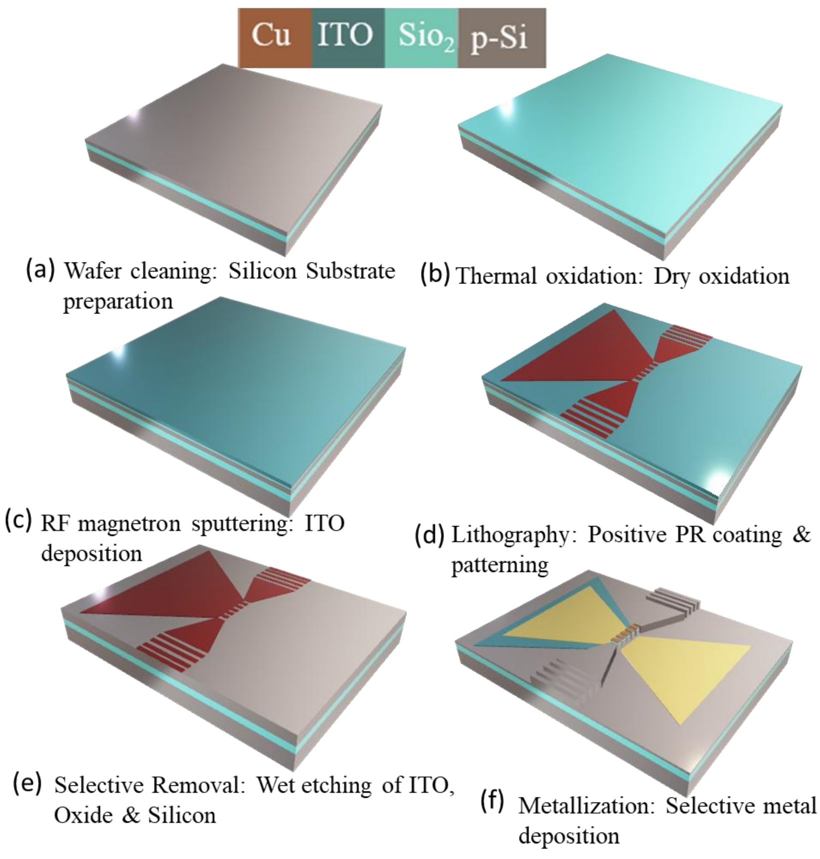

Figure:6.6 (a) Wafer cleaning with acetone, IPA and Pirahna solution (b) Dry oxidation at 1050 °C for oxide growth (c) RF magnetron sputtering for deposition of ITO (d) spin coating of *positive PR and lithography for pattering of structure (e) Wet etching for remove ITO and oxide followed by TMAH wet etching of silicon substrate (f) selective deposition of metal for formation of contact pads.*

7. Repeat the process of lithography for Lift off copper deposited via RF sputtering method
8. Final Steps: Clean the wafer thoroughly to remove any residual chemicals and etchants. Rinse the wafer with DI water and dry it using nitrogen gas. Inspect the wafer using optical microscopy to ensure the patterning and etching processes were successful and the device features are accurately defined.

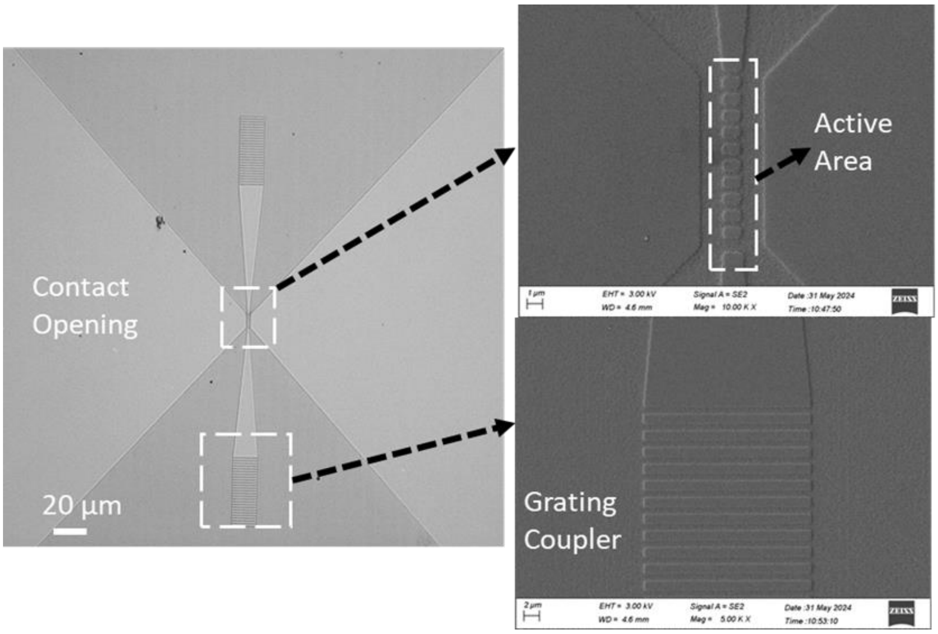

Fig.6.7 Scanning Electron Microscopic (SEM) images of the fabricated device.

6.6 Device Measurement

An illustrative diagram of the optoelectronic measurement setup is shown in Figure 6. The setup includes a highly precise optical spectrum analyzer (OSA), a microscope, a polarization controller, a device under test (DUT), and a tunable laser source operating between

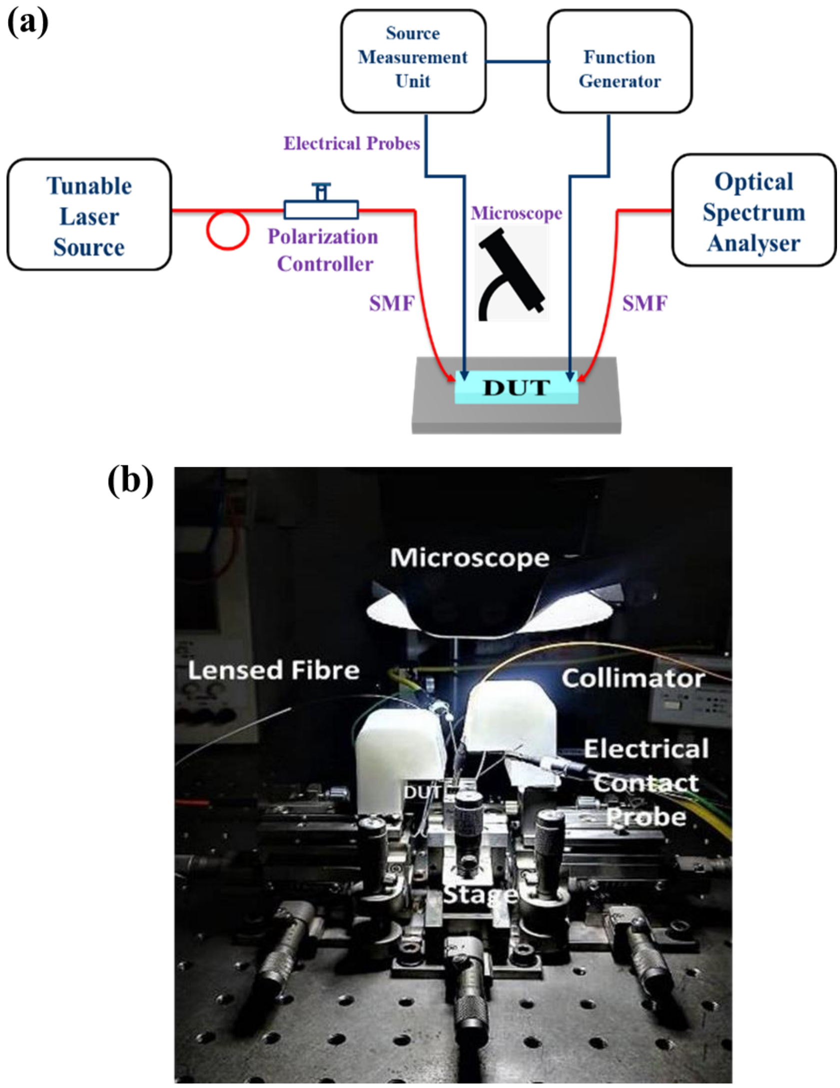

Figure 6.8: (a) An illustrative-representation of the experimental optoelectronic characterization setup composed of tunable laser source, polarization-controller, high resolution optical-spectrum- analyzer, SMF: single mode lensed fiber, vacuum-stage, DUT: device- under-test, source-measurement-unit, function-generator, and an optical-microscope (b) Photograph of the electrical and fiber-optic probe station used for device measurements.

1527 and 1566 nm in wavelength. The polarization controller receives the tunable laser source's fiber-optic output and activates the TM-polarized mode before feeding it via the lensed fiber to the input coupler of the device under test (DUT), i.e., Transmitted light is gathered at the opposite end of the DUT by a silicon-air grating coupler and collimator fiber. To calculate the maximum coupled to power and note that we receive the most power at the output coupler, the single-mode lensed fibers for the input and output are oriented at 0°, 5° and 10° about the test device's surface normal. We receive maximum output power when the input fiber is kept at an angle of 10°. An optical microscope is used to place the electrical probe arms on the contacts with high precision.

6.7 Results and Discussion

Figure 6.8 represents the experimentally measured transmission-spectrum of the fabricated incidence angle 10° with respect to the grating normal. The device is coupled with maximum power at 10^0 angles with normal [149]. The output power is normalized to the input power and plotted in dB. The maximum transmission of -22 dB is calculated at 1550 nm for a 10° angle of incidence form the grating normal. The choice of device is geometry is such that on one hand, it improves the light matter interaction for better modulation efficiency on the other hand it inherits grating type structure allows coupling of free-space light to the waveguide mode.

On applying the reverse-bias voltage on the fabricated device, the ENZ state of the ITO achieve at the applied bias of -4 V and large change of transmission spectrum is seen on Optical Spectrum Analyzer it is due to the absorption of the light The voltage-induced change in the complex effective index changes the intensity of the propagating beam with respect to the reverse-bias in accordance with the ENZ-effect and the

Drude model of ITO. Figure 6.11 (a) exhibits the transmission- spectrum at different reverse-bias voltage where output power is normalized to input power.

The maximum as well as the minimum output power achieved is -22 dB and -41 dB, respectively as shown in figure. The transmission from the fabricated device decreases with the increase in the reverse-bias due to a increment in the attenuation. After further increment of the

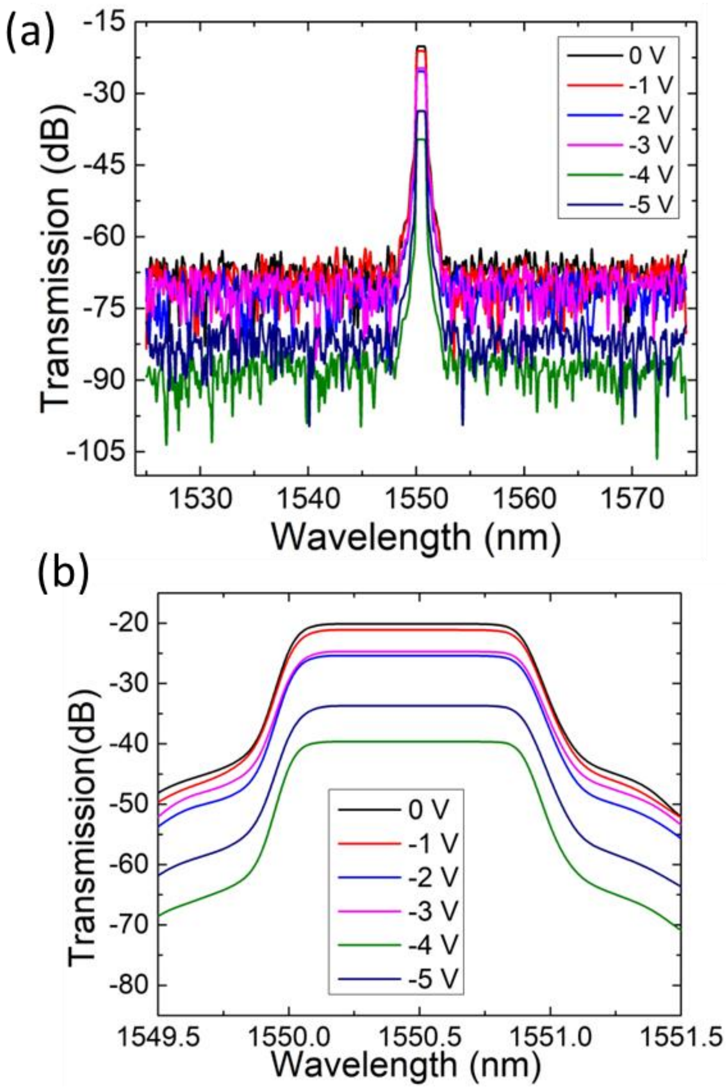

Figure 6.9: (a) Experimentally measured transmission spectrum with increasing reverse bias voltage. (b)The extinction ratio calculated from the transmission spectrum.

voltage to -5 V the transmission of the light further increases due to shift of plasma frequency to another wavelength. Figure 6.11(b) shows the experimental extinction-ratio calculated from the transmission-spectrum

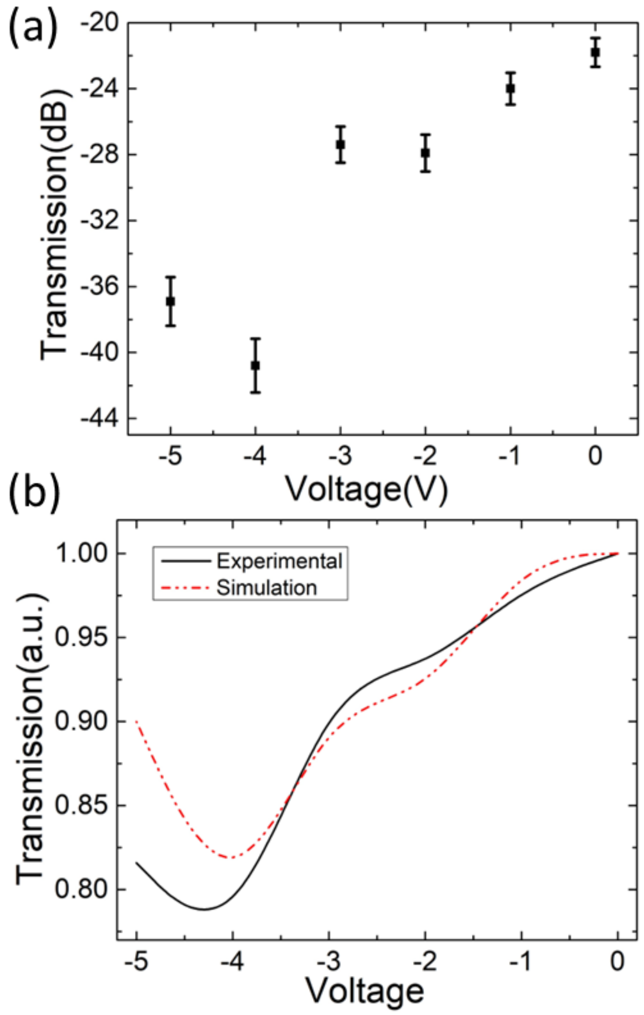

Figure 6.10: (a) Experimental fitting of transmission versus voltage at a fixed wavelength of 1550 nm for different sets of measurements on five sets of devices. The percentage of error may be because of fiber-misalignment or fabrication- tolerance. (b)The transmission spectrum of numerically calculated and experimentally measured

at different reverse-bias voltage. The extinction-ratio calculated is 1.9 dB/micron for the maximum voltage of -4 V and device length of 10 μm. Figure 6.12 (a) depicts the experimental fitting of transmission versus voltage at a fixed wavelength of 1550 nm for a different set of measurements on five different samples. The percentage of error may be because of fiber- misalignment or fabrication-tolerance.

6.8 Summary

The device described is an optical field-enhanced tunable plasmonic absorber integrated on a grating waveguide, utilizing the epsilon-near-zero (ENZ) state of indium tin oxide (ITO). This design enables precise control over light absorption and modulation, resulting in notable performance metrics. The device achieves an extinction ratio of 1.9 dB per micron, indicating its effectiveness in modulating light intensity. It offers a modulation depth of 1.9 dB/μm, ensuring substantial contrast between the on and off states. Furthermore, the device supports a 3 dB bandwidth of 72 GHz, which is suitable for high-speed optical communication applications. The energy required per bit for data transmission is remarkably low, at 56.25 femtojoules per bit, highlighting the device's efficiency in terms of power consumption. These attributes make this plasmonic absorber a promising candidate for advanced integrated photonic systems, particularly in applications requiring high-speed, low-energy optical modulation.

Chapter 7

7.1 Conclusion

This thesis explored the development of low-dimension photonic devices leveraging hybrid materials, focusing on both electrically tunable plasmonic absorbers and optically triggered semiconductor power transistors. The research introduced a highly efficient electrically tunable plasmonic absorber based on Cu-ITO subwavelength grating on a silicon-on-insulator (SOI) platform, optimized for operation at telecom wavelengths (1.55 µm). By utilizing the unique electro-optic properties of indium tin oxide (ITO) combined with copper's plasmonic capabilities, the device demonstrated high extinction ratios and low-voltage operation, paving the way for compact, energy-efficient optical components. In addition, an optically triggered AlGaN/GaN semiconductor power transistor was developed, incorporating a bi-layer anti-reflective structure of SiO_2 and TiO_2 to enhance optical triggering efficiency and overall performance. The transistor's ability to control device current through light intensity offers a significant advancement in power switching applications. Lastly, another plasmonic absorber featuring a Cu-ITO structure on silicon was created, further improving device performance by achieving efficient light confinement, low power consumption, and high optical tunability. Collectively, these contributions demonstrate the potential of hybrid materials and nanostructured designs for advancing photonic devices with applications in telecommunications, sensing, and power electronics.

Silicon photonics provides a promising platform for developing highly scalable and potentially cost-effective on-chip photonic devices. However, challenges such as its weak electro-optic effect, diffraction limit, and poor light-matter interaction led to large device footprints, high power consumption, and low extinction ratios in silicon-based tunable absorbers. These limitations raise doubts about whether silicon alone can meet the performance requirements for compact, highly tunable absorbers. Enhancing silicon photonics with additional materials or finding a cost-effective active material to combine with silicon is essential for achieving these performance goals. Indium tin oxide (ITO) has shown excellent electro-optic properties for efficient light tuning, while copper (Cu) is effective for nanoscale light confinement in plasmonic structures. This thesis explores a Cu-ITO-based tunable plasmonic absorber to achieve high extinction ratios, low voltage tuning, low power consumption, and higher bandwidth devices. Additionally, an optical control power transistor is incorporated due to its advantages over electrically gate-tunable power devices.

The research presents a comprehensive exploration of electrically controlled plasmonic absorbers, integrating copper (Cu) and indium tin oxide (ITO) structures within silicon-on-insulator (SOI) platforms. The work demonstrates both numerically and experimentally that incorporating Cu-ITO subwavelength gratings into waveguides enables highly efficient, tunable absorption at telecom wavelengths around 1.55 μm. The tunable permittivity of n-type ITO allows for significant modulation of optical absorption through applied voltages, with the devices achieving notable performance metrics, including extinction ratios of up to 22 dB and bandwidths exceeding 50 GHz.

Key findings highlight the ability of Cu-ITO structures to confine plasmonic modes efficiently, leading to high extinction ratios, small mode areas, and low power consumption. The epsilon-near-zero (ENZ) state of ITO is also exploited to enhance optical field effects, further improving the modulation depth and speed of the devices. With bandwidths reaching up to 72 GHz and energy efficiencies as low as

56.25 femtojoules per bit, these absorbers demonstrate significant potential for applications in high-speed optical communication, imaging, biosensing, and other nanophotonic devices that require tunable optical absorption.

This research also focusses on optically controlled AlGaN/GaN semiconductor power transistor with a low on-resistance and normally-off high electron mobility 2DEG channel offers a promising solution for efficient power control. By leveraging the photogenerated electron transitions at the n-AlGaN/GaN heterojunction, the device enables precise current control through light intensity modulation. This results in low conduction losses, fast switching capabilities, and minimal on-resistance, making the device highly efficient for power switching applications. The integration of an optical control mechanism enhances performance and provides significant advantages over conventional electrically controlled transistors.

7.2 Future Scope

The success of this research opens several avenues for further exploration and development:

1. **Performance Optimization**: Further refinement of the Cu-ITO grating design can be pursued to enhance absorption efficiency, reduce losses, and improve the quality factor of resonances. Optimization techniques such as machine learning algorithms can be employed to explore a broader parameter space.
2. **Material Innovation**: Investigation of alternative materials or composite structures that combine the benefits of Cu and ITO with other advanced materials (e.g., graphene, transition metal dichalcogenides) could lead to further improvements in performance and functionality.
3. **Advanced Fabrication Techniques:** Further research can focus on optimizing fabrication techniques to achieve even finer

control over the nano structuring of the subwavelength grating waveguide. Techniques such as electron-beam lithography, nanoimprint lithography, and advanced etching methods can be explored to enhance the precision and scalability of the plasmonic absorber.

4. **Broadband and Multi-band Absorbers**: Developing designs that can achieve broadband or multi-band absorption by incorporating additional layers or modifying the grating structure could expand the range of applications, including multi-wavelength optical communication systems and broadband photodetectors.
5. **Thermal and Mechanical Stability**: Assessing and enhancing the thermal and mechanical stability of the plasmonic absorber will be crucial for practical deployment in real-world environments, particularly in high-power or harsh conditions.
6. **Integration with Active Devices**: Exploring the integration of the plasmonic absorber with active optoelectronic components such as modulators, detectors, and light sources can lead to the development of fully integrated photonic circuits with enhanced functionality.
7. **Sensing Applications**: Leveraging the high sensitivity of the designed absorber for biosensing and environmental monitoring applications could be explored, utilizing its tunable properties to detect a wide range of analytes with high specificity and sensitivity.

The development of an optically triggered AlGaN/GaN semiconductor power transistor incorporating a bi-layer anti-reflecting (AR) structure marks a significant advancement in the field of power electronics. The promising results from this research open several avenues for further investigation and development:

1. **Broadband Anti-Reflecting Structures**: Future research can focus on developing broadband AR structures that can operate efficiently over a wider range of wavelengths, enhancing the versatility and application range of the optically triggered transistor.
2. **Integration with Photonic Systems**: Exploring the integration of these optically triggered transistors with advanced photonic systems could lead to the development of more efficient and compact optoelectronic devices, such as optical switches and modulators.
3. **Thermal Management Solutions**: Investigating advanced thermal management techniques will be essential to address the heat dissipation challenges associated with high-power operations, thereby improving the device's longevity and performance.
4. **Alternative Material Systems**: Exploring other wide-bandgap semiconductor materials, such as SiC or diamond, in conjunction with optimized AR structures, may yield devices with even higher performance metrics and broader application potential.
5. **Scalability and Manufacturing**: Addressing the challenges related to the scalability and manufacturability of the bi-layer AR structures and the overall device can pave the way for commercial production and widespread adoption in various industries.
6. **Reliability Testing**: Long-term reliability and robustness testing under different environmental conditions will be crucial to ensure the practical applicability of the developed transistor in real-world scenarios.

By building on the foundation laid by this research, future efforts can continue to push the boundaries of optically triggered semiconductor devices, leading to innovations that can significantly impact the fields of power electronics, telecommunications, and beyond.

In conclusion, the development of an optical field enhanced tunable plasmonic absorber on a subwavelength grating waveguide using the ENZ state of ITO opens up exciting possibilities in photonics. Continued research and development in this area will likely lead to significant technological advancements and a wide range of practical applications, from advanced sensors to integrated photonic circuits.

References:

1. L. Thylén and L. Wosinski, "Integrated photonics in the 21st century," 2014, doi: 10.1364/PRJ.2.000075.
2. "IntegratedPhotonicsSpringerLink." https://link.springer.com/chapter/10.1007/978-3-540-39913 1_2 (accessed Jun. 24, 2021).
3. C. R. Pollock and M. Lipson, *Integrated Photonics*. Boston, MA: Springer US, 2003.
4. F. G. Smith, T. A. King, and D. L. Dawes, "Optics and Photonics: An Introduction," *Cit. Am. J. Phys.*, vol. 69, p. 236, 2001, doi: 10.1119/1.1336840.
5. X. C. Zhang and J. Xu, *Introduction to THz wave photonics*. Springer US, 2010.
6. P. Cheben, R. Halir, J. H. Schmid, H. A. Atwater, and D. R. Smith, "Subwavelength integrated photonics," *Nature,* vol. 560, no. 7720. Nature Publishing Group, pp. 565–572, Aug. 30, 2018, doi: 10.1038/s41586-018-0421-7.
7. H. W. Hübers, "Terahertz technology: Towards THz integrated photonics," *Nat. Photonics*, vol. 4, no. 8, pp. 503–504, Aug. 2010, doi: 10.1038/nphoton.2010.169.
8. M. U. Khan, Y. Xing, Y. Ye, and W. Bogaerts, "Photonic integrated circuit design in a foundry+fabless ecosystem," *IEEE J. Sel. Top. Quantum Electron.*, vol. 25, no. 5, Sep. 2019, doi: 10.1109/JSTQE.2019.2918949.
9. K. Ohashi *et al.*, "On-chip optical interconnect," *Proc. IEEE*, vol. 97, no. 7, pp. 1186–1196, 2009, doi: 10.1109/JPROC.2009.2020331.
10. Wang, Jian, and Yun Long. "On-chip silicon photonic signaling and processing: a review." *Science Bulletin* 63, no. 19 (2018): 1267-1310.

11. Liu, Yitian, and Yaoguang Ma. "One-dimensional plasmonic sensors." *Frontiers in Physics* 8 (2020): 312.
12. Marpaung, David, Jianping Yao, and José Capmany. "Integrated microwave photonics." *Nature photonics* 13, no. 2 (2019): 80-90.
13. https://www.grandviewresearch.com/industry-analysis/silicon-photonics-market
14. Liu, Xiaofeng, Qiangbing Guo, and Jianrong Qiu. "Emerging low-dimensional materials for nonlinear optics and ultrafast photonics." *Advanced Materials* 29, no. 14 (2017): 1605886.
15. Tian, He, Jesse Tice, Ruixiang Fei, Vy Tran, Xiaodong Yan, Li Yang, and Han Wang. "Low-symmetry two-dimensional materials for electronic and photonic applications." *Nano Today* 11, no. 6 (2016): 763-777.
16. Gramotnev, Dmitri K., and Sergey I. Bozhevolnyi. "Plasmonics beyond the diffraction limit." *Nature photonics* 4, no. 2 (2010): 83-91.
17. Lee, Changhyoup, Frederik Dieleman, Jinhyoung Lee, Carsten Rockstuhl, Stefan A. Maier, and Mark Tame. "Quantum plasmonic sensing: beyond the shot-noise and diffraction limit." *Acs Photonics* 3, no. 6 (2016): 992-999.
18. Y. Lai and A. Badolato, "Integrated Nanophotonics with Genetically Designed Photonic Crystal Structures," 2016.
19. G. T. Reed, G. Mashanovich, F. Y. Gardes, and D. J. Thomson, "Silicon optical modulators," *Nature Photonics*, vol. 4, no. 8. pp. 518–526, Aug. 2010, doi: 10.1038/nphoton.2010.179.
20. D. K. Gramotnev and S. I. Bozhevolnyi, "Plasmonics beyond the diffraction limit," *Nature Photonics*, vol. 4, no. 2. pp. 83–91, Feb. 2010, doi: 10.1038/nphoton.2009.282.
21. D. A. B. Miller, "Rationale and challenges for optical

interconnects to electronic chips," *Proc. IEEE*, vol. 88, no. 6, pp. 728–749, 2000, doi: 10.1109/5.867687.

22. D. B. Strukov, G. S. Snider, D. R. Stewart, and R. S. Williams, "The missing memristor found," *Nature*, vol. 453, no. 7191, pp. 80–83, May 2008, doi: 10.1038/nature06932.
23. A. Gee, A. H. Jaafar, and N. T. Kemp, "Optical Memristors: Review of Switching Mechanisms and New Computing Paradigms," *Memristor Comput. Syst.*, pp. 219–244, 2022, doi: 10.1007/978-3-030-90582-8_10.
24. X. Chen, C. Li, and H. K. Tsang, "Device engineering for silicon photonics," *NPG Asia Mater.*, vol. 3, no. 1, pp. 34–40, 2011, doi: 10.1038/asiamat.2010.194.
25. R. Soref, "The Past, Present, and Future of Silicon Photonics," *IEEE J. Sel. Top. Quantum Electron.*, vol. 12, no. 6, pp. 1678–1687, Nov. 2006, doi: 10.1109/JSTQE.2006.883151.
26. V. R. Almeida, Q. Xu, C. A. Barrios, and M. Lipson, "Guiding and confining light in void nanostructure," Opt. Lett., vol. 29, no. 11, p. 1209, Jun. 2004, doi: 10.1364/ol.29.001209.
27. F. Dell'Olio and V. M. Passaro, "Optical sensing by optimized silicon slot waveguides," *Opt. Express*, vol. 15, no. 8, p. 4977, 2007, doi: 10.1364/oe.15.004977.
28. M. Hochberg et al., "Towards a millivolt optical modulator with nano-slot waveguides," Opt. Express, vol. 15, no. 13, p. 8401, 2007, doi: 10.1364/oe.15.008401.
29. J. S. Levy, A. Gondarenko, M. A. Foster, A. C. Turner-Foster, A. L. Gaeta, and M. Lipson, "CMOS-compatible multiple-wavelength oscillator for on-chip optical interconnects," Nat. Photonics, vol. 4, no. 1, pp. 37–40, Jan. 2010, doi: 10.1038/nphoton.2009.259.
30. X. Chen, Y. Chen, Y. Zhao, W. Jiang, and R. T. Chen, "Photonic

Crystal Waveguide Modulator,” *Opt. Lett.*, vol. 34, no. 5, pp. 602–604, 2009.

31. E. Yablonovitch, “E. Burstein et al. (eds.),” vol. 07701, pp. 841–842, 1995.
32. S. John, “Strong localization of photons in certain disordered dielectric superlattices,” *Phys. Rev. Lett.*, vol. 58, no. 23, pp. 2486–2489, 1987, doi: 10.1103/PhysRevLett.58.2486.
33. E. Yablonovitch, T. J. Gmitter, and K. M. Leung, “Photonic band structure: The face-centered-cubic case employing nonspherical atoms,” *Phys. Rev. Lett.*, vol. 67, no. 17, pp. 2295–2298, 1991, doi: 10.1103/PhysRevLett.67.2295.
34. C. Sirtori, S. Barbieri, and R. Colombelli, “Wave engineering with THz quantum cascade lasers,” *Nat. Photonics,* vol. 7, no. 9, pp. 691–701, 2013, doi: 10.1038/nphoton.2013.208.
35. C. Xiang and J. Wang, “Long-Range Hybrid Plasmonic Slot Waveguide,” *IEEE Photonics J.*, vol. 5, no. 2, pp. 4800311–4800311, Apr. 2013, doi: 10.1109/jphot.2013.2256887.
36. Pitarke, J. M., V. M. Silkin, E. V. Chulkov, and P. M. Echenique. "Theory of surface plasmons and surface-plasmon polaritons." *Reports on progress in physics* 70, no. 1 (2006): 1.
37. Hutter, Eliza, and Janos H. Fendler. "Exploitation of localized surface plasmon resonance." *Advanced materials* 16, no. 19 (2004): 1685-1706.
38. Oulton, Rupert F., Volker J. Sorger, D. A. Genov, D. F. P. Pile, and X. Zhang. "A hybrid plasmonic waveguide for subwavelength confinement and long-range propagation." *nature photonics* 2, no. 8 (2008): 496-500.
39. Mayer, Kathryn M., and Jason H. Hafner. "Localized surface plasmon resonance sensors." *Chemical reviews* 111, no. 6 (2011): 3828-3857.

40. Sharma, B. L., and R. K. Purohit. *Semiconductor heterojunctions*. Vol. 5. Elsevier, 2015.
41. Wang, Huanli, Lisha Zhang, Zhigang Chen, Junqing Hu, Shijie Li, Zhaohui Wang, Jianshe Liu, and Xinchen Wang. "Semiconductor heterojunction photocatalysts: design, construction, and photocatalytic performances." *Chemical Society Reviews* 43, no. 15 (2014): 5234-5244.
42. Calow, J. T., P. J. Deasley, S. J. T. Owen, and P. W. Webb. "A review of semiconductor heterojunctions." *Journal of Materials Science* 2 (1967): 88-96.
43. Li, Tingkai, Michael Mastro, and Armin Dadgar, eds. *III–V compound semiconductors: integration with silicon-based microelectronics*. CRC press, 2010.
44. Kamino, Brett A., and Timothy P. Bender. "The use of siloxanes, silsesquioxanes, and silicones in organic semiconducting materials." *Chemical Society Reviews* 42, no. 12 (2013): 5119-5130.
45. Krasavin, Alexey V., and Anatoly V. Zayats. "Silicon-based plasmonic waveguides." *Optics express* 18, no. 11 (2010): 11791-11799.
46. Lee, Jeong K., Kurt B. Smith, Cary M. Hayner, and Harold H. Kung. "Silicon nanoparticles–graphene paper composites for Li ion battery anodes." *Chemical communications* 46, no. 12 (2010): 2025-2027.
47. Khriachtchev, Leonid. *Silicon nanophotonics: basic principles, present status, and perspectives*. CRC Press, 2016.
48. R. Amin *et al.*, “Active material, optical mode and cavity impact on nanoscale electro-optic modulation performance,” *Nanophotonics*, vol. 7, no. 2, pp. 455–472, Oct. 2017, doi: 10.1515/nanoph-2017-0072.

49. M. Z. Alam, I. De Leon, and R. W. Boyd, “Large optical nonlinearity of indium tin oxide in its epsilon-near-zero region,” *Science (80-.).*, vol. 352, no. 6287, pp. 795–797, May 2016, doi: 10.1126/science.aae0330.
50. L. J. Meng and M. P. Dos Santos, “Structure effect on electrical properties of ITO films prepared by RF reactive magnetron sputtering,” *Thin Solid Films*, vol. 289, no. 1–2, pp. 65–69, Nov. 1996, doi: 10.1016/S0040-6090(96)08892-X.
51. J. Bregman, Y. Shapira, and H. Aharoni, “Effects of oxygen partial pressure during deposition on the properties of ion-beam-sputtered indium-tin oxide thin films,” *J. Appl. Phys.*, vol. 67, no. 8, pp. 3750–3753, 1990, doi: 10.1063/1.345017.
52. Liu, Ming, Xiaobo Yin, Erick Ulin-Avila, Baisong Geng, Thomas Zentgraf, Long Ju, Feng Wang, and Xiang Zhang. "A graphene-based broadband optical modulator." *Nature* 474, no. 7349 (2011): 64-67.
53. Armani, Deniz, Bumki Min, Andrea Martin, and Kerry J. Vahala. "Electrical thermo-optic tuning of ultrahigh-Q microtoroid resonators." *Applied physics letters* 85, no. 22 (2004): 5439-5441.
54. Aldous, Matthew, Jonathan Woods, Andrei Dragomir, Ritayan Roy, and Matt Himsworth. "Carrier frequency modulation of an acousto-optic modulator for laser stabilization." *Optics Express* 25, no. 11 (2017): 12830-12838.
55. R. A. Soref and B. R. Bennett, “Electrooptical effects in silicon,” *IEEE Journal of Quantum Electronics*, vol. 23, no. 1. pp. 123–129, 1987, doi: 10.1109/JQE.1987.1073206.
56. M. Qasymeh, M. Cada, and S. A. Ponomarenko, “Quadratic electro-optic Kerr effect: Applications to photonic devices,” *IEEE J. Quantum Electron.*, vol. 44, no. 8, pp. 740–746, 2008,

doi: 10.1109/JQE.2008.924430.

57. E. Feigenbaum, K. Diest, and H. A. Atwater, “Unity-Order Index Change in Transparent Conducting Oxides at Visible Frequencies,” vol. 10, pp. 2111–2116, 2010, doi: 10.1021/nl1006307.
58. G. Sinatkas and E. E. Kriezis, “Silicon-Photonic Electro-Optic Phase Modulators Integrating Transparent Conducting Oxides,” *IEEE J. Quantum Electron.*, vol. 54, no. 4, 2018, doi: 10.1109/JQE.2018.2852144.
59. C. E. Png, S. P. Chan, S. T. Lim, and G. T. Reed, “Optical phase modulators for MHz and GHz modulation in silicon-on-insulator (SOI),” *J. Light. Technol.*, vol. 22, no. 6, pp. 1573–1582, Jun. 2004, doi: 10.1109/JLT.2004.827655.
60. C. K. Tang and G. T. Reed, “Highly efficient optical phase modulator in SOI waveguides,” *Electron. Lett.*, vol. 31, no. 6, pp. 451–452, Mar. 1995, doi: 10.1049/el:19950328.
61. G. Sinatkas and E. E. Kriezis, “Silicon-Photonic Electro-Optic Phase Modulators Integrating Transparent Conducting Oxides,” *IEEE J. Quantum Electron.*, vol. 54, no. 4, 2018, doi: 10.1109/JQE.2018.2852144.
62. X. Zhang *et al.*, “High Performance Optical Modulator Based on Electro-Optic Polymer Filled Silicon Slot Photonic Crystal Waveguide,” *J. Light. Technol.*, vol. 34, no. 12, pp. 2941–2951, Jun. 2016, doi: 10.1109/JLT.2015.2471853.
63. Rajput, Swati, Vishal Kaushik, Prem Babu, Pragya Tiwari, Arvind K. Srivastava, and Mukesh Kumar. "Optical modulation via coupling of distributed semiconductor heterojunctions in a Si-ITO-based subwavelength grating." Physical Review Applied 15, no. 5 (2021): 054029.
64. Park, Junghyun, Ju-Hyung Kang, Xiaoge Liu, and Mark L.

Brongersma. "Electrically tunable epsilon-near-zero (ENZ) metafilm absorbers." *Scientific reports* 5, no. 1 (2015): 15754.

65. Mirshafieyan, Seyed Sadreddin, and Don A. Gregory. "Electrically tunable perfect light absorbers as color filters and modulators." *Scientific reports* 8, no. 1 (2018): 2635.
66. Q. Gao, E. Li, and A. X. Wang, “Ultra-compact and broadband electro-absorption modulator using an epsilon-near-zero conductive oxide,” Photonics Res., vol. 6, no. 4, p. 277, Apr. 2018, doi: 10.1364/prj.6.000277.
67. R. Amin, J. B. Khurgin, and V. J. Sorger, “Waveguide-based electro-absorption modulator performance: comparative analysis,” *Opt. Express*, vol. 26, no. 12, p. 15445, Jun. 2018, doi: 10.1364/oe.26.015445.
68. A. P. Vasudev, J.-H. Kang, J. Park, X. Liu, and M. L. Brongersma, “Electro-optical modulation of a silicon waveguide with an ‘epsilon-near-zero’ material,” *Opt. Express*, vol. 21, no. 22, p. 26387, Nov. 2013, doi: 10.1364/oe.21.026387.
69. Mazumder, Sudip K., and Tirthajyoti Sarkar. "Optically activated gate control for power electronics." *IEEE Transactions on Power Electronics* 26, no. 10 (2009): 2863-2886.
70. Mojab, Alireza, and Sudip K. Mazumder. "Low on-state voltage optically triggered power transistor for SiC emitter turn-off thyristor." *IEEE Electron Device Letters* 36, no. 5 (2015): 484-486.
71. Riazmontazer, Hossein, and Sudip K. Mazumder. "Optically switched-drive-based unified independent dv/dt and di/dt control for turn-off transition of power MOSFETs." *IEEE Transactions on Power Electronics* 30, no. 4 (2014): 2338-2349.
72. Cao, L., White, J.S., Park, J.S., Schuller, J.A., Clemens, B.M. and Brongersma, M.L., 2009. Engineering light absorption in

semiconductor nanowire devices. Nature materials, 8(8), pp.643-647, https://doi.org/10.1038/nmat2477

73. Baffou, G. and Quidant, R., 2013. Thermo-plasmonics: using metallic nanostructures as nano-sources of heat. Laser & Photonics Reviews, 7(2), pp.171-187, https://doi.org/10.1002/lpor.201200003
74. Anker, J.N., Hall, W.P., Lyandres, O., Shah, N.C., Zhao, J. and Van Duyne, R.P., 2010. Biosensing with plasmonic nanosensors. Nanoscience and Technology: A Collection of Reviews from Nature Journals, pp.308-319, https://doi.org/10.1142/9789814287005_0032
75. Adato, R. and Altug, H., 2013. In-situ ultra-sensitive infrared absorption spectroscopy of biomolecule interactions in real time with plasmonic nanoantennas. Nature communications, 4(1), pp.1-10, https://doi.org/10.1038/ncomms3154
76. Zhang, R., Zhang, Y., Dong, Z.C., Jiang, S., Zhang, C., Chen, L.G., Zhang, L., Liao, Y., Aizpurua, J., Luo, Y.E. and Yang, J.L., 2013. Chemical mapping of a single molecule by plasmon-enhanced Raman scattering. Nature, 498(7452), pp.82-86, https://doi.org/10.1038/nature12151
77. Atwater, H.A. and Polman, A., 2011. Plasmonics for improved photovoltaic devices. Materials for sustainable energy: a collection of peer-reviewed research and review articles from Nature Publishing Group, pp.1-11, https://doi.org/10.1142/9789814317665_0001
78. Hägglund, C., Zeltzer, G., Ruiz, R., Thomann, I., Lee, H.B.R., Brongersma, M.L. and Bent, S.F., 2013. Self-assembly based plasmonic arrays tuned by atomic layer deposition for extreme visible light absorption. Nano letters, 13(7), pp.3352-3357, https://doi.org/10.1021/nl401641v

79. Kim, S.J., Thomann, I., Park, J., Kang, J.H., Vasudev, A.P. and Brongersma, M.L., 2014. Light trapping for solar fuel generation with Mie resonances. Nano letters, 14(3), pp.1446-1452, https://doi.org/10.1021/nl404575e
80. Landy, N.I., Sajuyigbe, S., Mock, J.J., Smith, D.R. and Padilla, W.J., 2008. Perfect metamaterial absorber. Physical review letters, 100(20), p.207402, https://doi.org/10.1103/PhysRevLett.100.207402
81. Liu, N., Mesch, M., Weiss, T., Hentschel, M. and Giessen, H., 2010. Infrared perfect absorber and its application as plasmonic sensor. Nano letters, 10(7), pp.2342-2348, https://doi.org/10.1021/nl9041033
82. Zhou, H., Ding, F., Jin, Y. and He, S., 2011. Terahertz metamaterial modulators based on absorption. Progress In Electromagnetics Research, 119, pp.449-460, doi:10.2528/PIER11061304
83. Zhang, B., Zhao, Y., Hao, Q., Kiraly, B., Khoo, I.C., Chen, S. and Huang, T.J., 2011. Polarization-independent dual-band infrared perfect absorber based on a metal-dielectric-metal elliptical nanodisk array. Optics express, 19(16), pp.15221-15228, https://doi.org/10.1364/OE.19.015221
84. Aydin, K., Ferry, V.E., Briggs, R.M. and Atwater, H.A., 2011. Broadband polarization-independent resonant light absorption using ultrathin plasmonic super absorbers. Nature communications, 2(1), pp.1-7, https://doi.org/10.1038/ncomms1528
85. Hendrickson, J., Guo, J., Zhang, B., Buchwald, W. and Soref, R., 2012. Wideband perfect light absorber at midwave infrared using multiplexed metal structures. Optics letters, 37(3), pp.371-373, https://doi.org/10.1364/OL.37.000371

86. Cui, Y., Fung, K.H., Xu, J., Ma, H., Jin, Y., He, S. and Fang, N.X., 2012. Ultrabroadband light absorption by a sawtooth anisotropic metamaterial slab. Nano letters, 12(3), pp.1443-1447, https://doi.org/10.1021/nl204118h
87. Feng, N.N., Brongersma, M.L. and Dal Negro, L., 2007. Metal–dielectric slot-waveguide structures for the propagation of surface plasmon polaritons at 1.55$\mu {\hbox {m}} $. IEEE Journal of Quantum Electronics, 43(6), pp.479-485, 10.1109/JQE.2007.897913
88. Bian, Y. and Gong, Q., 2014. Bow-tie hybrid plasmonic waveguides. Journal of Lightwave Technology, 32(23), pp.4504-4509.
89. Grandidier, J., Des Francs, G.C., Massenot, S., Bouhelier, A., Markey, L., Weeber, J.C., Finot, C. and Dereux, A., 2009. Gain-assisted propagation in a plasmonic waveguide at telecom wavelength. Nano letters, 9(8), pp.2935-2939, https://doi.org/10.1021/nl901314u
90. Oulton, R.F., Sorger, V.J., Genov, D.A., Pile, D.F.P. and Zhang, X., 2008. A hybrid plasmonic waveguide for subwavelength confinement and long-range propagation. nature photonics, 2(8), pp.496-500, https://doi.org/10.1038/nphoton.2008.131
91. Feigenbaum, E., Diest, K. and Atwater, H.A., 2010. Unity-order index change in transparent conducting oxides at visible frequencies. Nano letters, 10(6), pp.2111-2116, https://doi.org/10.1021/nl1006307
92. Kou, Y., Ye, F. and Chen, X., 2011. Low-loss hybrid plasmonic waveguide for compact and high-efficient photonic integration. Optics express, 19(12), pp.11746-11752, https://doi.org/10.1364/OE.19.011746
93. Gao, L., Tang, L., Hu, F., Guo, R., Wang, X. and Zhou, Z., 2012.

Active metal strip hybrid plasmonic waveguide with low critical material gain. Optics express, 20(10), pp.11487-11495, https://doi.org/10.1364/OE.20.011487

94. Schuller, J.A., Barnard, E.S., Cai, W., Jun, Y.C., White, J.S. and Brongersma, M.L., 2010. Plasmonics for extreme light concentration and manipulation. Nature materials, 9(3), pp.193-204, https://doi.org/10.1038/nmat2630
95. Rajput, S., Kaushik, V., Jain, S., Tiwari, P., Srivastava, A.K. and Kumar, M., 2019. Optical modulation in hybrid waveguide based on Si-ITO heterojunction. Journal of Lightwave Technology, 38(6), pp.1365-1371, 10.1109/JLT.2019.2953690
96. Png, C.E., Chan, S.P., Lim, S.T. and Reed, G.T., 2004. Optical phase modulators for MHz and GHz modulation in silicon-on-insulator (SOI). Journal of lightwave technology, 22(6), p.1573, 10.1109/JLT.2004.827655
97. Tang, C.K. and Reed, G.T., 1995. Highly efficient optical phase modulator in SOI waveguides. Electronics letters, 31(6), pp.451-452.
98. Jain, S., Rajput, S., Kaushik, V. and Kumar, M., 2019. High speed optical modulator based on silicon slotted-rib waveguide. Optics Communications, 434, pp.49-53, https://doi.org/10.1016/j.optcom.2018.10.028
99. Tang, C.K., Reed, G.T., Walton, A.J. and Rickman, A.G., 1994. Low-loss, single-model optical phase modulator in SIMOX material. Journal of lightwave technology, 12(8), pp.1394-1400, 10.1109/50.317527
100. Park, J., Kang, J.H., Kim, S.J., Liu, X. and Brongersma, M.L., 2017. Dynamic reflection phase and polarization control in metasurfaces. Nano letters, 17(1), pp.407-413, https://doi.org/10.1021/acs.nanolett.6b04378

101. Huang, Y.W., Lee, H.W.H., Sokhoyan, R., Pala, R.A., Thyagarajan, K., Han, S., Tsai, D.P. and Atwater, H.A., 2016. Gate-tunable conducting oxide metasurfaces. Nano letters, 16(9), pp.5319-5325, https://doi.org/10.1021/acs.nanolett.6b00555
102. Rajput, S., Kaushik, V., Babu, P., Tiwari, P., Srivastava, A.K. and Kumar, M., 2021. Optical Modulation via Coupling of Distributed Semiconductor Heterojunctions in a Si-ITO-Based Subwavelength Grating. Physical Review Applied, 15(5), p.054029, https://doi.org/10.1103/PhysRevApplied.15.054029
103. Huang, Y.Z., Pan, Z. and Wu, R.H., 1996. Analysis of the optical confinement factor in semiconductor lasers. Journal of applied physics, 79(8), pp.3827-3830, https://doi.org/10.1063/1.361809
104. Dorodnyy, A., Salamin, Y., Ma, P., Plestina, J.V., Lassaline, N., Mikulik, D., Romero-Gomez, P., i Morral, A.F. and Leuthold, J., 2018. Plasmonic photodetectors. IEEE Journal of Selected Topics in Quantum Electronics, 24(6), pp.1-13, 10.1109/JSTQE.2018.2840339
105. Kaushik, V., Rajput, S., Srivastav, S., Singh, L., Babu, P., Heidari, E., Ahmed, M., Al-Hadeethi, Y., Dalir, H., Sorger, V.J. and Kumar, M., 2021. On-chip nanophotonic broadband wavelength detector with 2D-Electron gas. Nanophotonics, https://doi.org/10.1515/nanoph-2021-0365
106. Rajput, S., Kaushik, V., Singh, L., Pandey, S.S.K., Mishra, R.D. and Kumar, M., 2021. Efficient Photodetector Based on Sub-Bandgap Transition in Silicon-ITO Distributed-Heterojunctions. Journal of Lightwave Technology, 39(21), pp.6886-6892, 10.1109/JLT.2021.3106451
107. Chen, L., Liao, D.G., Guo, X.G., Zhao, J.Y., Zhu, Y.M. and

Zhuang, S.L., 2019. Terahertz time-domain spectroscopy and micro-cavity components for probing samples: a review. Frontiers of Information Technology & Electronic Engineering, 20(5), pp.591-607. https://doi.org/10.1631/FITEE.1800633

108. Chen, L., Xu, N., Singh, L., Cui, T., Singh, R., Zhu, Y. and Zhang, W., 2017. Defect-induced Fano resonances in corrugated plasmonic metamaterials. Advanced Optical Materials, 5(8), p.1600960. https://doi.org/10.1002/adom.201600960

109. Millan J, Godignon P, Perpiñà X, Pérez-Tomás A, Rebollo J. A survey of wide bandgap power semiconductor devices. IEEE transactions on Power Electronics. 2013 Jun 14;29(5):2155-63.

110. Bartolomeo L, Abbatelli L, Macauda M, Di Giovanni F, Catalisano G, Ryzek M, Kohout D. Wide band gap materials: revolution in automotive power electronics. InInternational Electric Vehicle Technology & Automobile Power Electronics Japan Conference (EVTec & APE Japan 2016) 2016 May 26.

111. Mahaboob I, Yakimov M, Hogan K, Rocco E, Tozier S, Shahedipour-Sandvik F. Dynamic control of AlGaN/GaN HEMT characteristics by implementation of a p-GaN body-diode-based back-gate. IEEE Journal of the Electron Devices Society. 2019 May 6; 7:581-8.

112. Shi Y, Huang S, Bao Q, Wang X, Wei K, Jiang H, Li J, Zhao C, Li S, Zhou Y, Gao H. Normally OFF GaN-on-Si MIS-HEMTs fabricated with LPCVD-SiN x passivation and high-temperature gate recess. IEEE Transactions on Electron Devices. 2016 Jan 6;63(2):614-9.

113. Wei J, Liu S, Li B, Tang X, Lu Y, Liu C, Hua M, Zhang Z, Tang G, Chen KJ. Low on-resistance normally-off GaN double-channel metal–oxide–semiconductor high-electron-mobility transistor. IEEE Electron Device Letters. 2015 Oct

9;36(12):1287-90.

114. Tang Z, Jiang Q, Lu Y, Huang S, Yang S, Tang X, Chen KJ. 600-V Normally Off ${\rm SiN} _ {x} $/AlGaN/GaN MIS-HEMT With Large Gate Swing and Low Current Collapse. IEEE Electron Device Letters. 2013 Sep 17;34(11):1373-5.

115. Saito W, Takada Y, Kuraguchi M, Tsuda K, Omura I. Recessed-gate structure approach toward normally off high-voltage AlGaN/GaN HEMT for power electronics applications. IEEE Transactions on electron devices. 2006 Jan 23;53(2):356-62.

116. Baltynov T, Narayanan ES. Simulation Study of AlGaN/GaN-based Optically controlled Power Transistor. InProc. ISPS 2014.

117. Mojab A, Hemmat Z, Riazmontazer H, Rahnamaee A. Introducing optical cascode GaN HEMT. IEEE Transactions on Electron Devices. 2017 Feb 6;64(3):796-804.

118. Ozpineci B, Tolbert LM. Comparison of wide-bandgap semiconductors for power electronics applications. United States. Department of Energy; 2004 Jan 2.

119. Millan J. A review of WBG power semiconductor devices. InCAS 2012 (International Semiconductor Conference) 2012 Oct 15 (Vol. 1, pp. 57-66). IEEE.

120. Kaushik V, Rajput S, Shrivastava S, Jain S, Singh L, Kumar M. Efficient sub-bandgap photodetection via two-dimensional electron gas in ZnO based heterojunction. Journal of Lightwave Technology. 2020 Nov 1;38(21):6031-7.

121. Kaushik V, Rajput S, Kumar M. Broadband optical modulation in a zinc-oxide-based heterojunction via optical lifting. Optics Letters. 2020 Jan 15;45(2):363-6.

122. A. Meyer, S. K. Mazumder and H. Riazmontazer, "Optical control of 1200-V and 20-A SiC MOSFET," 2012 Twenty-Seventh Annual IEEE Applied Power Electronics Conference

and Exposition (APEC), 2012, pp. 2530-2533, doi: 10.1109/APEC.2012.6166179.

123. Li J, Lu Y, Lan P, Zhang X, Xu W, Tan R, Song W, Choy KL. Design, preparation, and durability of TiO2/SiO2 and ZrO2/SiO2 double-layer antireflective coatings in crystalline silicon solar modules. Solar Energy. 2013 Mar 1;89:134-42.

124. Richards BS, Rowlands SF, Ueranatasun A, Cotter JE, Honsberg CB. Potential cost reduction of buried-contact solar cells through the use of titanium dioxide thin films. Solar Energy. 2004 Jan 1;76(1-3):269-76.

125. Pandey SK, Rajput S, Kaushik V, Babu P, Dev Mishra R, Kumar M. Electrically Tunable Plasmonic Absorber Based On Cu-ITO Subwavelength Grating On SOI At Telecom Wavelength. Plasmonics. 2022 May 19:1-8.

126. Rajput S, Kaushik V, Babu P, Tiwari P, Srivastava AK, Kumar M. Optical modulation via coupling of distributed semiconductor heterojunctions in a Si-ITO-based subwavelength grating. Physical Review Applied. 2021 May 13;15(5):054029.

127. Rajput S, Kaushik V, Singh L, Pandey SS, Mishra RD, Kumar M. Efficient photodetector based on sub-bandgap transition in silicon-ITO distributed-heterojunctions. Journal of Lightwave Technology. 2021 Nov 1;39(21):6886-92.

128. Zhao, Shuangyi, Zhenglin Jia, Yian Huang, Qingkai Qian, Qianqian Lin, and Zhigang Zang. "Solvent-Free Synthesis of Inorganic Rubidium Copper Halides for Efficient Wireless Light Communication and X-Ray Imaging." Advanced Functional Materials (2023): 2305858.

129. Guan, H., Zhao, S., Wang, H., Yan, D., Wang, M. and Zang, Z., 2020. Room temperature synthesis of stable single silica-coated

CsPbBr3 quantum dots combining tunable red emission of Ag–In–Zn–S for High-CRI white light-emitting diodes. Nano Energy, 67, p.104279.

130. Yan, Dongdong, Shuangyi Zhao, Yubo Zhang, Huaxin Wang, and Zhigang Zang. "Highly efficient emission and high-CRI warm white light-emitting diodes from ligand-modified CsPbBr 3 quantum dots." Opto-Electronic Advances 5, no. 1 (2022): 200075-1.

131. Liu, Na, Martin Mesch, Thomas Weiss, Mario Hentschel, and Harald Giessen. "Infrared perfect absorber and its application as plasmonic sensor." Nano letters 10, no. 7 (2010): 2342-2348.

132. Zhang, Yubin, Chunlian Cen, Cuiping Liang, Zao Yi, Xifang Chen, Meiwen Li, Zigang Zhou, Yongjian Tang, Yougen Yi, and Guangfu Zhang. "Dual-band switchable terahertz metamaterial absorber based on metal nanostructure." Results in Physics 14 (2019): 102422.

133. Minin, Igor V., and Oleg V. Minin. "Terahertz artificial dielectric cuboid lens on substrate for super-resolution images." Optical and Quantum Electronics 49, no. 10 (2017): 326.

134. Linic, Suljo, Phillip Christopher, and David B. Ingram. "Plasmonic-metal nanostructures for efficient conversion of solar to chemical energy." Nature materials 10, no. 12 (2011): 911-921.

135. Bruck, Roman, and Otto L. Muskens. "Plasmonic nanoantennas as integrated coherent perfect absorbers on SOI waveguides for modulators and all-optical switches." Optics express 21, no. 23 (2013): 27652-27661.

136. Lee, Kyu-Tae, Sungyong Seo, and L. Jay Guo. "High-Color-Purity Subtractive Color Filters with a Wide Viewing Angle Based on Plasmonic Perfect Absorbers." Advanced Optical

Materials 3, no. 3 (2015): 347-352.

137. Yu, Peng, Lucas V. Besteiro, Yongjun Huang, Jiang Wu, Lan Fu, Hark H. Tan, Chennupati Jagadish, Gary P. Wiederrecht, Alexander O. Govorov, and Zhiming Wang. "Broadband metamaterial absorbers." Advanced Optical Materials 7, no. 3 (2019): 1800995.
138. Zhu, Hong-Fu, Liang-Hui Du, Jiang Li, Qi-Wu Shi, Bo Peng, Ze-Ren Li, Wan-Xia Huang, and Li-Guo Zhu. "Near-perfect terahertz wave amplitude modulation enabled by impedance matching in VO2 thin films." Applied Physics Letters 112, no. 8 (2018): 081103.
139. Kocer, Hasan, Serkan Butun, Edgar Palacios, Zizhuo Liu, Sefaattin Tongay, Deyi Fu, Kevin Wang, Junqiao Wu, and Koray Aydin. "Intensity tunable infrared broadband absorbers based on VO2 phase transition using planar layered thin films." Scientific reports 5, no. 1 (2015): 13384.
140. Shu, Shiwei, Zhe Li, and Yang Yang Li. "Triple-layer Fabry-Perot absorber with near-perfect absorption in visible and near-infrared regime." Optics express 21, no. 21 (2013): 25307-25315.
141. Ding, Fei, Lei Mo, Jianfei Zhu, and Sailing He. "Lithography-free, broadband, omnidirectional, and polarization-insensitive thin optical absorber." Applied Physics Letters 106, no. 6 (2015): 061108.
142. Yao, Lin, Zhe Qu, Zili Pang, Jing Li, Siyao Tang, Junhui He, and Lili Feng. "Three-layered hollow nanospheres based coatings with ultrahigh-performance of energy-saving, antireflection, and self-cleaning for smart windows." Small 14, no. 34 (2018): 1801661.
143. Liu, Guiqiang, Jian Chen, Pingping Pan, and Zhengqi Liu.

"Hybrid metal-semiconductor meta-surface-based photo-electronic perfect absorber." IEEE Journal of Selected Topics in Quantum Electronics 25, no. 3 (2018): 1-7.

144. Le, Fei, Daniel W. Brandl, Yaroslav A. Urzhumov, Hui Wang, Janardan Kundu, Naomi J. Halas, Javier Aizpurua, and Peter Nordlander. "Metallic nanoparticle arrays: a common substrate for both surface-enhanced Raman scattering and surface-enhanced infrared absorption." ACS nano 2, no. 4 (2008): 707-718.

145. Landy, N. Iê, S. Sajuyigbe, Jack J. Mock, David R. Smith, and Willie J. Padilla. "Perfect metamaterial absorber." Physical review letters 100, no. 20 (2008): 207402.

146. Zhou, Hao, Fei Ding, Yi Jin, and Sailing He. "Terahertz metamaterial modulators based on absorption." Progress In Electromagnetics Research 119 (2011): 449-460.

147. Zhang, Bingxin, Yanhui Zhao, Qingzhen Hao, Brian Kiraly, Iam-Choon Khoo, Shufen Chen, and Tony Jun Huang. "Polarization-independent dual-band infrared perfect absorber based on a metal-dielectric-metal elliptical nanodisk array." Optics express 19, no. 16 (2011): 15221-15228.

148. Aydin, Koray, Vivian E. Ferry, Ryan M. Briggs, and Harry A. Atwater. "Broadband polarization-independent resonant light absorption using ultrathin plasmonic super absorbers." Nature communications 2, no. 1 (2011): 517.

149. Tang, C. K., and G. T. Reed. "Highly efficient optical phase modulator in SOI waveguides." Electronics letters 31, no. 6 (1995): 451-452.

150. Png, Ching Eng, Seong Phun Chan, Soon Thor Lim, and Graham T. Reed. "Optical phase modulators for MHz and GHz modulation in silicon-on-insulator (SOI)." Journal of lightwave

technology 22, no. 6 (2004): 1573.

151. Tong, Jinchao, Landobasa YM Tobing, and Dao Hua Zhang. "Electrically controlled enhancement in plasmonic mid-infrared photodiode." Optics express 26, no. 5 (2018): 5452-5460.

152. Rajput, Swati, Vishal Kaushik, Lalit Singh, Sulabh Suresh Kumar Pandey, Rahul Dev Mishra, and Mukesh Kumar. "Efficient photodetector based on sub-bandgap transition in silicon-ITO distributed-heterojunctions." Journal of Lightwave Technology 39, no. 21 (2021): 6886-6892.

153. Dorodnyy, Alexander, Yannick Salamin, Ping Ma, Jelena Vukajlovic Plestina, Nolan Lassaline, Dmitry Mikulik, Pablo Romero-Gomez, Anna Fontcuberta i Morral, and Juerg Leuthold. "Plasmonic photodetectors." IEEE Journal of Selected Topics in Quantum Electronics 24, no. 6 (2018): 1-13.

154. Feigenbaum, Eyal, Kenneth Diest, and Harry A. Atwater. "Unity-order index change in transparent conducting oxides at visible frequencies." Nano letters 10, no. 6 (2010): 2111-2116.

155. Melikyan, Argishti, N. Lindenmann, S. Walheim, P. M. Leufke, S. Ulrich, J. Ye, P. Vincze et al. "Surface plasmon polariton absorption modulator." Optics express 19, no. 9 (2011): 8855-8869.

156. Feigenbaum, Eyal, Kenneth Diest, and Harry A. Atwater. "Unity-order index change in transparent conducting oxides at visible frequencies." Nano letters 10, no. 6 (2010): 2111-2116.

157. Sorger, Volker J., Norberto D. Lanzillotti-Kimura, Ren-Min Ma, and Xiang Zhang. "Ultra-compact silicon nanophotonic modulator with broadband response." Nanophotonics 1, no. 1 (2012): 17-22.

158. Pandey, S.K., Rajput, S., Kaushik, V., Babu, P., Dev Mishra, R. and Kumar, M., 2022. Electrically tunable plasmonic absorber

based on Cu-ITO subwavelength grating on SOI at telecom wavelength. Plasmonics, 17(4), pp.1709-1716.

159. Chen, Meijie, Yurong He, Qin Ye, and Jiaqi Zhu. "Tuning plasmonic near-perfect absorber for selective absorption applications." Plasmonics 14 (2019): 1357-1364.

160. Png, Ching Eng, Seong Phun Chan, Soon Thor Lim, and Graham T. Reed. "Optical phase modulators for MHz and GHz modulation in silicon-on-insulator (SOI)." Journal of lightwave technology 22, no. 6 (2004): 1573.

161. Reed, Graham, David Thomson, Weiwei Zhang, Frederic Gardes, Lorenzo Mastronardi, Ke Li, Shinji Matsuo et al. "Optical modulators." In Integrated Photonics for Data Communication Applications, pp. 69-121. Elsevier, 2023.

162. Tang, C. K., G. T. Reed, A. J. Walton, and A. G. Rickman. "Low-loss, single-model optical phase modulator in SIMOX material." Journal of lightwave technology 12, no. 8 (1994): 1394-1400.

163. Katti, Rohan, and Shanthi Prince. "A survey on role of photonic technologies in 5G communication systems." *Photonic Network Communications* 38 (2019): 185-205.

164. Liu, Xiaofeng, Qiangbing Guo, and Jianrong Qiu. "Emerging low-dimensional materials for nonlinear optics and ultrafast photonics." *Advanced Materials* 29, no. 14 (2017): 1605886.

165. Khurgin, Jacob B., and Alexandra Boltasseva. "Reflecting upon the losses in plasmonics and metamaterials." *MRS bulletin* 37, no. 8 (2012): 768-779.

166. Gong, Chen, and Marina S. Leite. "Noble metal alloys for plasmonics." *Acs Photonics* 3, no. 4 (2016): 507-513.

167. L. J. Meng and M. P. Dos Santos, “Structure effect on electrical properties of ITO films prepared by RF reactive magnetron

sputtering," *Thin Solid Films*, vol. 289, no. 1–2, pp. 65–69, Nov. 1996, doi: 10.1016/S0040-6090(96)08892-X.

168. M. Z. Alam, I. De Leon, and R. W. Boyd, "Large optical nonlinearity of indium tin oxide in its epsilon-near-zero region," *Science (80-.).*, vol. 352, no. 6287, pp. 795–797, May 2016, doi: 10.1126/science.aae0330.

169. J. Bregman, Y. Shapira, and H. Aharoni, "Effects of oxygen partial pressure during deposition on the properties of ion-beam-sputtered indium-tin oxide thin films," *J. Appl. Phys.*, vol. 67, no. 8, pp. 3750–3753, 1990, doi: 10.1063/1.345017.

170. Wang, H., Zhang, L., Chen, Z., Hu, J., Li, S., Wang, Z., Liu, J. and Wang, X., 2014. Semiconductor heterojunction photocatalysts: design, construction, and photocatalytic performances. *Chemical Society Reviews*, *43*(15), pp.5234-5244.

171. R. A. Soref and B. R. Bennett, "Electrooptical effects in silicon," *IEEE Journal of Quantum Electronics*, vol. 23, no. 1. pp. 123–129, 1987, doi: 10.1109/JQE.1987.1073206.